People's Democratic Republic of Algeria
Ministry of Higher Education and Scientific Research

Batna 2 University – Mostefa Ben Boulaïd
Faculty of Technology
Department of Mechanical Engineering

Thesis

Performed at
(Laboratory of Structural Mechanics and Materials (LaMSM))

Presented for the degree of
LMD Doctor in Mechanical Engineering
Option: Mechanical Construction

Theme

Generation and modeling of the mechanical behavior in compression of stochastic foams

Defended by

KHENNAB Abdelghani

Before the Jury Composed of

Mr. KADDOURI Wahid	Professor	University of Batna 2	President
Mr. BENHIZIA Abdennour	MCA	University of Batna 2	Supervisor
Mr. MASMOUDI Mohamed	MCA	University of Batna 2	Examiner
Mr. CHEBBAH Mohamed-Saïd	Professor	University of Biskra	Examiner
Mr. SEDIRA Lakhdar	Professor	University of Biskra	Examiner

27/06/2024

To my dearest parents, ***KHENNAB Hadda*** *and* ***KHENNAB Hamid****,*

Throughout my life, you have been the unwavering pillar of love, support, and encouragement. Your sacrifices, dedication, and boundless belief in my potential have been the driving force behind my academic journey.

Mom, your nurturing care, resilience, and strength have inspired me in ways words cannot express. Dad, your wisdom, guidance, and unwavering belief in my abilities have been a constant source of motivation.

To my beloved brother, ***Sifeddin****, and my cherished sisters,* ***Chahra*** *and* ***Ritej****,*

Your unwavering support, love, and understanding have been the foundation upon which I've built my dreams. Your belief in my abilities and the countless moments of laughter and encouragement have been a source of inspiration.

To ***TAIEB Kahina*** *Your invaluable assistance, wisdom, and kindness have played a crucial role in this work.*

It is with the deepest gratitude and love that I dedicate this work to all of you, knowing that every achievement I have earned is a reflection of our shared values and the strong bonds that tie us together.

Thank you for being my role models, my greatest champions, and my constant sources of love and support. This is for all of you.

With all my love,

KHENNAB ABDELGHANI

JANUARY, 2024

ACKNOWLEDGEMENTS

I express my deepest and sincere gratitude to **Dr. BENHIZIA Abdennour**, whose unwavering support, profound guidance, and constant encouragement were the cornerstone of my doctorate. **Dr. BENHIZIA** was more than just my advisor, he was a mentor in every sense of the word, a contact who guided me through the maze of academic challenges, and a beacon of wisdom and support. Under his tutelage, I developed greatly, both as a researcher and as an individual. I consider myself lucky to have been his student. His influence was essential in achieving the objectives and milestones of my doctoral research.

This work was carried out within the Laboratory of Structural and Materials Mechanics, and for this, I would like to express my sincere thanks and gratitude to the Director of the laboratory **Pr. OUTTAS Toufik**, and to all the members of the laboratory, in particular **Pr. MADANI Salah**, **Pr. KADDOURI Wahid** and **Dr. MASMOUDI Mohamed** for their professionalism and for all the facilities and advice they provided me.

My gratitude extends to the honorable members of the jury: **Pr**. **KADDOURI Wahid**, **Dr**. **MASMOUDI Mohamed**, **Pr**. **SEDIRA Lakhdar**, and **Pr**. **CHEBBAH Mohamed-Saïd**, for their time and consideration. Your evaluation and insights are highly appreciated and respected.

I would also like to extend my heartfelt thanks TO **BOUTERAI Fadda, Dr. Rahmouni khaoula, Nacer Sara, Dr. DJEBARA Youcef**, **Dr. BENSALEM Ilyas**, **SAADNA Mohamed**, **SAADI Aymen** and **ODACCHI Shoaib** for their unwavering support and encouragement throughout this Ph.D.

I thank my family for encouraging me to register for the doctorate. They have been my strength and inspiration throughout. It wouldn't have been possible without them.

A warm thanks to all my teachers and the whole Mechanical Engineering Department.

Completing this PhD has been a journey that I could not have undertaken without the support and encouragement of all those mentioned above, and many others who have crossed my path over the last few years. I am eternally grateful to every one of you.

TABLE OF CONTENTS

LIST OF FIGURES

LIST OF TABLES

Notations and abbreviations

MF	Metal foam
OCF	Open cell foam
ρ_F	Foam density
ρ_s	Solid density
V_P	Volume of pores
V_s	Solid volume
P	Porosity
ρ	Relative density
PCMFP	Powder Compact Melt Foaming Process
SLM	Selective Laser Melting
CAD	Computer aided design
UTM	Universal Testing Machine
σ_{ple}	Plateau end stress
ε_{ple}	Plateau end strain
W	The energy absorption per unit volume
SEA	The specific energy absorption
Δσ	Difference between peak stress and 1st low valley stress
σ_{peak}	Peak stress
Ave.	Average
Std. Dev.	Standard deviation
SHPB	Split Hopkinson Pressure Bar
Dp	Apparent pore diameter,
lp	Deformation in mm corresponding to the 1st stress drop
ε_y	Compressive yield strain
σ_y	Compressive yield stress
PS	Lower plateau stress
HSR	High strain rate
CMF	Composite metallic foams
SiC	Silicon Particles
PCS	Plastic collapse stress
qs	Quasi-satatic
dyn	Dynamic
AFSS	Aluminum foam sandwich with steel panel
P_{cr}	Peak load
S_{cr}	Displacement at peak load
B	Bending stiffness of specimens
c	Thickness
SSFs	Syntactic steel foams
AL	Aluminum
UTS	Ultimate tensile strength
ρ_{SSFs}	Density of the syntactic foams
TYS	Tensile yield strength
PDE	Partial differential equation
R	Scaling ratio
S_f	The polyhedrons faces scale factor
S_v	The polyhedrons volume scale factor

ρ_{app}	Density of the 3D-printed PLA sample
ρ_{PLA}	Density of the rigid polymer
AM	Additive Manufacturing
η	Energy absorption efficiency
ε_d	Densification strain
σ_{pl}	Plateau stress
σ_c	Collapse stress
PLA	Polylactic Acid

GENERAL INTRODUCTION

1. Context

Metal foam is a porous material having a cellular structure comprising metal and gas bubbles [1]. The special combination of lightweight, high thermal stability, good electrical insulating properties, air and water permeability, exceptional acoustic properties, energy absorption, good environmental and corrosion characteristics make it suitable for various applications. However, the MF applications are still limited due to the high cost of its manufacturing processes.

Several methods have been developed to produce porous metals since they were discovered, which result in foams with different features. The foam microstructure depends on how it is manufactured [2], for example, the density and cell size can be controlled by selecting certain manufacturing parameters, such as gas injection or nozzle vibration [3-5].

While conventional techniques allow for the manipulation of certain parameters, isolating the effect of individual morphological parameters is challenging due to the complexity and cost associated with manufacturing methods and experimental tests.

Additive Manufacturing (AM) is an efficient process for creating a three-dimensional object by gradually adding materials together. Along with computer-aided design (CAD), it has gained popularity in the field of quick prototyping and customized design solutions. It enables the rapid production of preliminary iterations of a product to evaluate its design and functionality.

2. Problem and objectives of the thesis

The majority of recent studies on cellular structures created by 3D printing have focused primarily on periodic lattice structures formed by repeating unit cells or OCF with consistent strut cross-sections. Although these models yield substantial outcomes, they are greatly constrained by their inability to consider the microstructural defects present in real OCF. Open-cell foam have cell structures that are commonly characterized by their non- periodic nature, lack of order, and the presence of struts with a non-uniform cross-section shape [6-8]. These morphological factors significantly influence the open-cell foam performances. Hence, additional research may be necessary to examine the mechanical behavior and energy dissipation properties of OCF, while considering all morphological factors, including variations in strut sections with diverse cross-sectional forms.

The current study involved subjecting a 3D-printed PLA OCF with real morphological features to a quasi-static load. The objective was to analyze the relationship between the structures' elastoplastic mechanical responses and their topological features.

3. Contributions

The Voronoi approach is used to generate the 3D morphology of the stochastic open-cell foam that is next produced using 3D printing. An in-depth analysis was conducted to investigate the impact of several parameters such as relative density, pore number, random realization, and cross-sectional morphologies of struts on the compressive mechanical properties of the manufactured PLA foam. It was found that both of relative density and cross-sectional shape of the strut have an important influence on the overall mechanical behavior of the studied structures. The mechanical characteristics of the 3-D printed PLA foam with various cross-sectional shapes during quasi-static compression, specifically collapse stress, plateau stress, and densification strain, are assessed using the energy-efficient approach. These properties are then quantified using commonly employed equations that are used to calculate the mechanical properties of cellular structures during deformation.

This thesis is composed of 4 chapters and is organized as follows:

- Chapter 1 provides an overview of the classification, production, and most relevant applications of metal foams.
- Chapter 2 presents detailed information on the methodology of experimental investigations of metallic foams and the main microstructural parameters affecting the mechanical behavior of these materials.
- Chapter 3 reviews the methodology devoted to generating 3D solid models of open-cell foams and its validation through comparison with available experimental data from literature and by 3D printing tests.
- Chapter 4 presents the experimental study of the mechanical behavior of the 3D printed samples under compression test.

Finally, a general conclusion summarizes the main findings and recommendations and gives a strategy for future studies.

CHAPTER I METAL FOAMS MANUFACTURING PROCESSES AND APPLICATIONS

I.1. Introduction

Cellular materials are defined by their porous microstructure consisting of solid and void networks. These materials are already present in nature and utilized like bone, marine sponges, wood, and cork, in which they have significantly impacted and advanced the development of cellular materials research.

Novel cellular solids mimicking natural structures, such as honeycomb materials and foams, have been produced. These materials possess unique properties such as lightness, insulation, cushioning, and energy absorption due to their cellular composition, making them suitable for various applications.

Metal foams exhibit superior qualities compared to other lightweight materials, including increased deformation resistance, compressive strength, and crashworthiness. The foam material's characteristics and foaming behavior strongly depend on the fabrication methods.

This chapter comprehensively delves into the definition, classification, and manufacturing processes of metal foams utilizing diverse production techniques. Additionally, it sheds light on several industrial sectors that have successfully incorporated these foams into their applications.

I.2. Cellular materials

Cellular materials are defined as materials that have a porous microstructure, consisting of solid and void networks. They can be found in both natural and artificial forms, such as cork, plant stems, wood, and human bones [1].

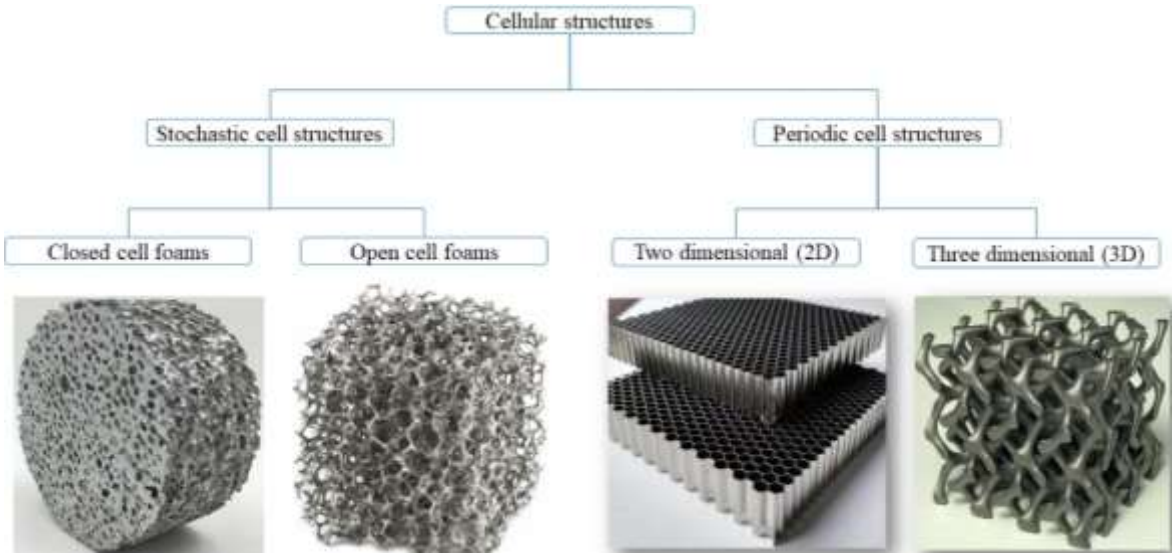

Figure I.1 Cellular Materials examples.

Cellular materials are typically divided into two primary categories: open-cell and closed-cell structures. This classification is based on the nature of the cells, with open-cell structures featuring cells connected by edges, and closed-cell structures having cells that are separated from each other by solid faces [1]. The structural design of cells plays a crucial role in defining the mechanical characteristics and density of these substances, impacting an array of additional properties [2].

Due to their unique combination of properties, including high strength-to-weight ratio, energy absorption, and thermal insulation, these materials are used to create micro-lattices with graded porosity, truss structures optimized for specific loading conditions, and other architected cellular materials with varying properties to match specific requirements [1].

I.3. Metal foams

Metal foams consist of a solid matrix including a substantial quantity of gas-filled voids. it can be created using various base materials such as metals (like copper, nickel, aluminum, and various alloys), carbon, or polymers, a key characteristic of these materials is their high porosity, generally between 75% and 95%, which contributes to their extremely lightweight nature.

Generally, there are two parameters used to represent metal foams:

- Porosity
- Relative density

Metal foams typically maintain the majority of the physical characteristics inherent in their base metal. The characteristics of any metal foam can be encapsulated by its proportional density:

$\frac{\rho_F}{\rho_S}$ Where ρ_F and ρ_S denote foam and solid density, respectively.

The porosity P of these porous materials is defined by a specific formula [1]:

$$P(\%) = \left[\left(\frac{V_P}{V_P+V_S}\right) \times 100\right](\%) \quad \text{(I. 1)}$$

Where V_P represents the volume of pores and V_S stands for the solid volume. The relative density of the foam ρ is determined experimentally by [1]:

$$\rho(\%) = [(1 - P) \times 100](\%) \quad \text{(I. 2)}$$

I.3.1. Classification

The metallic foams are broadly divided into two categories based on

a) Pore type

- Closed Cell (sealed pores)

Closed-cell foams are a type of foam material characterized by completely closed cells, which are pressed together to prevent moisture and air from entering the foam Figure I.2.

Figure I.2 Closed-Cell Aluminum Foam.

- Open Cell (interconnected network formed pores)

Open-cell foam is a type of foam material characterized by cells that are not completely closed, allowing air to pass through the foam Figure I.3.

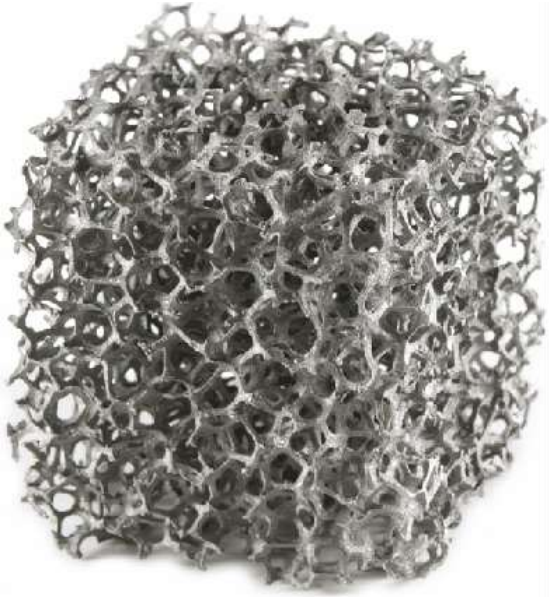

Figure I.3 Open-Cell Aluminum Foam.

b) Pore structure

Considering the geometries and topologies of microstructures, metal foam can be categorized into two main types: stochastic cells and periodic cells.

- *Stochastic (pores distribution is irregular)*

Stochastic metal foams refer to metallic materials with a cellular or porous structure where the arrangement of the cells follows a random or stochastic pattern Figure I.4.

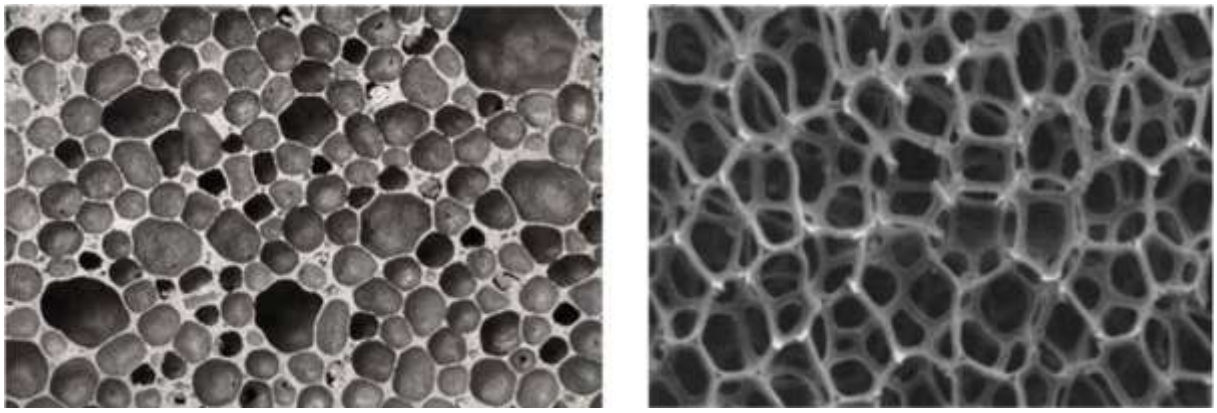

Figure I.4 Stochastic metal foams.

- *Regular (periodic)*

Regular foams refer to materials with a structured and ordered arrangement of cells or pores within a matrix Figure I.5.

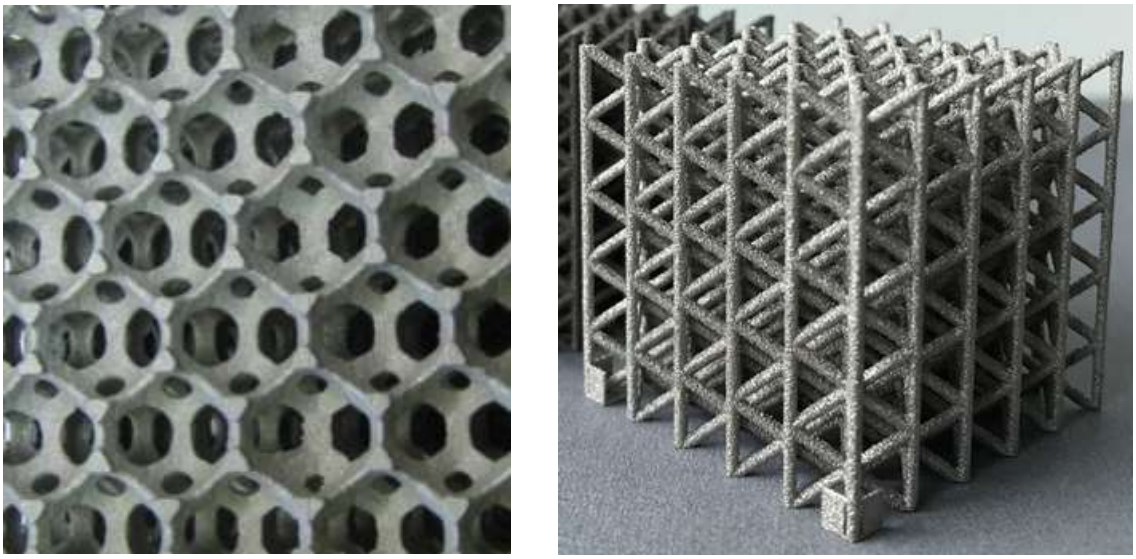

Figure I.5 Regular metal foams.

I.4. Foam production techniques

The different techniques may be categorized according to the condition in which the metal is manipulated. There are five distinct categories of operations, as shown in Figure I.6, that define different families in foam manufacturing. These various approaches result in a wide range of products. Foams vary in terms of pore size, relative density, porosity, and other characteristics.

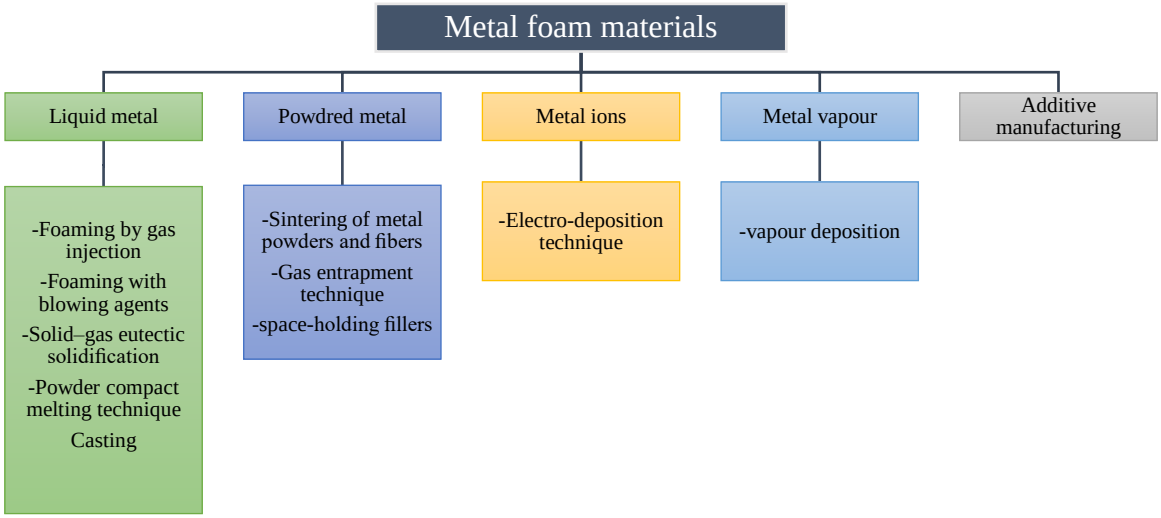

Figure I.6 Manufacturing methods of cellular metallic materials.

I.4.1. Liquid metal

Liquid metals like aluminum, copper, or steel alloys are versatile materials extensively utilized in the manufacturing of metal foams. These foams are engineered to have a cellular structure, which provides them with unique properties. The production processes involve various techniques that allow the liquid metal to form a porous structure.

a) Foaming by gas injection

The process of creating metal foams by gas injection involves several steps. Initially, the metal is melted, and then a gas or a foaming agent is introduced into the melt. When using inert gases, the process needs to be conducted at temperatures close to the metal's melting point.

The gas forms bubbles in the molten metal, which are trapped as the metal cools and solidifies, creating the foam structure.

Key Factors in the Process:

- Gas Choice and Control: The type of gas and the rate at which it is injected play crucial roles in determining the size and distribution of the pores within the metal foam.

- Cooling Rate: The rate of cooling can affect the foam's cell structure. Faster cooling may result in finer, more uniform cells. [3-5].

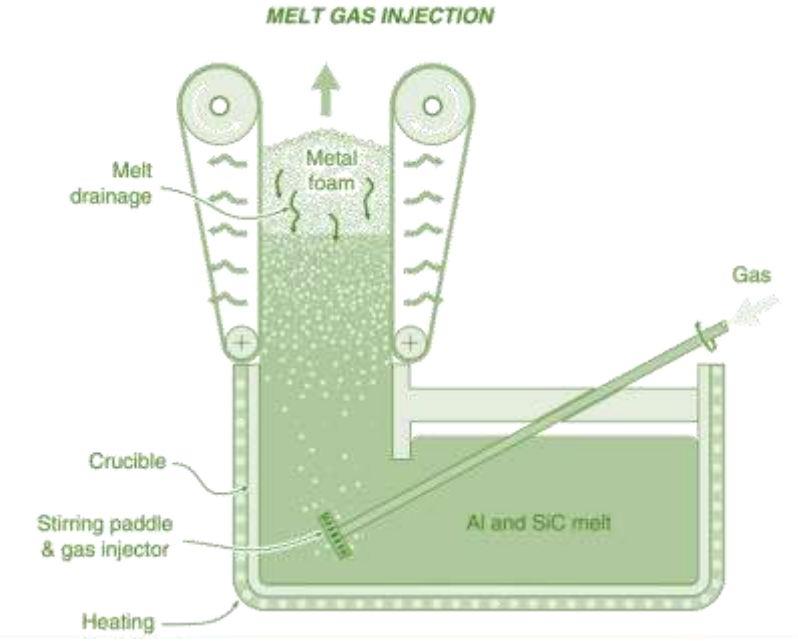

Figure I.7 Illustration of the melt gas injection manufacturing method of metal foam.

b) Foaming with blowing agents

The use of blowing agents in the production of metal foams involves the introduction of substances that decompose under heat, releasing gas to propel the foaming process. In the context of metal foam production, blowing agents such as hydrides and carbonates are utilized to create closed-cell metal foams. These blowing agents are introduced close to the melting point of the metal to facilitate the formation of the foam structure. The selection of an appropriate blowing agent is a critical aspect of the manufacturing process, influencing the physical properties and characteristics of the resulting metal foam [5-7].

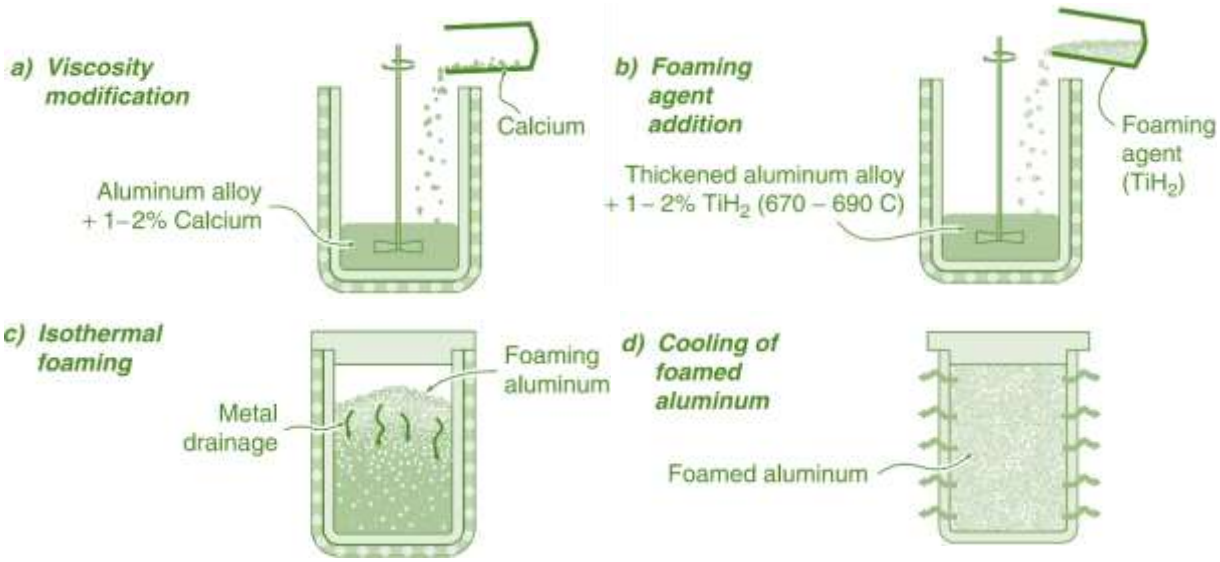

Figure I.8 The processes and steps of the foaming with blowing agents manufacturing method decomposition in the melt (Alporas technique).

c) Solid–gas eutectic solidification ‘‘gasars’’

The solid-gas eutectic solidification process is used for the production of metallic foams. This approach was devised due to the tendency of some liquid metals, such as aluminum, magnesium, and copper, to create eutectic systems when combined with hydrogen gas. When liquid metal is heated in a high-pressure hydrogen environment, it forms a two-phase eutectic melt that contains hydrogen gas. Upon cooling and solidification, the liquid metal assimilates the hydrogen gas, resulting in the formation of pores inside the metal. The process is referred to as GASAR, an abbreviation derived from the Russian term "gas-reinforced." Nevertheless, this procedure has limitations, including challenges in regulating pore structure and inapplicability for very reactive metals as titanium [5, 8].

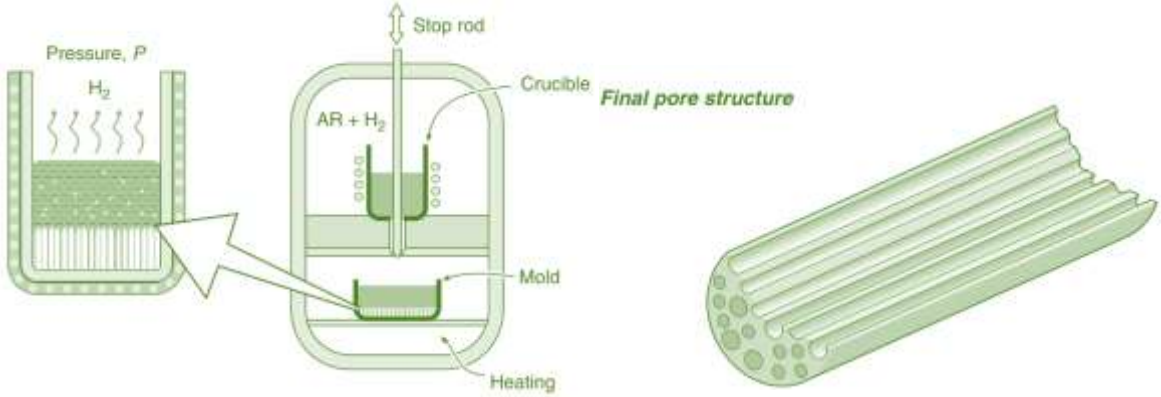

Figure I.9: Gas–metal eutectic solidification for the manufacture of GASARs.

d) Powder compact melting technique

The powder compact melting technique is a well-established method for manufacturing metallic foams. This process involves mixing metal powder with a blowing agent to create a foamable precursor, which is then compacted and heated to initiate foam formation. The Powder Compact Melt Foaming Process (PCMFP) is a specific application of this technique, where the foaming occurs during the melting process.

The powder compact melting technique is suitable for metals with high melting points and reactive properties, such as titanium and stainless steel. The process layout of the powder compact melt technique involves heating the precursor to initiate cell growth and foam formation [5, 9].

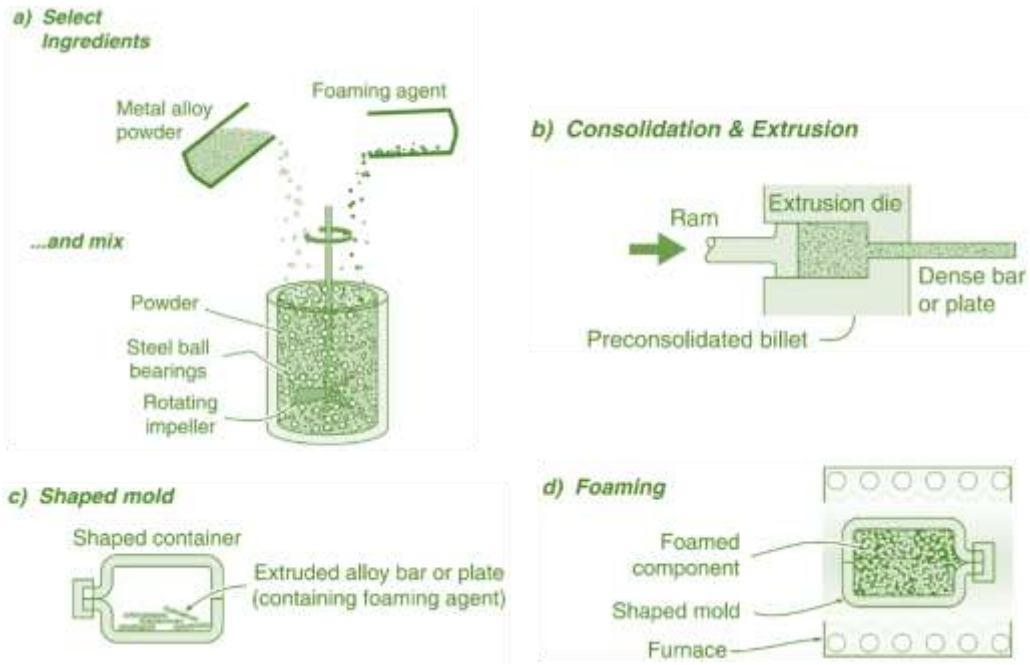

Figure I.10 Powder compact melting technique.

e) Casting methods

During this procedure, a polymer is originally chosen to form a preliminary shape utilizing the injection molding technique using polymer lattices or wax. Subsequently, the polymer form is coated with a layer of ceramic material. Following the application of this coating, a further drying phase occurs, resulting in the creation of an inverse copy of the foams present in the initial material, which functions as a mold. The selected metal was progressively introduced into the object, following precise criteria. Applying mild pressure is permissible to provide a uniform and equitable flow and dispersion.

This stage initiates a process of freezing and cooling in a specific direction, resulting in the restoration of the original structure of the polymer foam. After the chilling step is over, a structure that looks like an open-cell foam is formed, with a porosity of about 95%.
Figure I.11 illustrates the procedural phases of the Duocel method [5].

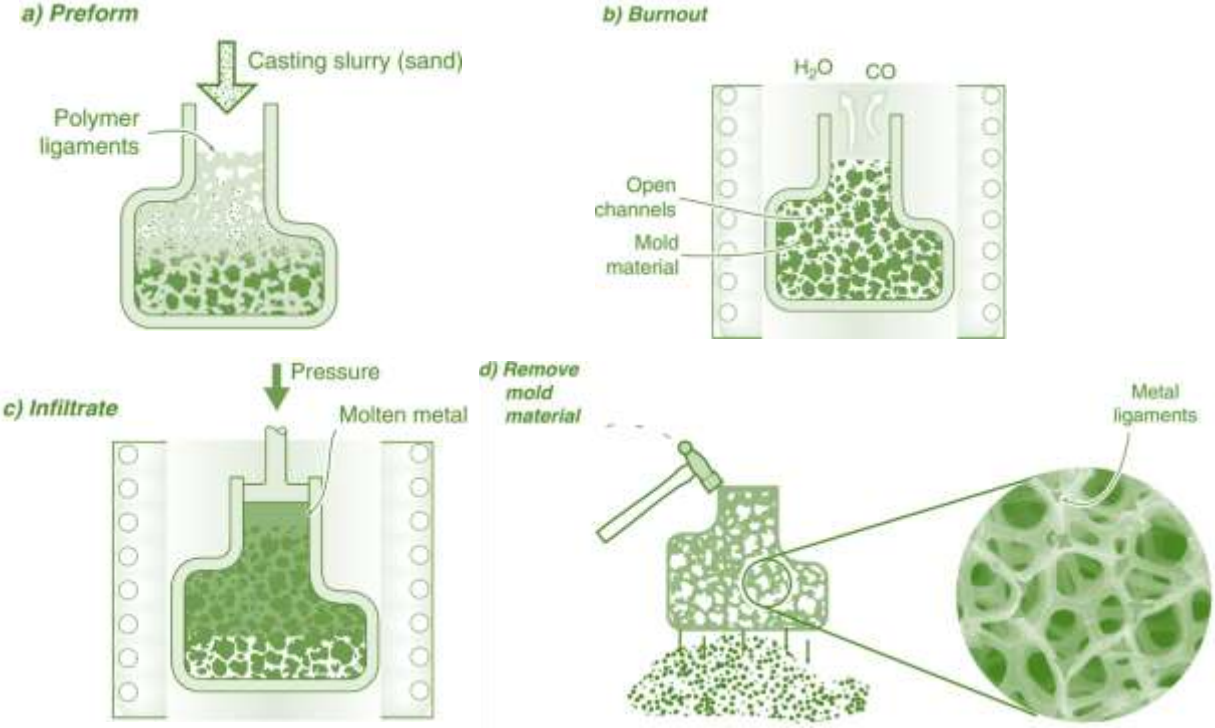

Figure I.11 Investment casting method used to manufacture open cell foams (DUOCEL process).

I.4.2. Powdered metal

Powdered metals are integral to the manufacturing of MF, offering diverse techniques and applications that enhance their versatility and performance across industries. One prominent method involves utilizing powdered metals within the powder metallurgy process. This technique allows for the creation of metal foams with tailored properties such as specific pore sizes, distribution, and mechanical strengths.

a) Sintering of metal powders and fibers

The sintering of metal powders and fibers is a process used for the manufacturing of metallic foams. This process involves the following steps: Metal powder and fibers are mixed with a blowing agent to create a foamable precursor; The mixture is then compacted using compression or extrusion techniques.

The compacted mixture is heated to a temperature in close proximity to the metal's melting point, which initiates cell growth and foam formation.

Sintering is a solid-state processing method that is suitable for metals with high melting points and reactive properties, such as titanium and stainless steel [10]. The process layout of sintering involves heating the precursor to produce metal foams [10].

b) Gas entrapment technique

This process involves the use of gas to create voids within the metal structure, resulting in the formation of foams. The technique typically begins with the placement of metal powder into a mold, followed by the introduction of gas to create the desired porosity within the material. Gas entrapment is a promising approach for manufacturing metal foams and has been the subject of various studies and numerical investigations [5,10,11]. This method offers an alternative to traditional foam production processes and has been the focus of research aimed at understanding its effects on porosity and foam properties [11].

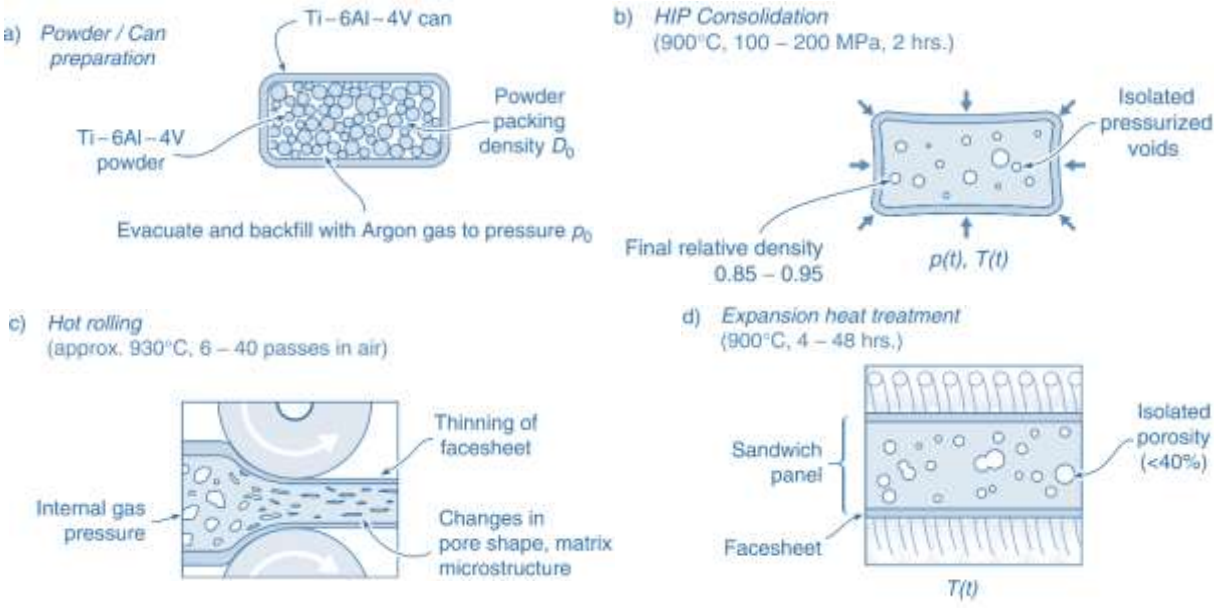

Figure I.12 manufacture process used for closed-cell titanium alloy sandwich panels.

c) Space-holding fillers

This method involves the use of fillers that create voids within the metal matrix, contributing to the cellular structure of the material.

The fillers can be removed by thermal treatment or the use of an aqueous solvent, leaving behind a porous metallic network. The use of polymer spheres as space holders is one way to manufacture titanium foams [10]. The use of space-holding fillers is a promising technique for manufacturing metal foams with tailored properties for various industrial applications.

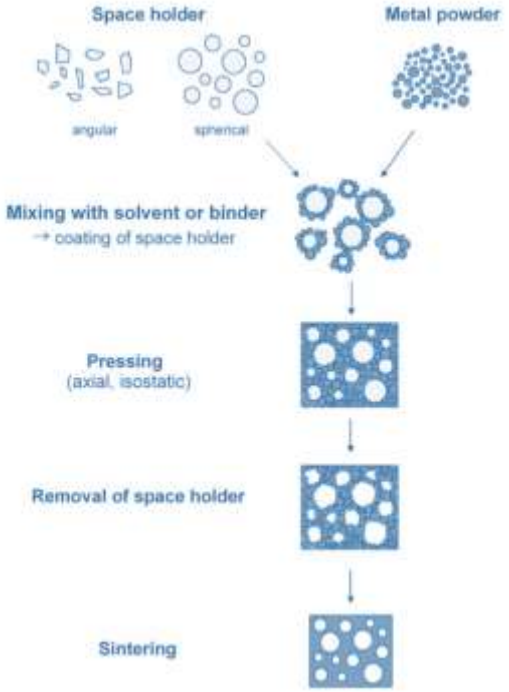

Figure I.13 Space holder technique for making porous metallic structures from metal powders.

I.4.3. Metal ions (Electro-deposition technique)

The Electro-deposition technique for manufacturing metal foams is a process where a metallic layer is deposited on a preformed substrate through electroplating. This substrate, often a polymeric foam, defines the structure of the foam. The metal, such as nickel or copper, is deposited onto the substrate in an electrolytic bath. After the desired thickness is achieved, the substrate is removed, typically by thermal decomposition or chemical dissolution, leaving behind the metal foam. This method allows for precise control over the foam's structure and is particularly useful for creating foams with complex geometries and fine features [4].

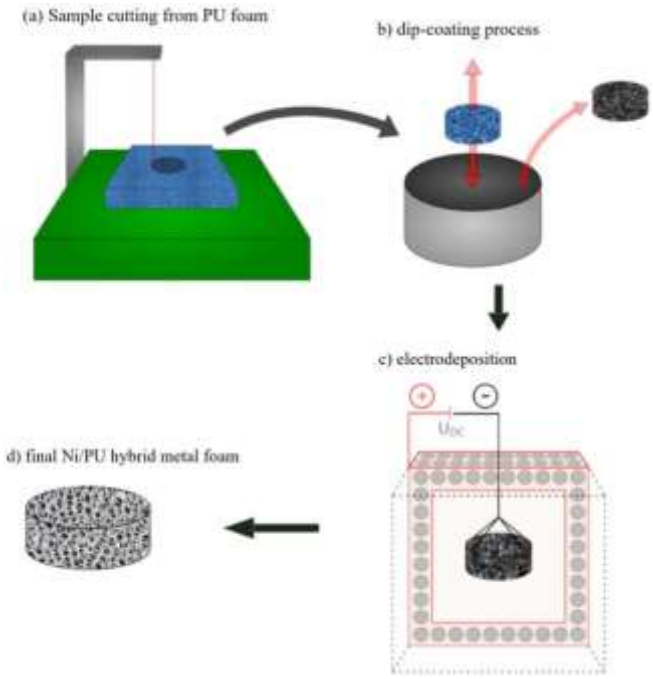

Figure I.14 Schematic illustration of the electro-deposition technique.

I.4.4. Additive manufacturing

Additive manufacturing of metal foams involves the application of advanced techniques such as Selective Laser Melting (SLM). In the SLM process, a fine layer of metal powder is meticulously deposited on a build platform, and a high-powered laser selectively melts and fuses the powder in accordance with a numerically designed model. The process is then repeated layer by layer, each time lowering the build platform and applying a new layer of powder. This results in the formation of a three-dimensional structure with controlled porosity. Laser additive manufacturing has been used for the fabrication of metal foams, offering the ability to design and build random metal foam structures for specific applications [12, 13].

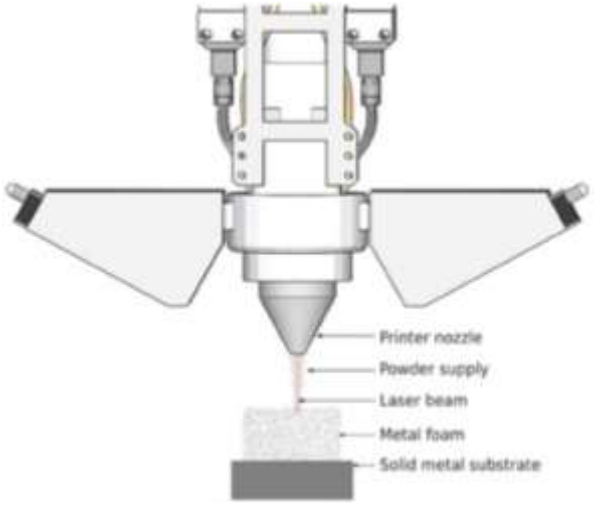

Figure I.15 Schematic illustration of the additive manufacturing process.

I.5. Metal foams applications

In today's rapidly advancing technological era, metal foams have become a prominent lightweight material option for numerous uses. Beginning in the 1990s, the range of applications for metal foams has expanded considerably [14, 17]. Their distinctive qualities have led to their widespread adoption in a variety of engineering fields, including structural, chemical, functional and biomedical applications [15-17]. The use of metallic foams in industrial applications remains somewhat restricted, primarily because of their higher expense compared to other materials. A significant limiting factor is the lack of a cost-effective manufacturing method that can produce metal foams on a large scale.

I.5.1. General Considerations

The use of metal foams in conventional or novel applications is influenced by many factors, including porosity, economic factors, and appropriateness for certain purposes, as outlined in the following literature [15, 16]:

Figure I.16 illustrates the many uses of metal foams based on their level of porosity, whether they are open or closed, as described in reference [14, 15].

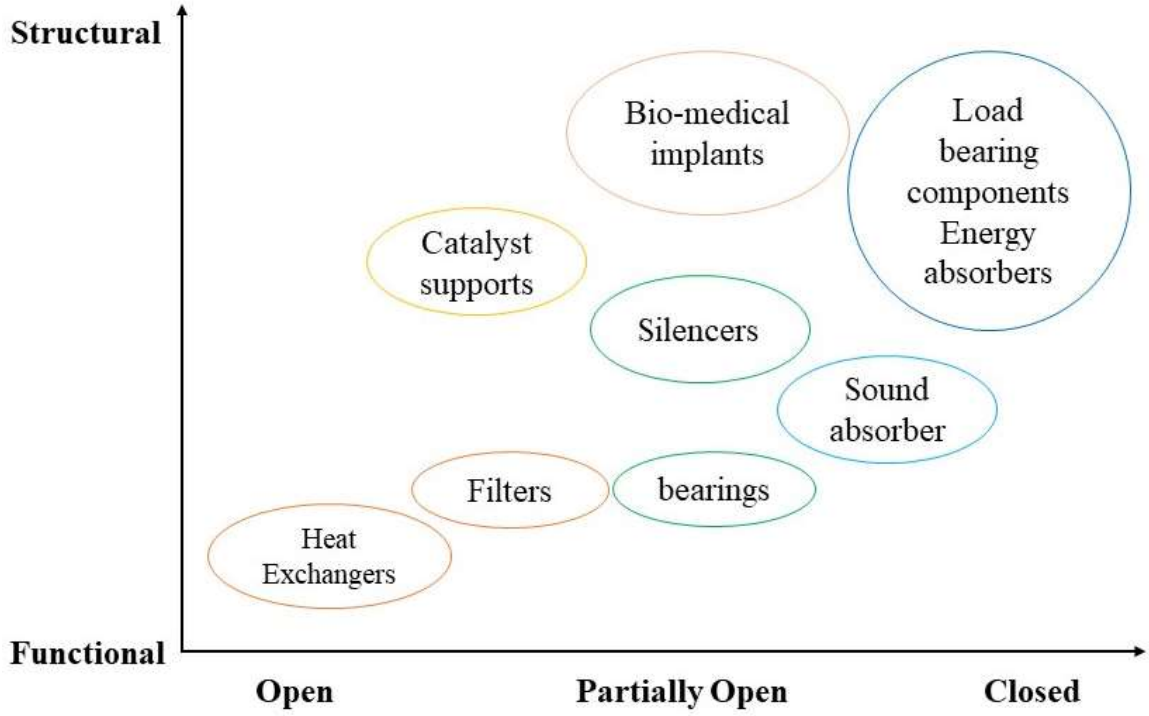

Figure I.16 Application of metallic foams based on the porosity degree.

I.5.2. Structural Applications

Metal foams find numerous structural applications across various industries due to their unique properties that combine lightweight construction with excellent mechanical performance.

a) Automotive Industry

Metal foams have found various applications in the automotive industry due to their unique properties, including high porosity, low weight, stiffness, and high impact resistance. Some of the specific applications of metal foams in the automotive sector include:

- Anti-intrusion Bars: MF are extensively used in anti-intrusion bars in ground vehicles and passenger cars to protect passengers by absorbing the kinetic energy of colliding vehicles.
- Heat Exchangers: MF offer superior thermal conductivity, making them valuable in heat exchanger applications within automotive systems.
- Sound Insulation: The use of MF contributes to sound insulation in vehicles, thereby enhancing the comfort of passengers.
- Lightweight Structures: MF are employed in the manufacturing of lightweight structures in vehicles, leading to reduced fuel consumption and improved safety due to their damping and shock absorbability properties.

The use of MF in the automotive industry is expected to continue growing, driven by their cost-effectiveness, lightweight characteristics, and specific functional properties [14][18].

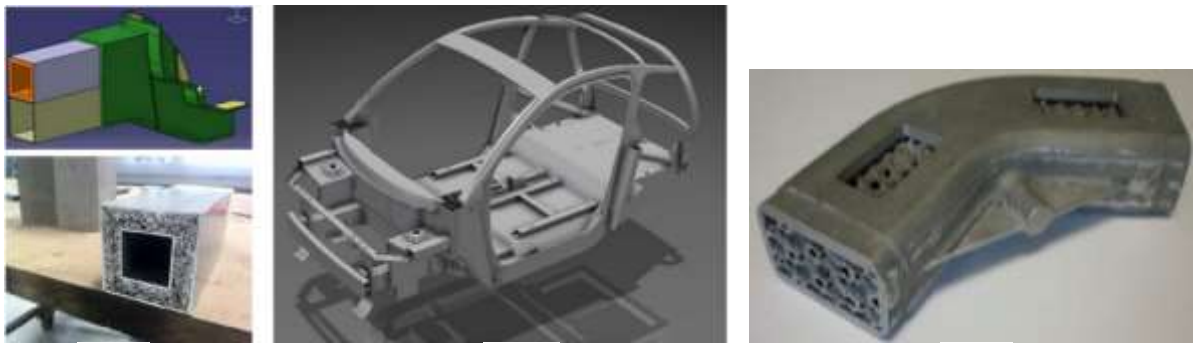

(a) **(b)** **(c)**

Figure I.17 Examples of application of MF in automotive industry: a) electric car Crash box prototype made with rectangular Al-profiles filled with Al-foam, b) CAD design of the body and c) Crash box for domestic car.

b) Noise/Sound Management

MF are the chosen materials for managing and controlling noise [19]. In scenarios where a car passenger might encounter loud sounds both from inside and outside the vehicle (like engine noise), aluminum foams like Alporas are effective for dampening and managing these sounds. When used in combination with polymeric foam, these MF demonstrate an impressive ability to absorb sound, achieving up to 99% effectiveness for specific frequencies between 1–5 kHz [14,15].

Figure I.18 a) Audience Hall, b) Restaurant covered by Alusion foam for sound control.

c) Aerospace Industry

The aircraft industry relies on lightweight materials and structures. Foam-filled structures are used as a cost-effective alternative to honeycomb structures, resulting in improved efficiency and reduced expenses. MF have the benefit of increased buckling and crippling resistance. In addition, they provide uniform mechanical qualities in all directions and allow for the creation of composite structures without the need for adhesive agents.

The fire-resistant characteristic also plays a crucial role in maintaining the structural integrity of a building. Boeing, as a result of these benefits, the aerospace industry is progressively using MF sandwiches [20-22]. Turbine blades and engine seals may use these materials to achieve both high rigidity and improved damping properties. Aluminum foams are being increasingly used in spacecraft, energy storage components, and satellites.

Figure I.19 Aircraft Air Oil Separator.

d) Railway Industry

Like the automotive sector, aluminum foam, are well-suited for the railway industry. This foam was employed in this context for three primary reasons:

- Lightweight construction.
- Energy absorption.
- Noise management.

For example, trains in Japan utilize energy absorbers constructed from blocks of Alporas aluminum foam, each measuring 2.3 cubic meters [14].

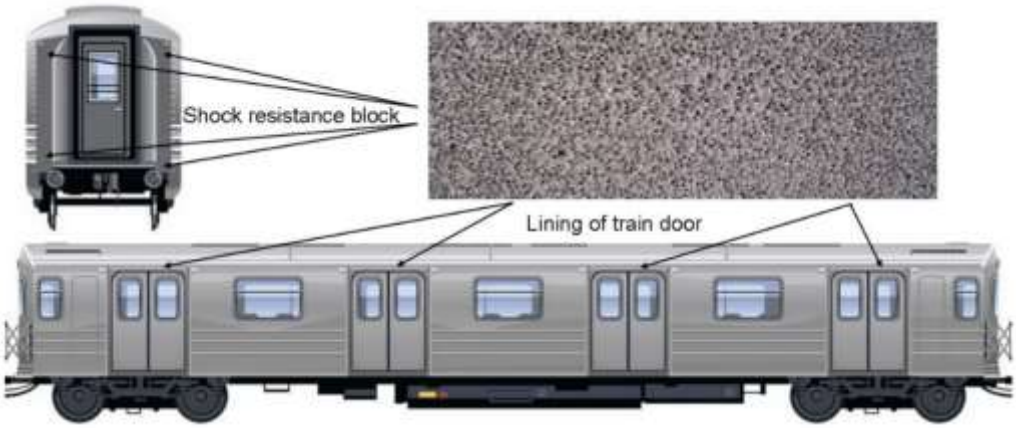

Figure I.20 Diagrammatic sketch of aluminum foams used in subway train compartment.

e) Building Industry

MF offer several advantages in the building industry, including insulation, sound reduction, electromagnetic shielding, and structural applications. They are particularly useful for lightweight and rigid materials, such as aluminum, which can be used in various applications, including building skins, noise reduction, and structural reinforcement.

Figure I.21 Aluminum foam used for construction projects (ALUSION by Cymat Technologies Ltd).

f) Biomedical Industry

MF have significant applications in the biomedical industry. They are used in the manufacturing of bone implants. This is attributed to Their capability to mimic the mechanical properties of natural bone and promote bone ingrowth.

Metals such as titanium and its alloys, magnesium, and tantalum are porously produced and used as biomaterials [23]. Additionally, metallic foams are utilized in the development of scaffolds for tissue engineering, where their porous structure allows for cell growth and nutrient transport. These applications demonstrate the versatility and importance of metallic foams in advancing biomedical technologies [23].

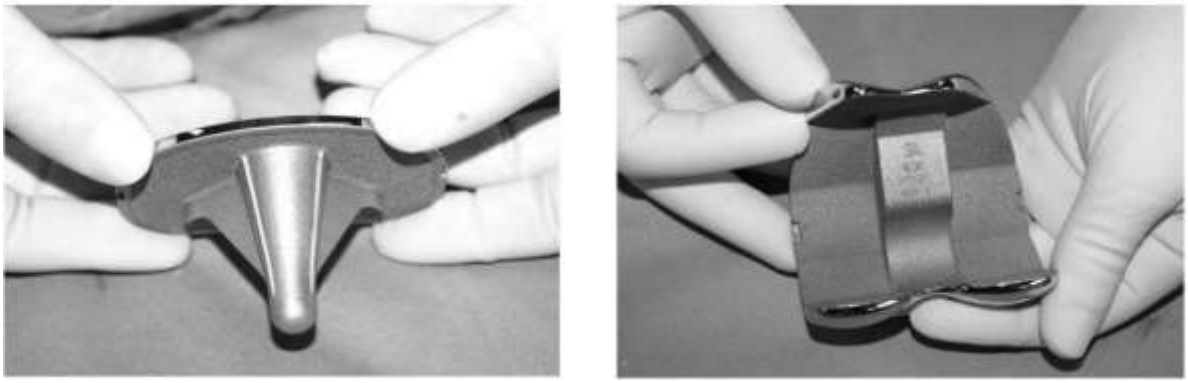

Figure I.22 Porous titanium components: Tibial (left) and Femural (right).

g) Heat Exchangers and Cooling Machines

Copper and aluminum foam materials are suitable for creating components with high conductivity. Such components require open-cell structures. The heat exchange process in foams involves the flow of liquids or gases through them, leading to a reduction in pressure drop [24]. Enhancing the performance coefficient in MF is possible by maintaining low stream resistance and high thermal conductivity, although achieving this balance can be challenging due to their inherent conflict [14, 25].

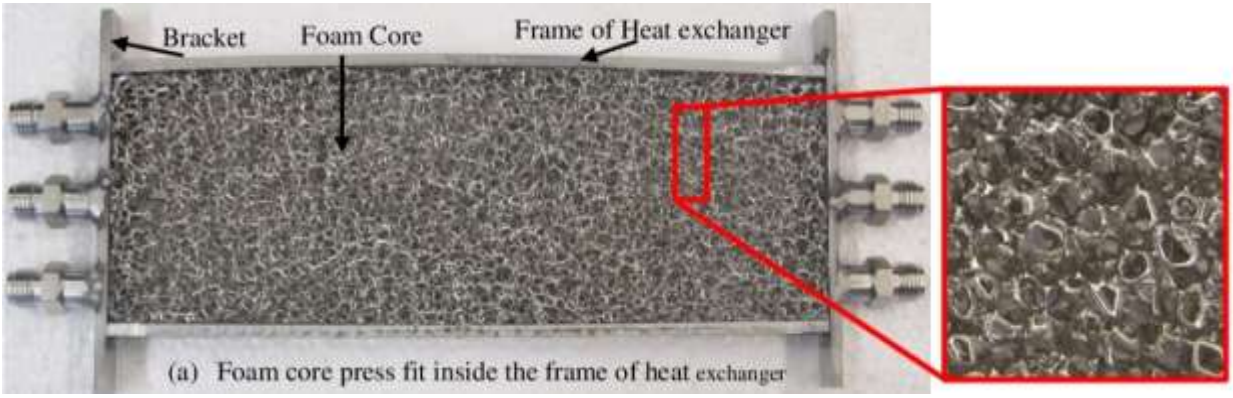

Figure I.23 Photographic of heat exchangers.

I.6. Conclusion

In conclusion, a comprehensive overview of the properties and applications of cellular materials, with a particular emphasis on metal foam has been provided in this chapter. Starting from the fundamental characteristics of cellular materials. This foundational knowledge serves as a critical backdrop for understanding the specific attributes and advantages of MF.

The preparation methods of MF were explored next, showcasing the diverse techniques available for creating these materials. We discussed how each method influences the final properties of the MF, underscoring the importance of the preparation phase in determining the quality and applicability of the product.

In the manufacturing section, we navigated through the processes involved in producing MF, highlighting the technological advancements and the challenges faced in this domain. The focus on manufacturing underlined the critical role of production techniques in enhancing the efficiency and sustainability of MF.

Finally, we surveyed the wide-ranging applications of MF, demonstrating its versatility and effectiveness in various sectors such as automotive, aerospace, construction, and biomedical engineering.

This exploration into the applications not only showcased the practical utility of MF but also highlighted their potential to address complex engineering challenges and contribute to innovative solutions.

CHAPTER II

CHARACTERISTICS OF METAL FOAMS UNDER MECHANICAL TESTS

II.1. Introduction

Understanding the properties of MF is essential for several applications where they exhibit specialized behaviors, such as lightweight structural uses, bone implants, filters, and electrodes. Various experimental methods were used to investigate the reaction of MF, based on tensile, compression, and bending tests. This chapter is dedicated to a comprehensive investigation into the mechanical properties of MF under different mechanical tests, specifically focusing on critical parameters such as Young's modulus, tensile strength, relative density, collapse stress, and densification strain.

II.2. Mechanical response under static compression

Static loading refers to the process of applying a consistent and continuous load to MF over a prolonged duration. Understanding the behavior of MF under prolonged stresses or weights is crucial in various structural applications, making this form of loading essential.

The centerpiece of the setup is a compression testing machine (Figure II.1), often a Universal Testing Machine (UTM). These machines are designed to apply controlled compressive forces to a specimen and measure the corresponding deformations. They come in various sizes and force capacities, suitable for different types of materials and tests.

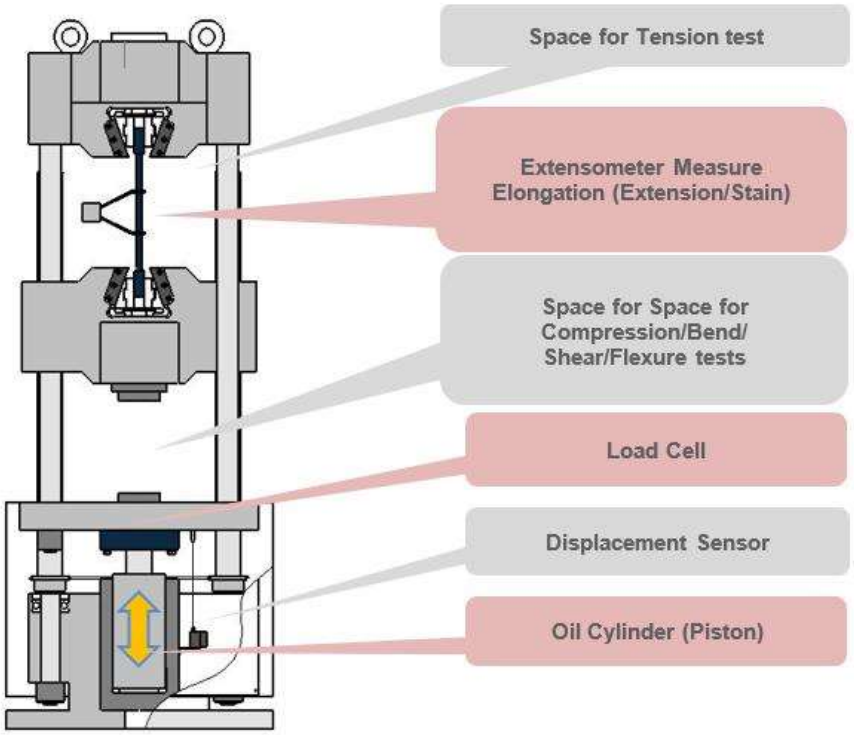

Figure II.1 Compression testing machine.

Static Loading and Mechanical Response:

- Creep Phenomenon: MF demonstrate creep under prolonged static stresses. Creep refers to the gradual deformation that occurs over time when a steady load is applied. The creep rate and magnitude in metal foams are contingent upon variables such as the foam's density, cell structure, and the qualities of the underlying material [26].
- Yield Strength and Elastic Modulus: The yield strength, when subjected to static loading, refers to the stress level at which the MF initiates plastic deformation. The elastic modulus quantifies the foam's rigidity in such circumstances. Both features are essential for accurately forecasting the performance of metal foams in load-bearing applications [27].
- Compression Behavior: MF are frequently analyzed for their compression behavior under static loading circumstances. This encompasses the stress-strain relationship observed during compression, which provides valuable insights into key factors such as the point at which elastic deformation ceases, the maximum stress reached during the plateau phase, and the extent of strain resulting in densification. This characteristic is crucial in applications involving MF for energy absorption or as materials for cushioning [28].

II.2.1. Illustrations of the static loading test

a) Example 1 [29]

The compression test was performed according to DIN 53 291 [30] using a servo-hydraulic testing machine SHM250/4 model. The quadratic specimens are produced with a side length of 40 mm. The specimen is positioned inside the confines of two parallel plates Figure II.2.

Figure II.2 Before and After Compression Testing: Aluminum Foam Sandwich Specimen with t_s= 34mm Thick Sandwich Core.

The compressive stress-strain curves initially display elasticity at low stress levels, followed by plastic and non-uniform deformation. These curves consistently demonstrate remarkable reproducibility in fully expanded foam. Furthermore, increasing foam density results in greater stiffness.

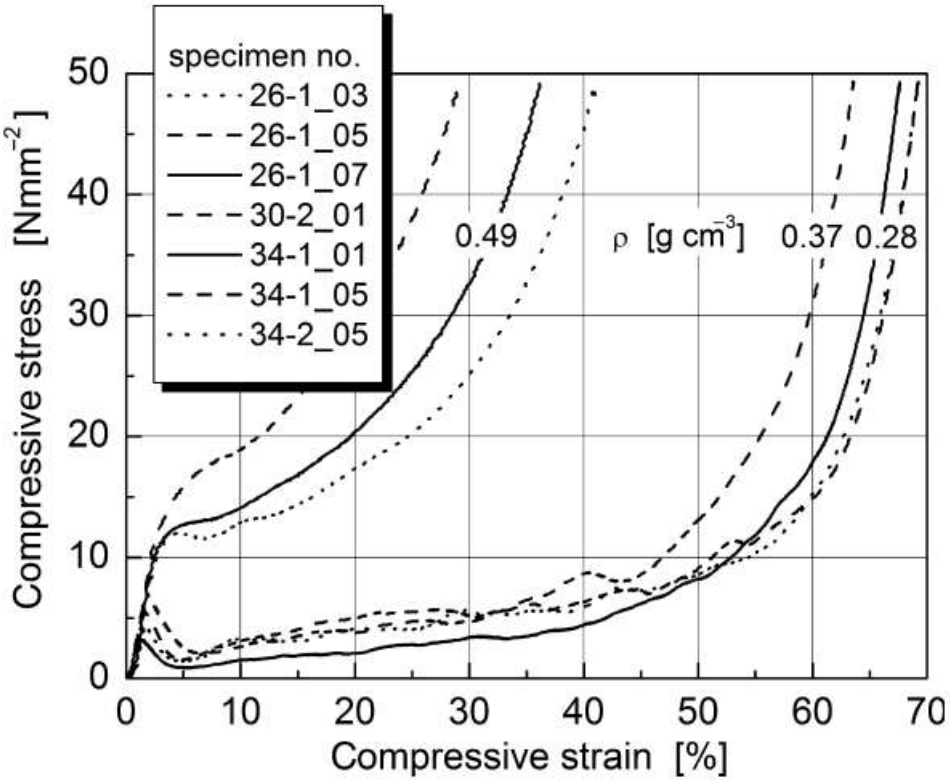

Figure II.3 Stress–strain curves of aluminum foam sandwich specimens under compression test with different densities and thicknesses.

The MF exhibits a blend of elastic and plastic characteristics when subjected to static stress, rendering it appropriate for applications that necessitate energy absorption and crush behavior.

II.3. Mechanical response under quasi-static compression

During a quasi-static compression test, the MF specimen undergoes compression at a deliberately slow and controlled pace. This enables the meticulous observation of the deformation process. Quasi-static tests exhibit a slower rate of compression compared to dynamic testing, hence maintaining a stress state in the material that is in close proximity to equilibrium throughout the test. The quasi-static test is usually conduct using the universal mechanical testing machine as shown in Figure II.4.

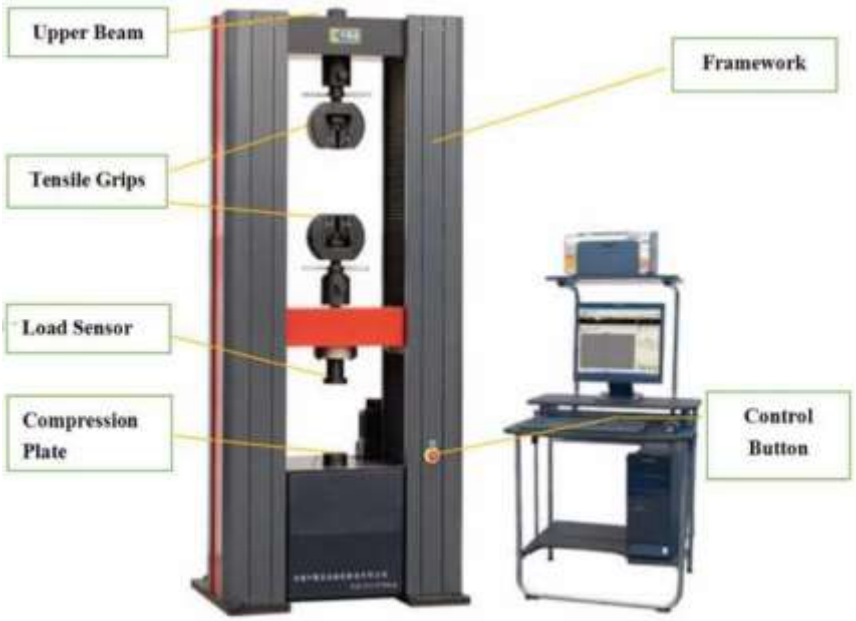

Figure II.4 WDW-200E Universal Testing Machine.

MF demonstrate distinctive characteristics and behavior when subjected to quasi-static loading, rendering them appropriate for a range of applications including energy absorption, impact mitigation, and structural components in aerospace vehicles [31,32]. Key facets of their behavior encompass:

- Elastoplastic behavior of Closed-cell aluminum foams show elastic-plastic behavior under transverse uniaxial compressive loads [33]. This means the material exhibits elastic and plastic deformation, which can benefit energy absorption and damping [31].
- In the Quasi-static compression, the material strength increases as the strain rate increases.
- Yield behavior of a material foam under compression combined loadings has been investigated [34]. The material foam exhibits different yield modes under combined loadings, which are dependent on the loading angle [34]. Metallic foams are being extensively utilized for energy absorption, particularly in lightweight buildings, to withstand blast and impact loads [35]. Due to their ability to absorb substantial amounts of energy, they are highly successful in applications involving impact protection.

The standardized methodologies employed to carry out these examinations are crucial to guarantee uniformity, reproducibility, and comparability of findings across various investigations and applications. The predominant norms or standards utilized in material testing, including metallic foams, are as follows:

- ASTM Standards, established by the American Society for Testing and Materials, provide a diverse array of guidelines for conducting material testing.

Standards such as ASTM E9, which pertains to the compression testing of metallic materials, could be applicable to metallic foams. The standards provide specific instructions for performing the tests, specifying the appropriate equipment, the compression rate, and the method for recording the results [36].

- ISO (International Organization for Standardization) Standards: such as ISO 13314, are designed expressly for testing MF and comparable materials. specifically, ductility and compression for porous and cellular metals [37].

II.3.1. Illustrations of the quasi-static loading test

a) Example 1 [38]

Compressive tests at a loading velocity of 4 mm/min performed using the WDW-200E universal testing machine are presented in Figure II.5, for aluminum foam samples with different porosity percentages Table II.1.

Table II.1 Porosities percentage of aluminum foam specimens used for compression

Foam number	1	2	3	4	5	6	7	8	9	10
Porosity (%)	75.9	77.8	81.0	882.1	84.3	85.3	88.8	91.7	91.9	95.0

The deformation mode under the quasi-static compression test is presented in Figure II.5.

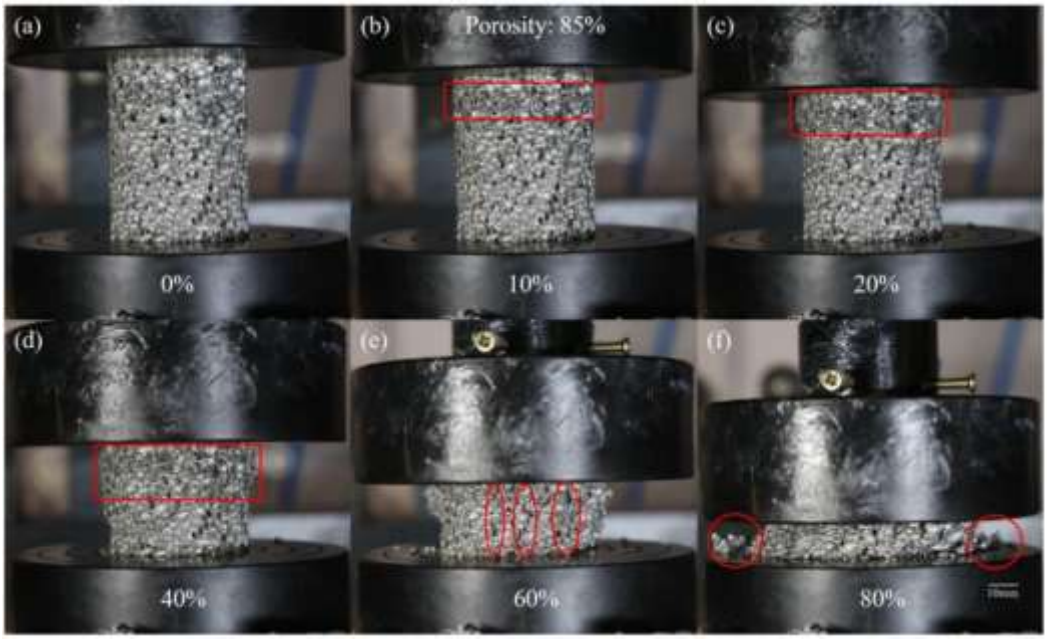

Figure II.5 Deformation mode of aluminum foam under compression.

The Stress-strain curves of the tested aluminum foams are illustrated in Figure II.6.

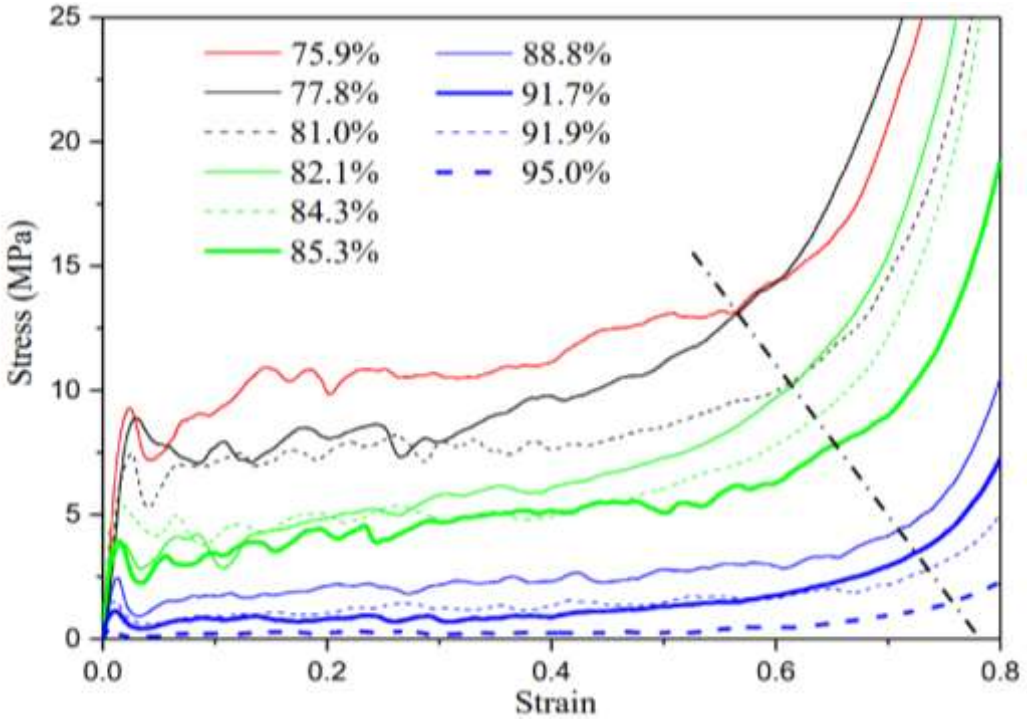

Figure II.6 Stress-strain curves of aluminum foams.

The results demonstrate a direct correlation between decreased cell size (approximately 1 mm) and heightened plateau stresses. These foams exhibit brittle deformation behavior during quasi-static compression, commonly resulting in failure through either post-buckling fracture or direct cell wall fracture. This study underscores the paramount importance of reducing and homogenizing cell sizes to significantly enhance the mechanical efficacy of aluminum foams.

b) Example 2 [39]

Using the universal testing machine, the compression test was performed with a load velocity of 2 mm/min.

Table II.2 The density of different samples used in the experiment.

No	Compression test	Density
1	Quasi-static experiment	0.23-0.25 g/cm^3
2		0.41-0.45 g/cm^3
3		0.62-0.68 g/cm^3
4		0.73-0.79 g/cm^3

Figure II.7 shows the deformation mode of the tested aluminum foam sample under quasi static compression at different times.

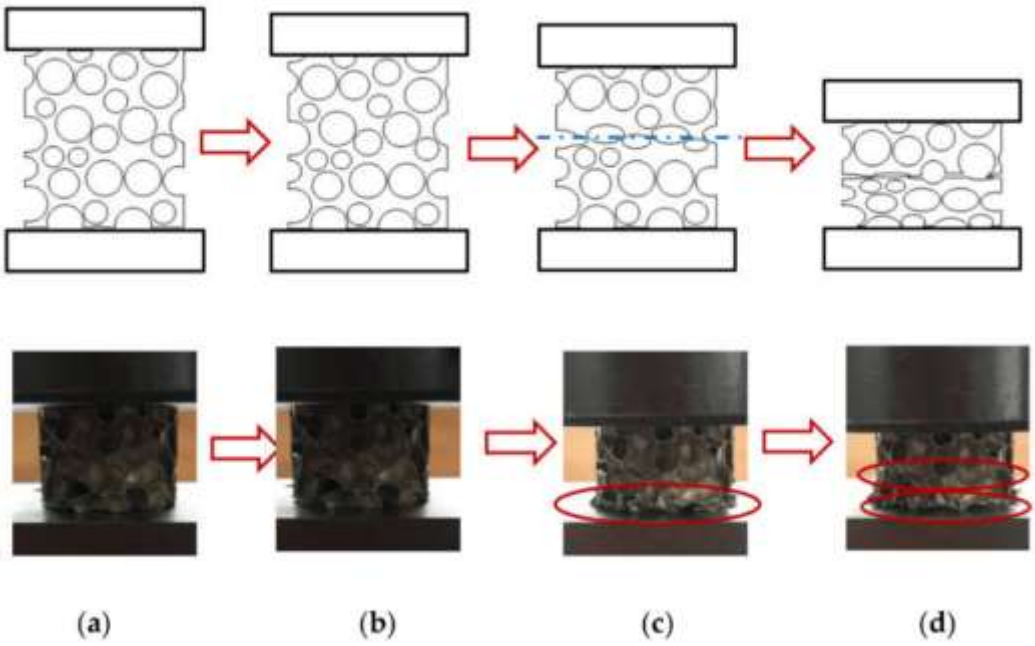

Figure II.7 deformation mode of aluminum foam at different times under quasi static compression.

Table II.3 Result parameters of aluminum foam under quasi-static test.

Structural parameters Ω	Density (g/cm³)	Plastic yield strain	Elastic modulus (MPa)	Yield stress (MPa)	Initial strain of yield plateau stage	Yield plateau stress (MPa)	Densification strain
0.138	0.237	0.0351	78.57	2.043	0.0914	2.07	0.738
0.1519	0.423	0.0654	252.78	7.41	0.1695	7.89	0.687
0.1735	0.725	0.0685	491.47	19.779	0.1727	14.5	0.673
0.2011	0.662	0.0787	401.11	16.356	0.1764	14.23	0.637

The observation revealed that:

- Bigger cell sizes typically led to reduced strength and stiffness, since they were more prone to buckling when subjected to compressive pressures.

- Smaller cells, on the other hand, displayed increased strength and stiffness due to their superior ability to resist buckling.

- Thicker cell walls greatly enhance the elastic modulus of the foam. This is because the increased thickness of the walls offers more material to withstand deformation. The increased thickness of the walls also enhanced the ability of the material to deform without breaking, resulting in greater energy absorption capacity.

- The study also found that diverse failure modes occurred due to changes in the structural configurations of the foam. Specifically, foams with thinner cell walls tended to fail through buckling, whereas foams with thicker walls were more prone to tearing or plastic collapse.

During quasi-static compression, the aluminum foam exhibited a consistent collapse pattern, where each layer collapsed uniformly.

c) Example 3 [40]

The compression test with a speed of 0.5mm/min was conducted on open-cell aluminum foams produced using the pressurized infiltration process as shown in Figure II.8. The compression test is performed using the SANTAM STM-250 universal testing machine by ISO 13314 standards.

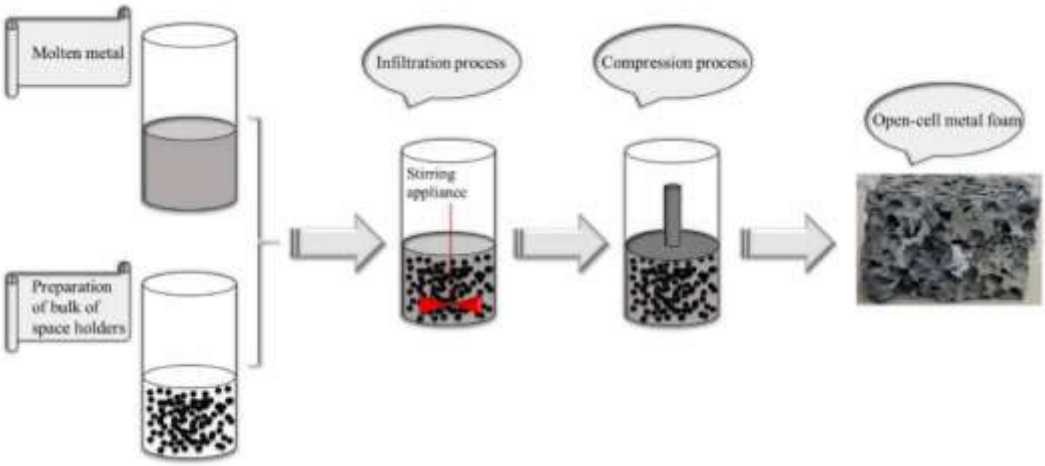

Figure II.8 The process of producing open-cell metal foam.

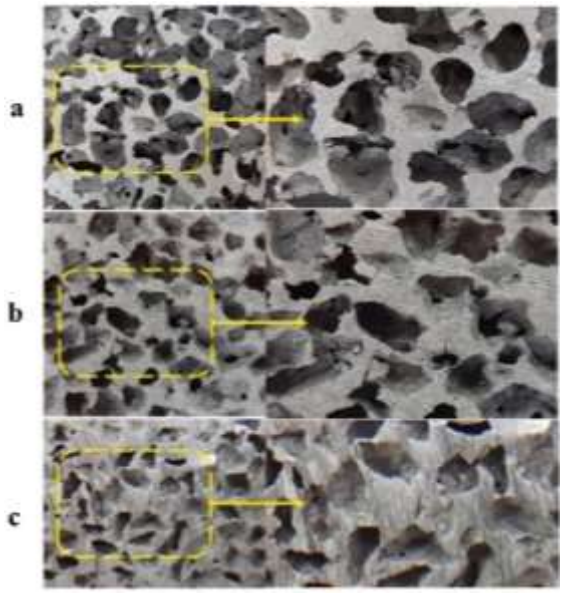

Figure II.9 Aluminum foams specimen with different pore size. a= 5 mm, b= 4 mm pore, c= 3 mm pore.

Figure II.10 shows the stress-strain curves of the tested aluminum foam samples under compression test.

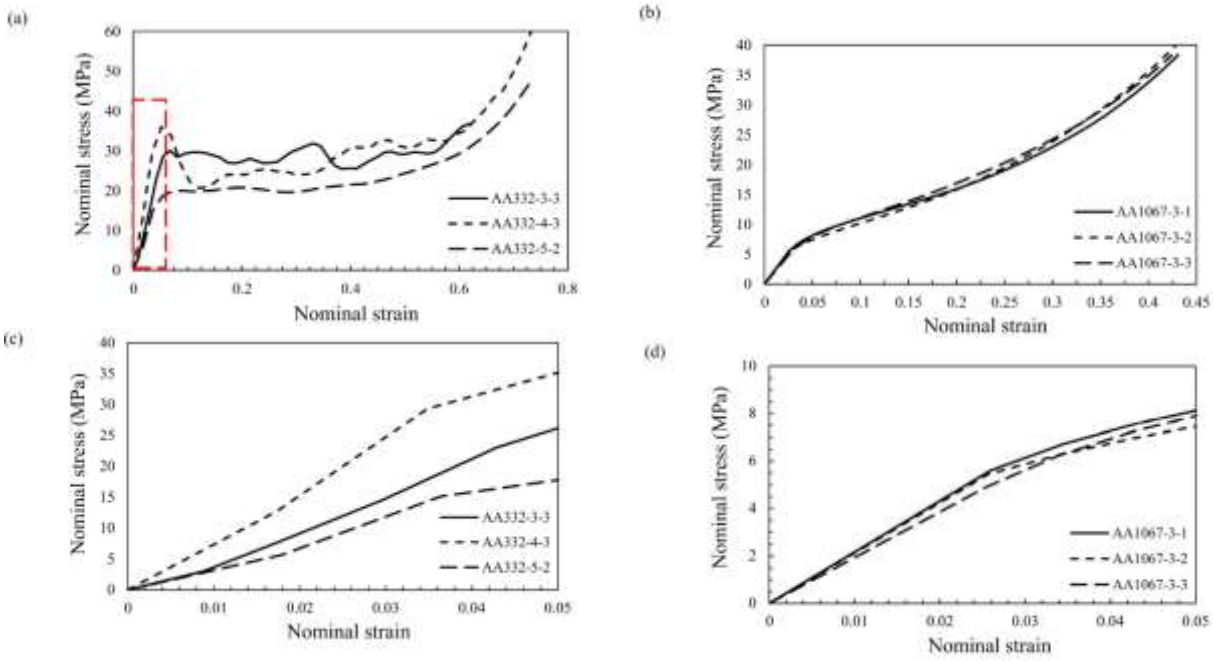

Figure II.10 Stress-strain response of aluminum foams under compression test: a) and b) represent different base material c) and d) highlight of the linear elastic region of the two different base material.

Figure II.11 Deformation mode of aluminum foam specimen under quasi-static compression test.

The obtained mechanical performance under the quasi-static test is reported in Table II.4.

Table II.4 Compression results of open-cell aluminum foams.

Test code	λ (mm)		ρ %	σ_{pl} (MPa)	σ_{peak} (MPa)	$\Delta\sigma$ (MPa)	σ_{ple} (MPa)	ε_{ple}	W^* MJ/m^3	SEA * J/g	η_m (%)
AA332-3-1	3		46.2	27.64	32.77	1.59	35.93	0.631	17.05	13.66	75.20
AA332-3-2			45.9	27.37	30.85	0.57	35.58	0.705	17.03	13.73	67.89
AA332-3-3			46.5	27.77	30.04	0.75	36.11	0.592	16.22	12.92	75.88
		Ave.	46.2	27.59	31.22	0.97	35.87	0.643	16.77	13.43	73.0
		Std. Dev.	0.24	0.17	1.15	0.44	-	-	0.39	-	-
AA332-4-1	4		42.3	22.76	38.76	12.79	29.58	0.613	14.62	12.80	80.6
AA332-4-2			42.7	19.26	34.05	11.73	25.03	0.65	12.99	11.27	79.8
AA332-4-3			41.6	24.73	35.98	15.39	32.15	0.515	13.74	12.23	83.0
		Ave.	42.2	22.25	36.27	13.30	28.92	0.593	13.78	12.10	81.2
		Std. Dev.	0.45	2.26	1.93	1.54	-	-	0.67	-	-
AA332-5-1	5		37.6	22.49	21.97	2.16	29.24	0.553	12.19	12.01	75.4
AA332-5-2			38.5	19.99	20.78	1.20	25.99	0.521	10.47	10.07	77.3
AA332-5-3			38.3	20.27	19.65	2.43	26.36	0.499	9.94	9.61	75.6
		Ave.	38.1	20.92	20.8	1.93	27.20	0.524	10.87	10.56	76.1
		Std. Dev.	0.39	1.12	0.95	0.53	-	-	0.96	-	-
AA1067-3-1	3		42.0	19.16	-	-	24.91	0.313	4.43	3.91	56.8
AA1067-3-2			43.5	19.8	-	-	25.74	0.31	4.33	3.69	54.3
AA1067-3-3			46.0	20.38	-	-	26.49	0.316	4.69	3.78	56.0
		Ave.	43.8	19.78	-	-	25.71	0.313	4.48	3.79	55.7
		Std Dev.	1.65	0.50	-	-	-	-	0.15	-	-

This study used commercial NaCl particles with a purity of over 99% and varying particle sizes (3 mm, 4 mm, and 5 mm) as the space holder.

The findings showed that, except for energy absorption efficiency, all the characteristics decreased as NaCl particle size increased, which confirmed the influence of space holder particle size on the mechanical response of the foam.

II.4. Mechanical response under dynamic compression

The dynamic compression test for MF is an important evaluation method in materials science and engineering, particularly for assessing the mechanical properties of MF under high strain-rate conditions. This test is crucial for applications where MF are subjected to rapid deformations, such as in automotive, aerospace, and protective structures.

The primary equipment used for dynamic compression tests on metallic foams is typically a high-speed testing machine, such as a Split Hopkinson Pressure Bar (SHPB) Figure II.12 or drop weight testing Figure II.13.

The Split Hopkinson Pressure Bar equipment consists two long bars (incident and transmission bars) with a specimen placed between them. A striker bar hits the incident bar, sending a stress wave through the specimen into the transmission bar. The strain and stress in the specimen are calculated from the measured strain in these bars.

In the drop weight test, a weight is dropped from a known height onto a specimen, generating a dynamic impact.

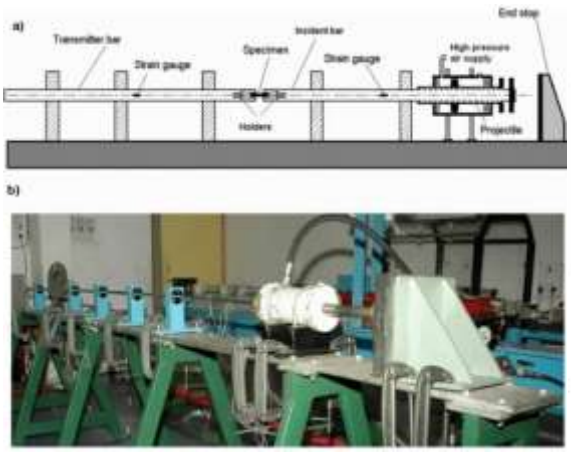

Figure II.12 Setup of Split Hopkinson Pressure Bar (SHPB) apparatus.

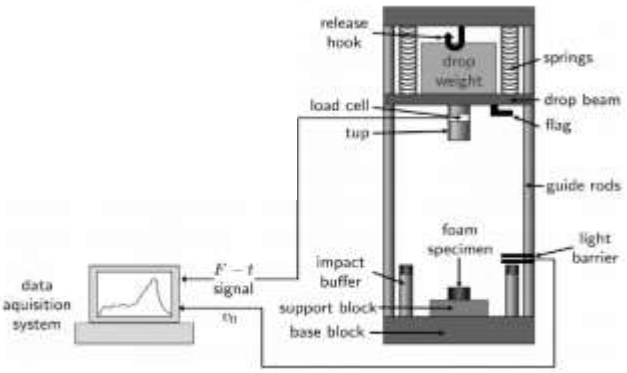

Figure II.13 Setup of drop weight testing.

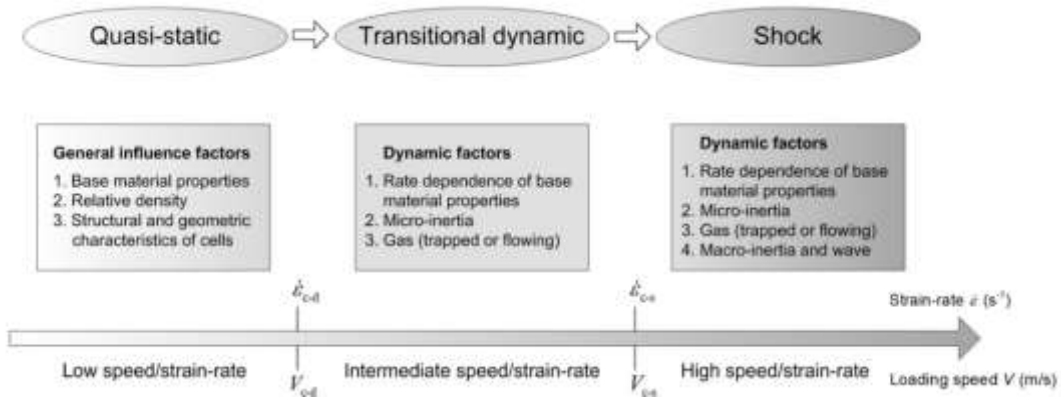

Figure II.14 Compression regimes at different loading rates (strain-rates or loading speeds).

There is no established protocol for conducting dynamic compression experiments on MF. Nevertheless, several correlated standards and methodologies have been employed to investigate the mechanical properties of materials when subjected to compression. The criteria encompassed are as follows:

- ISO 844 and ASTM D1621 are standards utilized to conduct compression tests on rigid cellular polymers. These standards offer guidance on how to determine the compression properties of such materials [41].

- ISO 13314:2011 is a standard that is employed to conduct mechanical tests on metals, with a specific focus on evaluating their ductility [37].

Although these standards are primarily intended for inflexible cellular polymers and permeable metals, they can be modified to examine the mechanical properties of MF during dynamic compression. Scientists have employed these criteria as a foundation for their investigations, adapting the examination methods and variables to accommodate the particular requirements of their research.

II.4.1. Illustrations of the dynamic Loading Test

a) Example 1 [42]

The study involved dynamic tests by the Instron-Dynatup impact testing system. The foam samples included in the experiments exhibited densities ranging from 350 to 550 kg/m³. The dynamic tests were conducted with a crosshead speed of 3.72 m/s. The experiments were conducted by the guidelines outlined in reference [43].

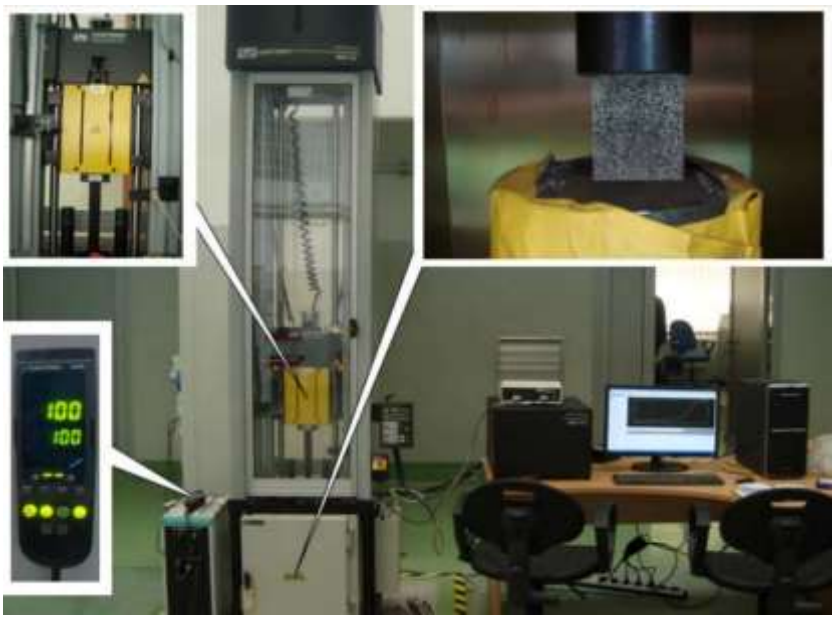

Figure II.15 Dynamic Instron – Dynatup testing machine.

Figure II.16 shows the stress-strain curves of the tested aluminum specimens foam under dynamic compression test.

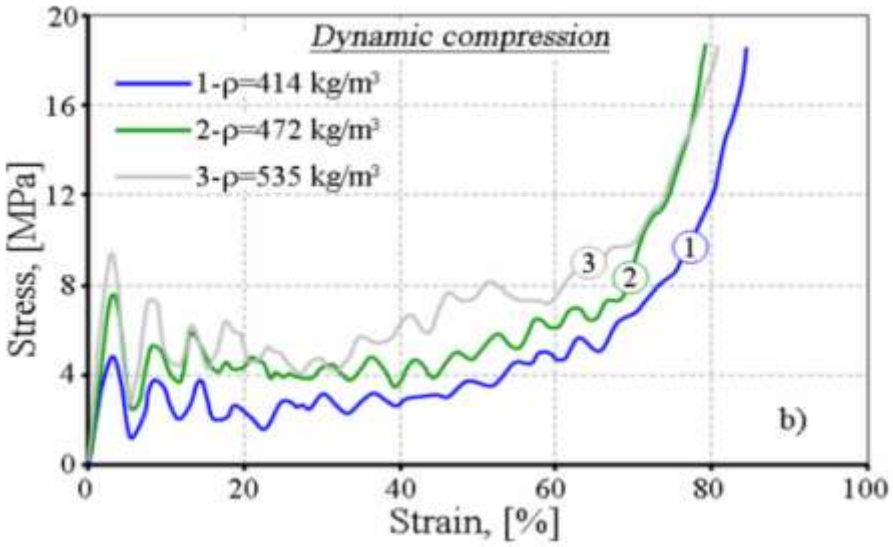

Figure II.16 Stress-strain curves of the aluminum specimen foam under dynamic compression test.

The stress-strain curves derived from dynamic compression testing show that the increase of the foam density leads to an increase their mechanical properties. The curves exhibit pronounced oscillations, signifying the gradual brittle fracture of cells occurring in almost parallel planes. The initial stress reduction seen following the attainment of the compressive yield stress during dynamic tests was around 74% of the yield stress, which is greater than quasi-static test results. The variation can be ascribed to micro-insertial phenomena occurring within the foam. The reduction in yield stress observed during dynamic compression can be attributed to the characteristics of the foam material.

Table II.5 The 1st stress drops result for the dynamic loading.

Spec. No.	Density	D_p	σ_y	Ps	ε_d	ε_y	1st minima	Strain@1st minima	Δ_{strain}	Δ_{stress}	l_p	l_p/D_p	Δ_S/σ_y
	[Kg/m³]	[mm]	[MPa]	[MPa]	[%]	[%]	[MPa]	[%]	[MPa]	[%]	[mm]	[%]	[%]
1	404	3.87	6.49	6.49	61.62	3.274	1.95	5.791	4.54	2.52	1.289	33.30	69.95
2	414	3.96	5.06	5.06	53.38	3.308	1.27	5.774	3.79	2.47	1.260	31.79	74.90
3	421	3.03	4.37	4.37	53.28	2.313	1.21	5.715	3.16	3.40	1.742	57.56	72.31
4	468	4.66	6.92	6.92	60.21	3.058	1.49	5.340	5.43	2.28	1.168	25.05	78.47
5	472	2.92	7.6	7.33	53.61	3.260	2.40	5.586	5.20	2.33	1.191	40.72	68.42
6	535	6.02	9.45	10.00	56.78	2.64	2.64	5.370	6.81	2.36	1.206	20.05	72.06
7	550	3.9	10.0	9.445	64.63	2.22	2.22	6.531	7.78	3.28	1.641	35.75	77.80
							average		5.24	2.66	1.366	35.75	73.42
							Standard deviation		1.63	0.47	0.233	12.11	3.81

The obtained results was compared to quasi-static tests conducted at a crosshead speed of 1.67.10-4 m/s and a linear link between quasi-static and dynamic compressive strength at 20% and 50% strain is suggested based on the experimental data.

b) Example 2 [44]

The work showed compression tests on the composite MF (CMFs) using the (SHPB). The high strain rate (HSR) varied from 520 s^{-1} to 1560 s^{-1}.

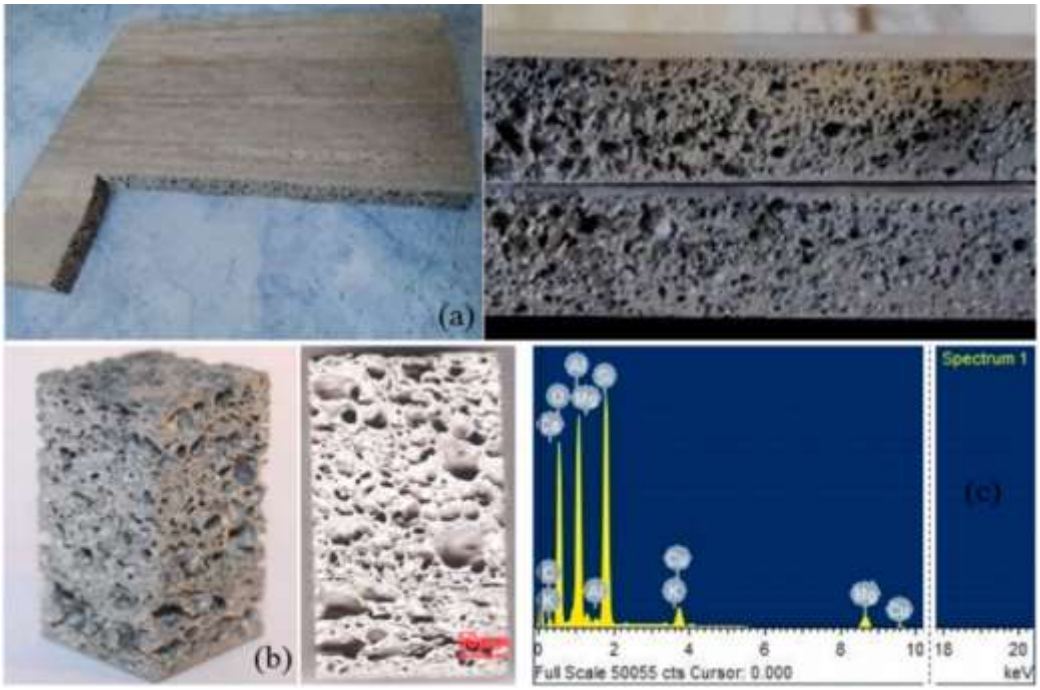

Figure II.17: a) CMF blocks, b) the pore shape and c) EDAX analyses of the sample.

Table II.6 Physical parameters of SiC metallic foam reinforced specimen.

Sample number	Mass (g)	Height (mm)	Diameter (mm)	Cross-section area (mm^2)	Volume (mm^3)	Density (g/cm^3)
1	11.823	35.02	20.03	401.20	14050.05	0.84
2	11.625	35.06	20.04	401.60	14080.15	0.83
3	11.081	35.04	20.01	400.40	14030.01	0.79
4	10.926	35.05	20.07	402.80	14118.31	0.78

Figure II.18 displays stress-strain curves of the CMFs at various relative densities (0.289, 0.293, 0.307, and 0.31) under high strain rates.

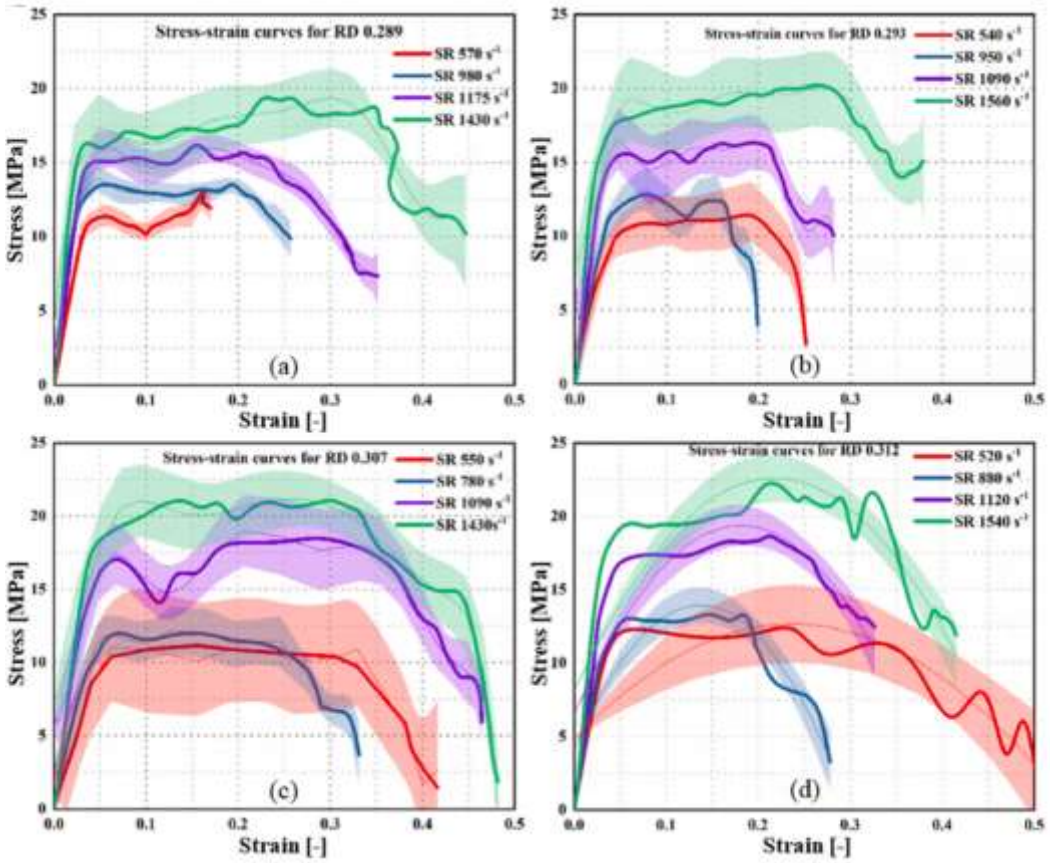

Figure II.18 stress-strain curves of CMFs with different relative densities: a) 0.289, b) 0.293, c) 0.307 and d) 0.31 under high strain rates (HSR).

Table II.7 displays the mean values of yield stress, plateau stress, and energy absorption parameters obtained from CMF samples, categorized by relative density and strain rate.

Table II.7 mechanical properties of CMFs obtained from HSR dynamic test.

Relative density (-)	Strain rate (s^{-1})	Yield Stress (MPa)	Plateau stress (MPa)	Energy absorption (MJ m^{-3})
0.289	570	10.82 ± 0.10	10.20 ± 0.20	2.04 ± 0.04
	980	13.94 ± 0.05	12.30 ± 0.33	3.69 ± 0.09
	1175	15.73 ± 0.09	14.80 ± 0.23	5.18 ± 0.08
	1430	17.26 ±0.11	15.50 ± 0.12	6.97 ± 0.06
0.293	540	11.12 ± 0.17	10.12 ± 0.43	2.53 ± 0.10
	950	13.18 ± 0.06	12.10 ± 0.22	2.54 ± 0.07
	1090	16.57 ± 0.03	15.10 ± 0.32	4.53 ± 0.09
	1560	19.29 ± 0.19	17.50 ± 0.13	6.65 ± 0.05
0.307	550	11.06 ± 0.29	10.30 ± 0.31	4.12 ± 0.12

Figure II.19 illustrates how the strain rate affects each density's strength and energy absorption characteristics.

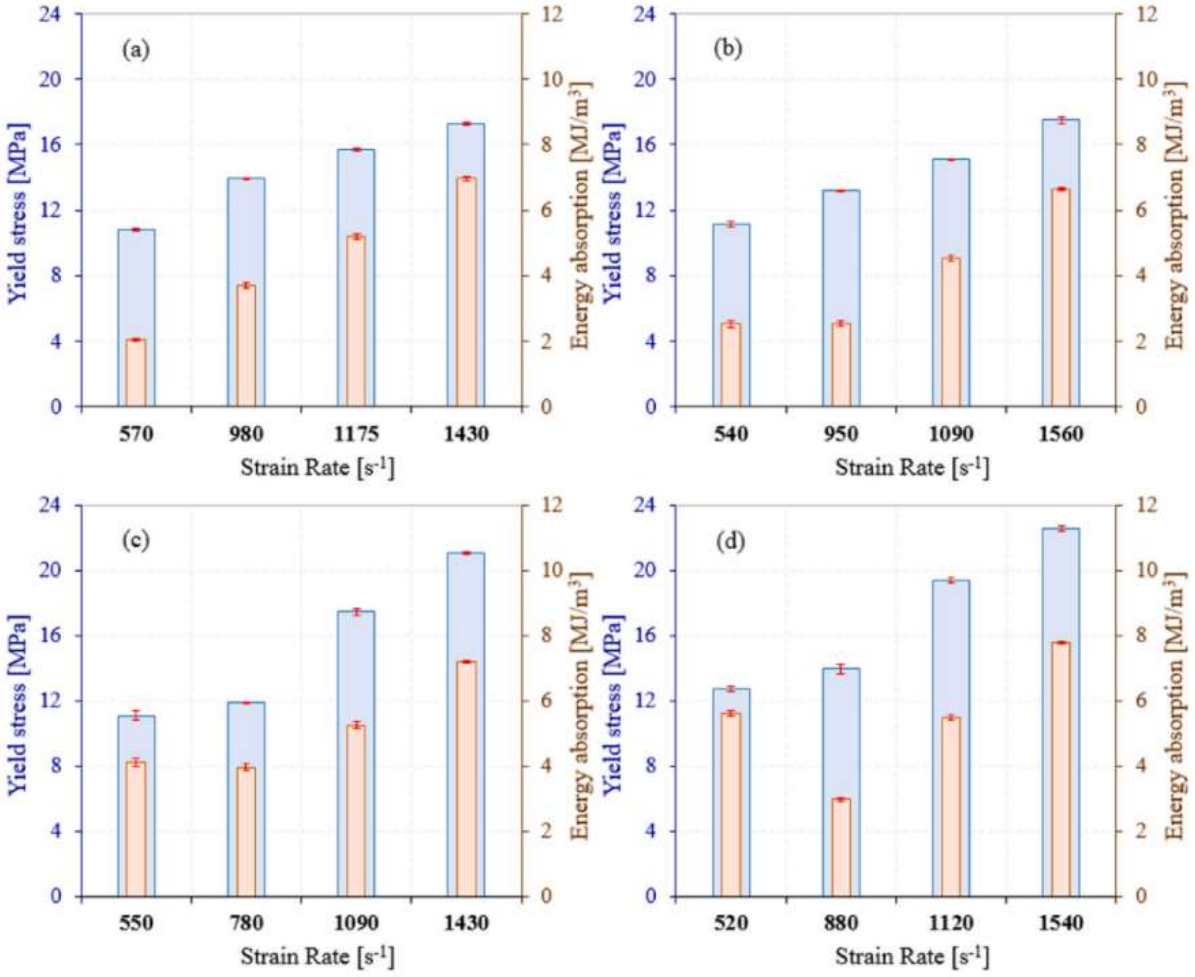

Figure II.19 strain rate influence on mechanical properties of CMFs with different relative densities: 0.28 (a), 0.29(b), 0.30(c) and 0.31(d).

The results show that:

- The strain rate and relative density, have an important influence on the mechanical response of the CMFs.
- Under dynamic loading conditions, the CMFs exhibited typical behavior of cellular materials.
- This behavior indicates the occurrence of main collapse mechanisms in the foam.
- It was found that the strain rate was the most contributing factor to the energy absorption capabilities of these foams.

The SHPB technique is used in many works for investigating the mechanical response of different materials at HRS [45, 46].

c) Example 3 [46]

The research on the High Strain-Rate effect using a traditional split-Hopkinson pressure bar equipment (Figure II.20) and compared the findings with quasi- static compression tests.

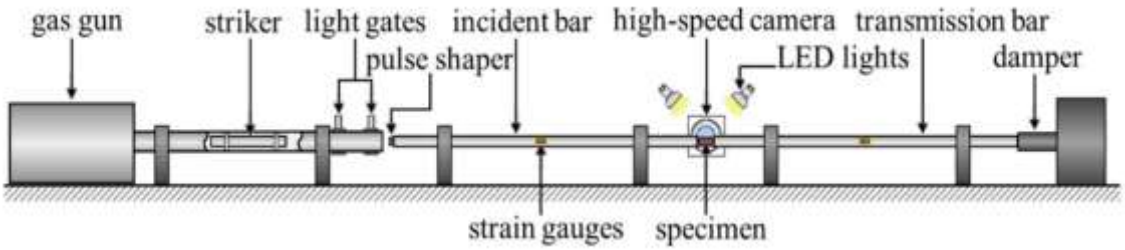

Figure II.20 representation of the experimental SHPB.

Table II.8 Description of the specimens used in the experiment.

Height	Quantity	Density [g cm^{-3}]
10	16	0.796 ± 0.116
20	14	0.926 ± 0.039

The experiment used two specimens with a diameter of 20 mm and a length of 10 mm and 20 mm, respectively. [47]. under impact velocities from 20 up to 45 ms^{-1}.

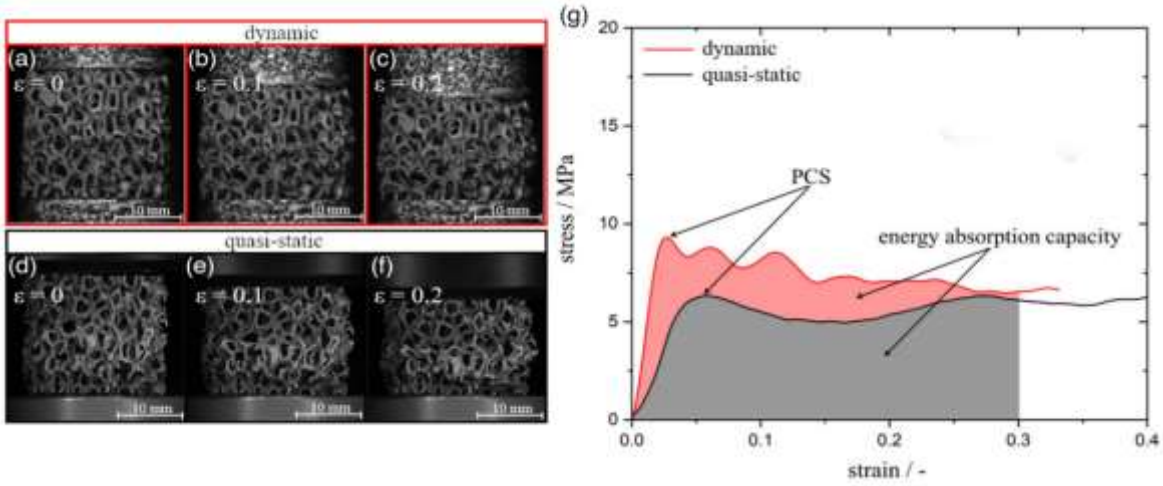

Figure II.21 Ni/PU hybrid MF under a–c) dynamic and d–f) quasi-static compression test, g) a representative stress–strain relation.

Table 2 displays the specific energy absorption capacity per density and specific compressive strength per density up to a strain of 0.3 for Ni/PU hybrid MF studied under quasi-static and dynamic impact speeds using the SHPB approach.

Table II.9 Density-Normalized Performance Compression Strength (PCS) and Energy Absorption of Ni/PU Hybrid MF up to ε = 0.3 under Quasi-Static and Enhanced Dynamic Conditions.

Length [mm]	mode	Norm. PCS [MPa cm^3 g^{-1}]	PCS deviation [%]	Energy abs. cap. [MPa cm^3 g^{-1}]	Energy deviation [%]
10	qs	13.8 ± 4.9		3.4 ± 1.1	
	dyn	17.4 ± 2.4	26.1	3.8 ± 0.6	12.2
20	qs	11.5 ± 2.3		2.9 ± 0.1	
	dyn	18.1 ± 1.7	57.4	3.7 ± 0.3	26.8

The Ni/PU hybrid MF exhibit significant sensitivity to strain rates. This means that the mechanical response of the used hybrid foams exhibits sensitivity to strain rates, this means that the mechanical response, specifically the plastic collapse stress (PCS) and energy absorption capacity changes considerably when subjected to different rates of dynamic loading.

The study found that the PCS of the used hybrid MF shows a distinct increase under dynamic conditions compared to quasi-static conditions. This indicates that the foam becomes more resistant to collapse under faster loading rates.

The strain rate effect on the compressive stress/strain behavior of open-cell Ni/PU hybrid composite MF is examined in the work of [47], using an Instron Dynatup 9250HV drop-weight tower Figure II.22.

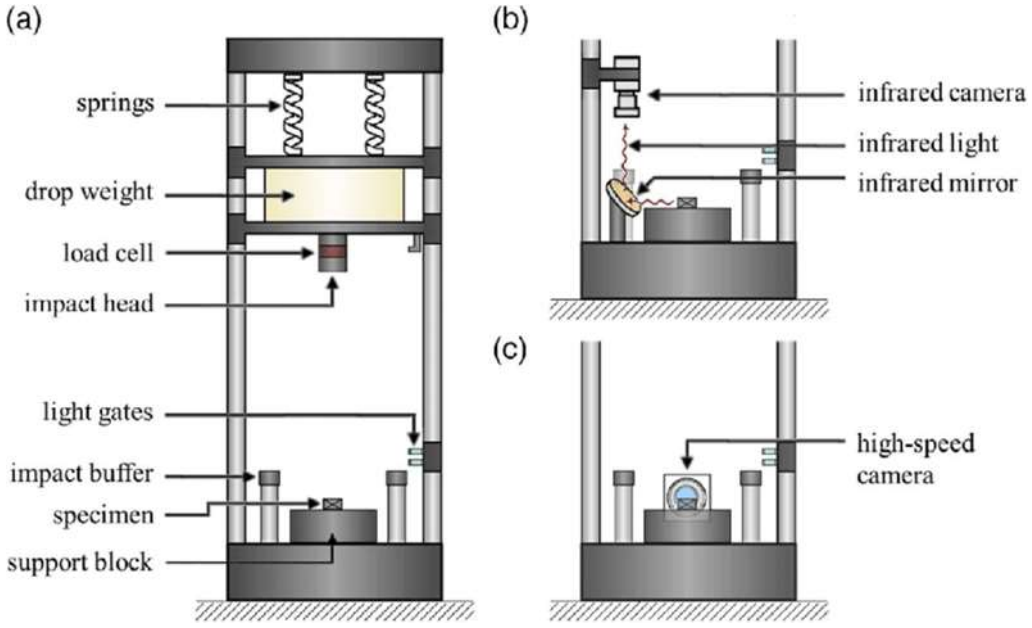

Figure II.22 Schematic illustration of the experimental configuration. a) Complete drop-weight tower, b) arrangement for the IR camera, and c) the high-speed camera.

The Digital Image Correlation (DIC) analysis of the tests showed a variation in the unique micromechanical deformation process between quasi-static and dynamic loading. Deformation bands are activated progressively under quasi-static pressures, but several bands are already activated after the PCS under dynamic loads, resulting in a greater PCS due to micro-inertia effects.

The ability of these foams to absorb energy under compression is a critical factor, especially for their application in energy absorption systems. The studies highlight that the energy absorption capacity of these MF is enhanced under dynamic loading conditions, which is beneficial for applications where high-impact resistance is required.

II.5. Three-point bending

The three-point bending test is a widely used method for characterizing the mechanical properties of materials, including the fatigue behavior of materials. The test involves applying a cyclic load to the specimen, which causes the material to undergo flexure and potential failure.

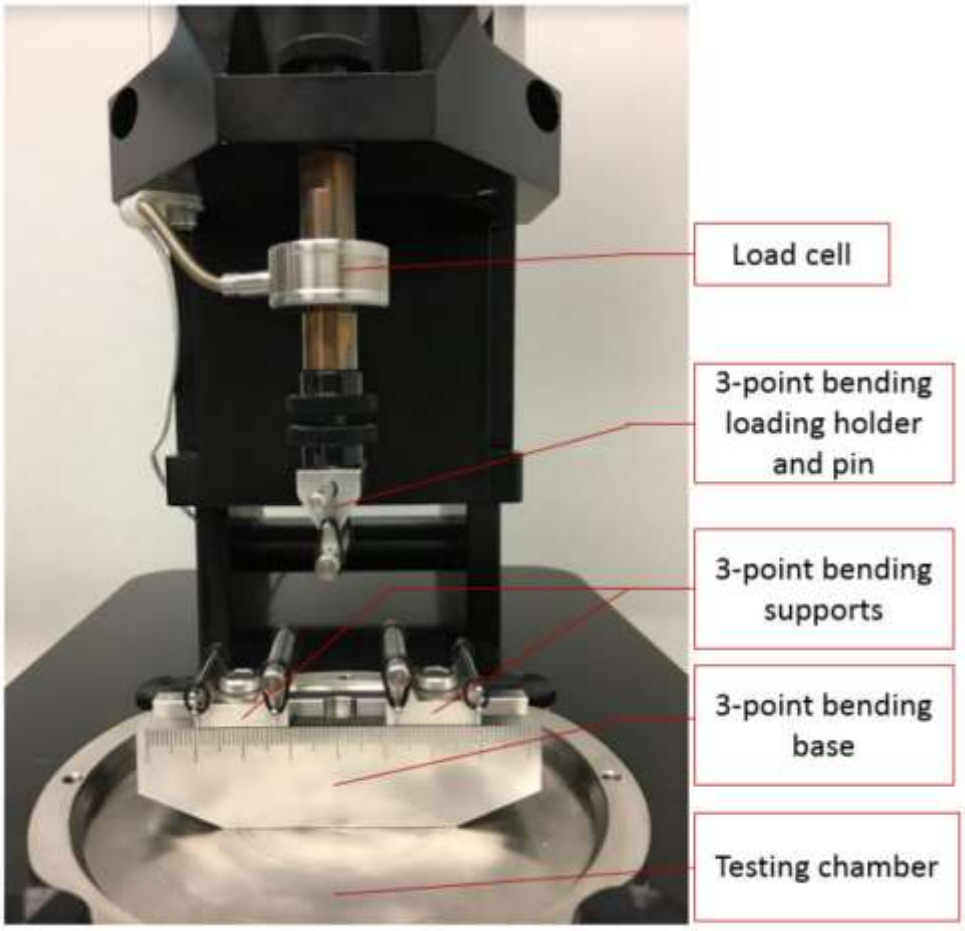

Figure II.23 Tester setup for bending test.

There isn't a specific standard for the three-point bending test of MF. However, some related standards and methods have been used to study the mechanical behavior of materials under bending. These standards include:

- ISO 7204, ASTM E290: This standard is used for bending tests on rigid cellular plastics, and it provides information on the determination of bending properties [48].
- EN 826: This standard is also related to bending tests on rigid cellular plastics, and it is similar to ISO 7204 and ASTM E290[48].
- ISO 13314:2011: This standard is used for mechanical testing of metals, specifically for ductility testing, and it includes a bending test for cellular metals [6].

II.5.1. Illustrations of the three-point bending test

a) Example 1 [49]

The user performed static three-point bending tests on a CMT 5105 materials testing equipment. With speed of 5 mm/min on aluminum foam cores produced by the melt foaming technique.

Figure II.24 displays the results of the Bending Test.

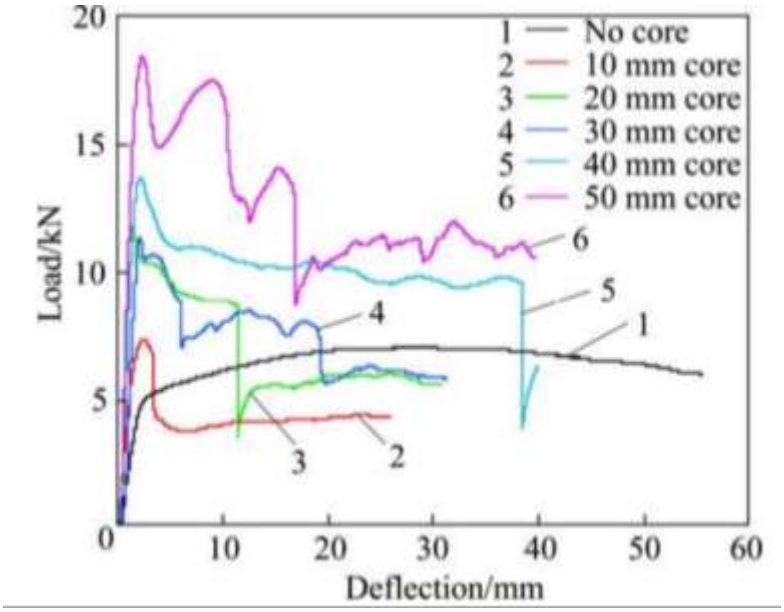

Figure II.24 Bending Test Results Showing Load versus Deflection for AFSS with Differing Core Thicknesses.

The comparative static three-point bending performance of AFSS with a 3 mm steel panel across various core thicknesses is displayed Table II.10.

Table II.10 Comparative Static Three-Point Bending Performance of AFSS with a 3 mm Steel Panel Across Various Core Thicknesses.

Core Thickness /mm	Maximum bending load/kN	Deflection at maximum bending load /mm
10	7.37	2.39
20	11.91	1.62
30	11.4	2.16
40	13.7	2.34
50	18.52	2.42

Figures II.25 and II.26 display the deformation mode during a bending test at various time intervals, as well as the relationship between Core Thickness and Maximum Bending Load Variation.

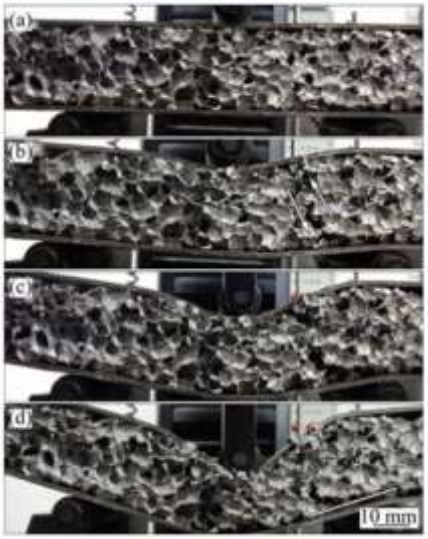

Figure II.25 deformation mode of AFSS under bending test with 3 mm steel panel and 40 mm foam core at different time.

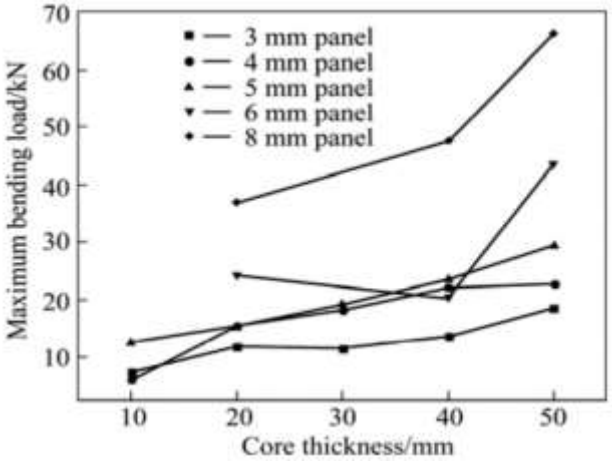

Figure II.26 Correlation between Core Thickness and Maximum Bending Load Variation.

The studies demonstrated that increasing the thickness of both foam core and steel panel leads to an increase in the maximum bending load capacity of an AFSS. Nevertheless, certain instances revealed mechanical discrepancies at the adhered interface. The results also showcased the significance of aluminum foam core in enhancing energy absorption, especially evident in sandwiches with thicker cores.

b) Example 2 [50]

The study performed a three-point bending test utilizing a universal testing machine on three types of foams made of aluminum with different densities (0.37 g/cm3, 0.57 g/cm3, and 0.75 g/cm3) (as shown in Table II.11). The loading rate was 2 mm/min (quasi- static).

Table II.11 Specimen parameters used in the experiment.

Specimens	c(mm)	Density of Foam (g/cm³)
10-0.37	10	0.37
20-0.37	20	0.37
30-0.37	30	0.37
20-0.57	20	0.57
20-0.75	20	0.75

Figure II.27 displays the load-displacement curves of tested aluminum foam sandwich during the three-point bending test, with variations in core densities and core thicknesses.

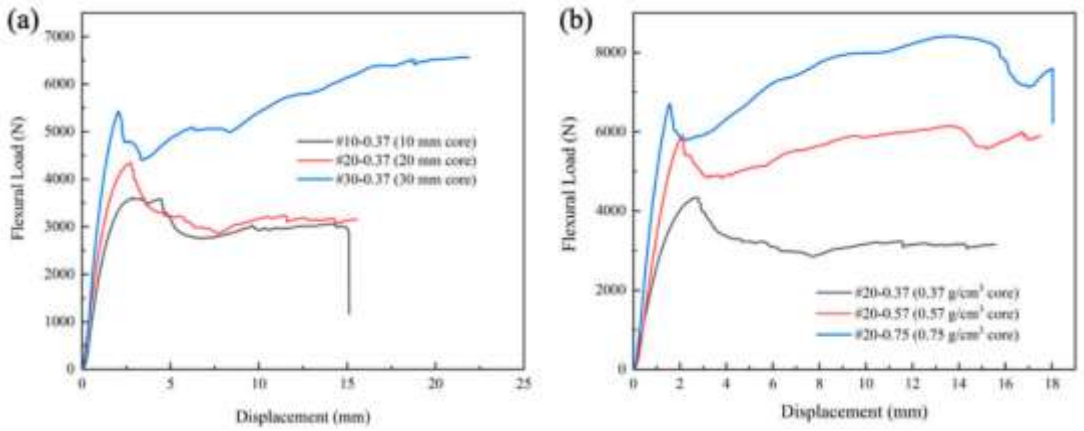

Figure II.27 load-displacement curves of aluminum foam sandwich under three-point bending test with a) different core densities, b) different core thicknesses.

The Three-point bending results of specimens are listed in Table II.12.

Table II.12 Three-point bending results of specimens.

Specimens	P_{cr} (N)	S_{cr} (mm)	B (N.m²)
10-0.37	3599	2.86	13.42
20-0.37	4340	2.72	17.02
30-0.37	5396	2.06	27.94
20-0.57	5880	2.11	29.73
20-0.75	6683	1.56	45.70

Figure II.28 and Figure II.39 display the deformation morphology of the foam sandwich panel with varying thicknesses and densities respectively.

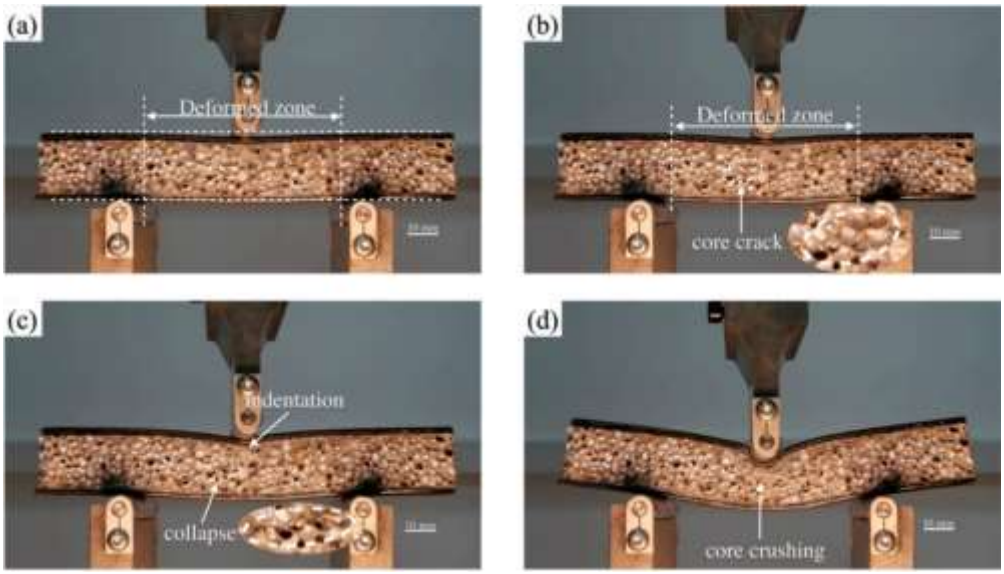

Figure II.28 Deformation morphology of the foam sandwich panel.

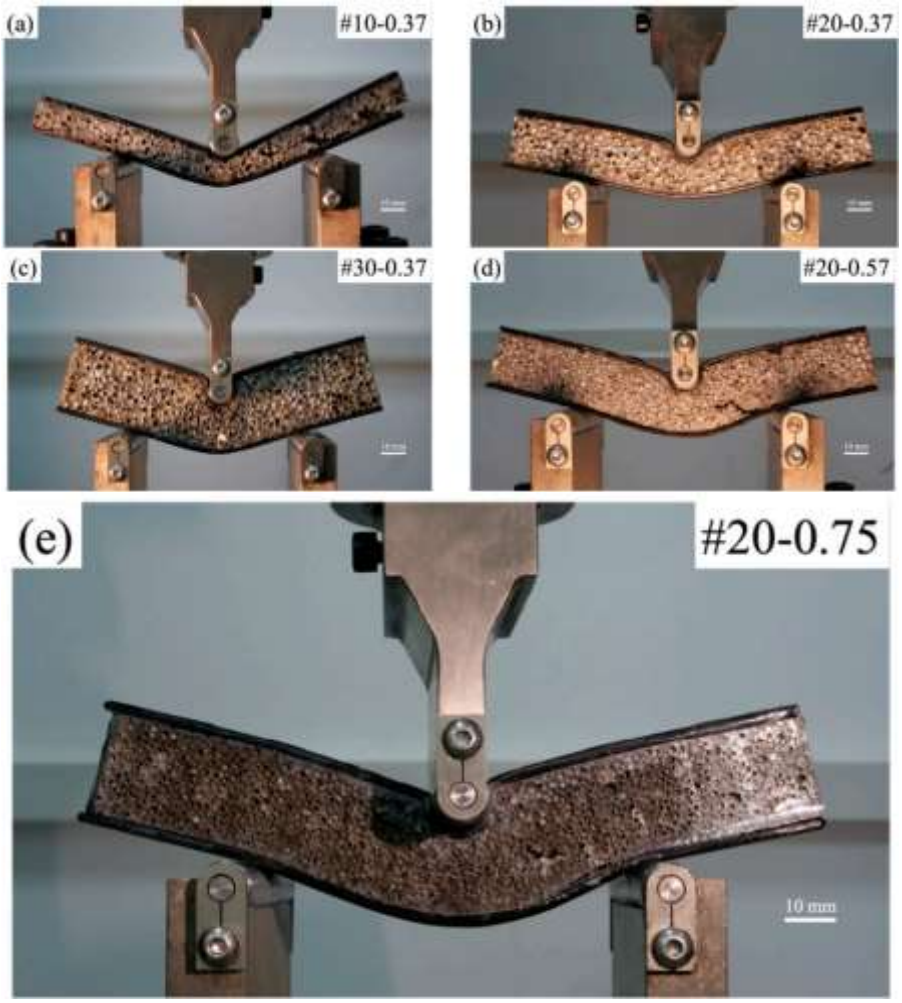

Figure II.29 Deformation morphology of the foam sandwich panel with different thicknesses and densities.

The study summarized that enhancing both the density and thickness of the aluminum foam core leads to a rise in the ability to withstand bending loads and rigidity against bending. These findings suggest that foam cores with larger density and thickness can endure greater bending loads without experiencing failure, therefore enhancing the structural strength of the panel.

The aluminum foam core has a crucial function in absorbing energy during the process of bending. This phenomenon is especially noticeable in sandwich structures that have thicker aluminum foam cores. In these designs, the core undergoes continual crushing when bent, which enhances its ability to absorb energy.

II.6. Under Tension

Tensile tests are essential for determining parameters such as Young's modulus, ultimate tensile strength, and yield strength. The stress-strain curve from a tensile test usually displays the yield strength, ultimate tensile strength, and initial stiffness. The results of MF under tensile test occurrence of plastic deformation at sufficiently high loads.

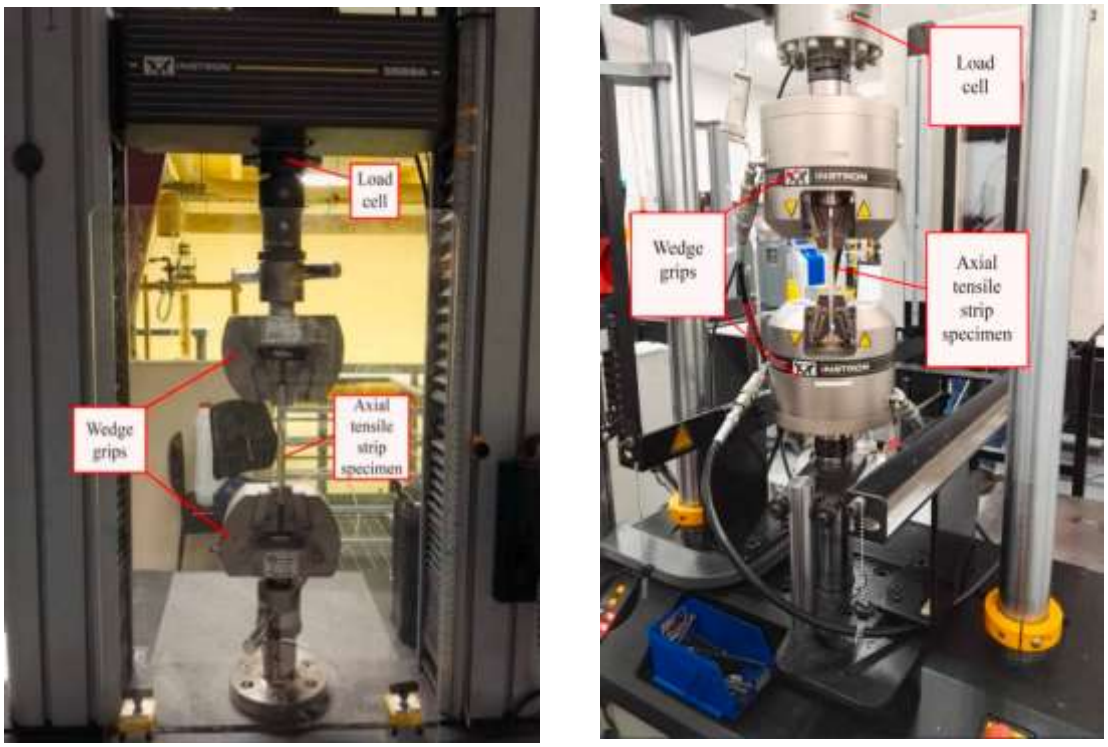

Figure II.30 the setup for tensile test.

The predominant standard for conducting tensile testing on metallic materials, including foams, are:

- ASTM-E8 (2010) [51]. This standard is employed to guarantee the precision and uniformity of tensile testing outcomes. A lesser proportion of studies have explored the characteristics of open or hollow sphere foams [51].
- The ASTM-E8 standard, along with several additional tests and procedures, has been employed to investigate the mechanical behavior of metal foams [52].

Essentially, the ASTM-E8 standard is widely used for conducting tensile tests on metallic materials, including foams. Nevertheless, literature is scarce regarding the tensile behavior of MF. Consequently, alternative tests and methodologies have been employed to examine their mechanical properties under diverse loading conditions.

II.6.1. Illustrations of the Tensile Test

a) Example 1 [53]

The study examined the SSFs. The precise approach for the preparation of the foams has been detailed in another source [54]. Figure II. 31 depicts a diagram of the manufacturing process.

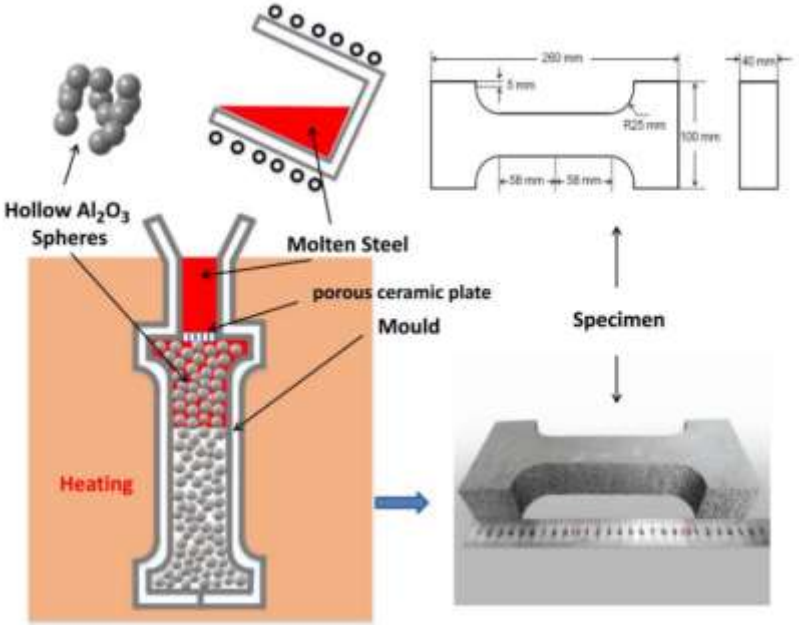

Figure II.31 the manufacturing process (infiltration) and the tensile specimen.

Based on the ASTM-E8 standard uniaxial tensile tests with speed of 1 mm/min (quasi-static) were conducted using a DNS 300 test machine. The foam specimens were fabricated with 260 mm in length, central cross-section measuring 40 × 40 mm.

The deformation mode under tensile load conditions and the Tensile fracture mode of the specimens are illustrated in Figure II.32.

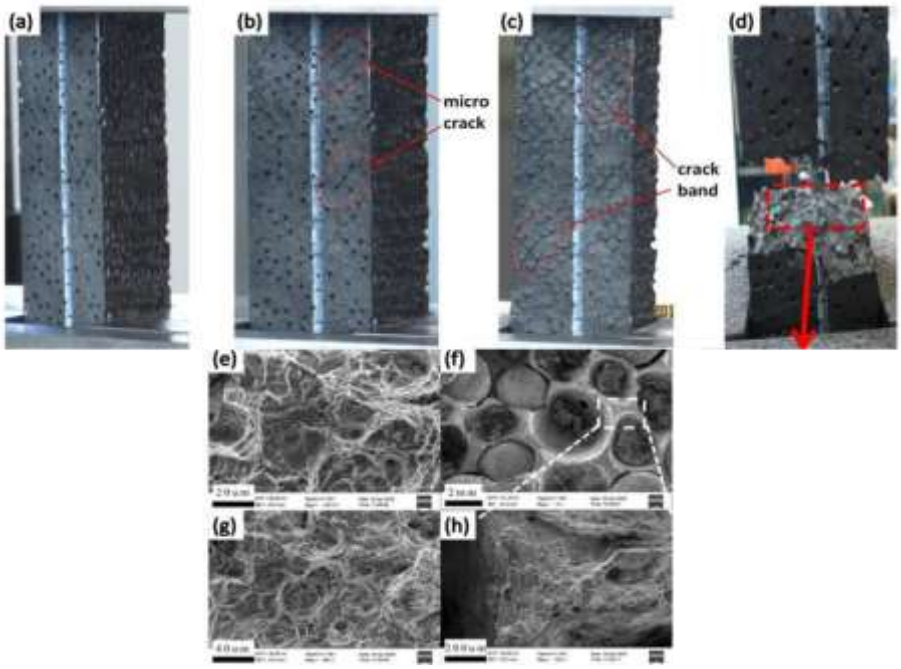

Figure II.32 (a–d) the deformation mode of SSFs under tensile load condition. (e–h) Tensile fracture mode.

The stress–strain curve under tensile test and the comparison of the UTS for different types of MF are presented in Figure II.33.

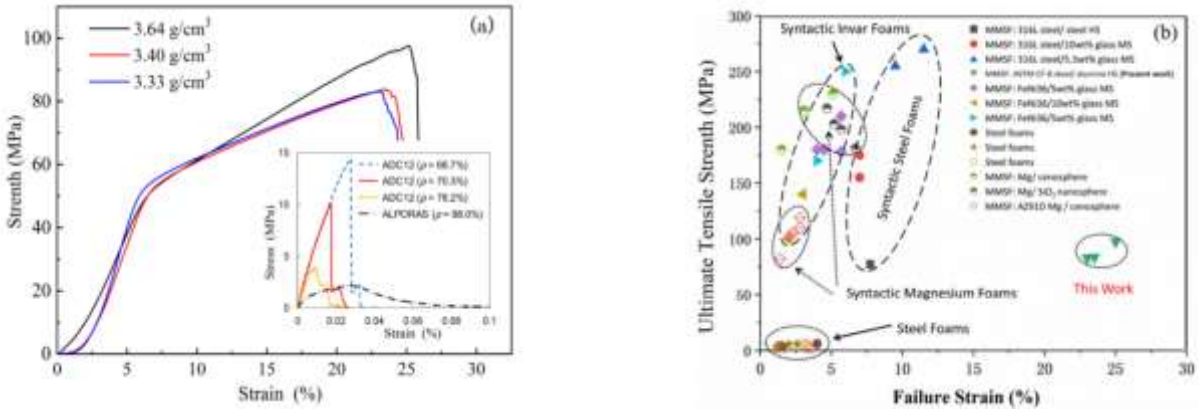

Figure II.33 a) stress–strain curve of SSFs and AL- foam [50] under tensile test. b) Comparison of the UTS of different types of metal foams.

Table II.13 Tensile properties of SSFs and solid metal.

Sample	HS Diameter (mm)	ρ_{SSFs} (g/cm³)	Max load (kN)	UTS (MPa)	TYS (MPa)
SSFs-1	4.79	3.64	161.546	97.6	52.3
SSFs-2	3.97	3.40	139.790	83.8	50.7
SSFs-3	3.11	3.33	138.656	83.1	49.6
Bulk metal matrix	-	7.8	-	485	205

The SSFs exhibited a spectrum of (UTS) ranging from 83.1 to 97.6 MPa. The material demonstrated notable ductility, as indicated by visible plastic deformation occurring prior to ductile fracture during the tensile testing.

The tensile deformation of SSFs exhibits similarities to plastic bulk metals, although it is distinct from typical MF.

Overall, the SSFs exhibited notable tensile strength and ductility, which were affected by factors such as density, size of the hollow spheres, and the ductility of the metal matrix. The study's findings enhance comprehension of the tensile characteristics and failure mechanisms of iron-matrix syntactic foams with high melting points, hence potentially expanding their utilization in diverse engineering domains.

b) Example 2 [55]

The mechanical reaction during uniaxial stress tests is measured used specimens as shown in Figure II.36. Passive during the entire examination. The specimens are subjected to uniaxial tension testing at a strain rate of 3×10^{-4} s^{-1}, which is in line with the results obtained from the uniaxial compression tests.

Figure II.34 Specimens for uniaxial tension.

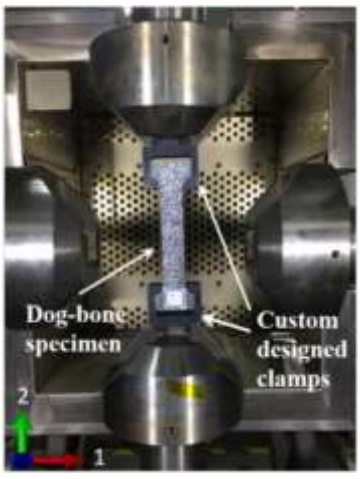

Figure II.35 test set-up of the tension experiment.

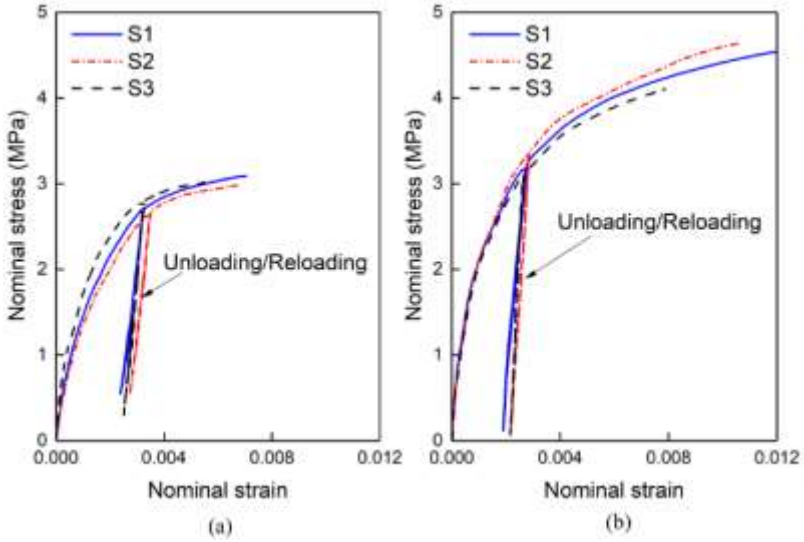

Figure II.36 nominal strain stress curves of Alporas foams with different relative density (a) 11.7% and (b) 17.2%. of three different specimens (S1, S2 and S3) under tensile test.

The aluminum foam demonstrates a greater resistance to deformation when subjected to tensile forces as opposed to compressive forces. This is apparent from the increased amounts of stress measured at specific strain levels during tension tests.

The foam exhibited excellent tensile ductility, as seen by the fracture of dog-bone specimens at substantial tensile strains. This demonstrates the material's capacity to endure large elongation prior to failure.

II.7. Conclusion

This chapter clarified the main characteristics of MF when subjected to various types of loads. The review revealed that significant progress has been made in understanding the mechanical properties of MF.

- When subjected to static loading, MF exhibit distinctive deformation characteristics, where parameters like pore size and metal type have a substantial influence on their mechanical properties.
- When subjected to quasi-static loading, MF exhibit an intricate relationship between strain rate and deformation. This section highlighted the intermediate character of quasi-static circumstances, serving as a connection between static and dynamic behaviors.
- The part on dynamic loading concentrated on the mechanical response of foams under high strain rates. MF have been found to possess remarkable energy absorption and dissipation characteristics, rendering them highly suitable for mitigating impacts in diverse industrial applications.

- In the context of three-point bending tests, we emphasized the anisotropic mechanical behavior of MF. The tests yielded useful information regarding the flexural properties of MF, which are essential for structural applications.
- Under Tension test: it provided information about the tensile strength and ductility properties of MF.

CHAPTER III 3D MODELING OF STOCHASTIC OPEN-CELL FOAM

III.1. Introduction

This chapter outlines the proposed technique for creating three-dimensional (3D) accurate models of Open-cell foams. The primary limitation of experimental studies is the challenge of isolating and examining the impact of individual morphological parameters due to their complexity and the expensive nature of manufacturing methods and experimental tests. These factors constrain the use of experimental methods and indicate the need for an alternative approach.

The utilization of dependable finite element models for numerical simulation of foam materials emerges as a significant methodology, enabling the isolated examination of individual parameters.

However, many numerical models in the literature fail to accurately reflect the local morphological features present in the geometry of solid foams due to the significant level of unpredictability in their microstructure. The primary obstacle that hinders the study of this new material is the lack of a comprehensive 3D solid model that accurately represents the intricate geometry of actual closed-cell foams. This limitation serves as a driving force for the advancement of a sophisticated model.

In this study, an efficient method for generating three-dimensional (3D) realistic models of open-cell foams is presented. The modeling approach was effectively validated by 3D printing the designed 3D models and comparing the morphological characteristics of the generated models with those observed experimentally.

III.2. Three-Dimensional Modeling of Foam Structures -Historical Overview-

The historical overview of three-dimensional modeling of foam structures involves the study of foam rheology, foam structure, and physical quantities associated with foam dynamics.

Researchers have used various techniques, including phase-field modeling, Voronoi models, and computed tomography (CT) scan techniques, to generate three-dimensional foam models for porous material design and mechanical behavior analysis [56-59].

Most of the investigations on the mechanical properties of MF have been carried out by quasi-static and dynamic compression tests, using mesoscopic numerical analysis [60].

The use of three-dimensional printed foam structures has also been explored for various structural applications. These studies demonstrate the potential of three-dimensional modeling of foam structures in understanding foam rheology, foam structure, and mechanical behavior analysis, providing insights into the design and development of foams for various applications.

III.2.1. Phase-field modeling

Phase-field modeling is a computer method used to predict the progression of microstructures in MF. The multi-phase-field approach is used, whereby each bubble is shown as a distinct "phase" that occupies a specific location in space. The phase field function assigns a value of 1 to places that are filled by a bubble and a value of 0 to points that do not have a bubble [61]. The phase-field model enables the examination of foam generation and development in three dimensions. To entirely prohibit the merging of bubbles, a non- merging criterion may be applied to the phase fields and the free energy penalty linked to additives can be increased. This allows for the concentration on the development of a compact and permeable microstructure [61]. The model may also be used to examine the start of coalescence and the development of open foam formations. The model can mimic the development and deformation of bubbles until a semi-stable configuration is achieved by modifying the criteria and energy barriers.

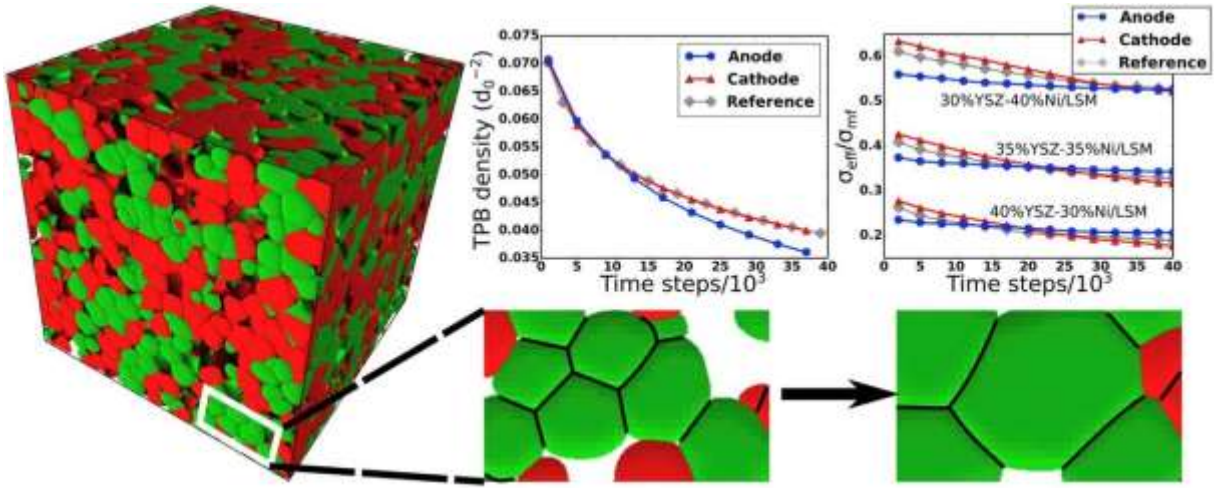

Figure III.1 Phase field modeling of microstructure evolution.

Phase-field modeling is a useful tool for comprehending the processes involved in the creation of microstructures in MF. It also allows for the investigation of how various parameters and situations impact the structure and characteristics of the foam. The user's text consists of two references, [56] and [61].

The methode represents the interface between different phases or components of a material using a continuous scalar field, known as the phase field. In the context of foams, this field helps distinguish between the gas phase (bubbles) and the surrounding liquid or solid phase. The phase field smoothly transitions from one value to another across the interface, allowing for the modeling of interfacial phenomena.

The evolution of the phase field is described by a partial differential equation (PDE), often referred to as the Cahn-Hilliard equation or the Allen-Cahn equation. This equation captures the dynamics of the foam structure, including bubble growth, coarsening, and coalescence. It takes into account factors such as surface tension, capillarity, and diffusion.

To solve the phase-field equation, numerical methods such as finite difference, finite element, or spectral methods are employed. These methods discretize space and time to simulate the evolution of the phase field over time. Advanced numerical techniques are often used to handle the complex dynamics of foams, including bubble coalescence, rupture, and rearrangement.

Phase-field modeling for foams has a wide range of applications, including in the manufacturing of materials with controlled porosity, the study of foam stability, and the design of foams for various industrial and consumer products. It is also used to investigate foam behavior under different conditions, such as changes in temperature, pressure, and surfactant concentration.

The limitations of phase-field modeling for three-dimensional foam structures include:

- Computational Complexity

Phase-field modeling requires significant computational resources, making it computationally expensive and time-consuming [56].

- Assumptions and Simplifications

The accuracy of the model depends on the assumptions and simplifications made during the modeling process, which may not always reflect the real-world behavior of foam materials [56].

- Limited Validation

The model's accuracy and reliability depend on the availability of experimental data for validation, which may be limited for some foam materials [61].

- Limited Applicability

The model's applicability may be limited to specific types of foam materials, and it may not be suitable for all types of foam structures [56].

These limitations highlight the need for further research and development to improve the accuracy and reliability of phase-field modeling for three-dimensional foam structures.

III.2.2. X-ray computed tomography (CT)

X-ray tomography is a non-destructive imaging technique that uses X-rays to produce high-resolution 2D and 3D images of the internal structure of objects. The principle of X-ray tomography involves directing X-rays at an object from multiple orientations and measuring the intensity of the X-rays that pass through the object. The X-rays are absorbed by the object, and the degree of absorption depends on the material and thickness of the object.

A specialized algorithm is then used to reconstruct the distribution of X-ray attenuation in the object, producing a 3D image of its internal structure. X-ray tomography is based on the principles of X-ray physics, including the generation, propagation, and attenuation of X-rays, as well as the detection, digitization, and processing of X-ray images [65, 66].

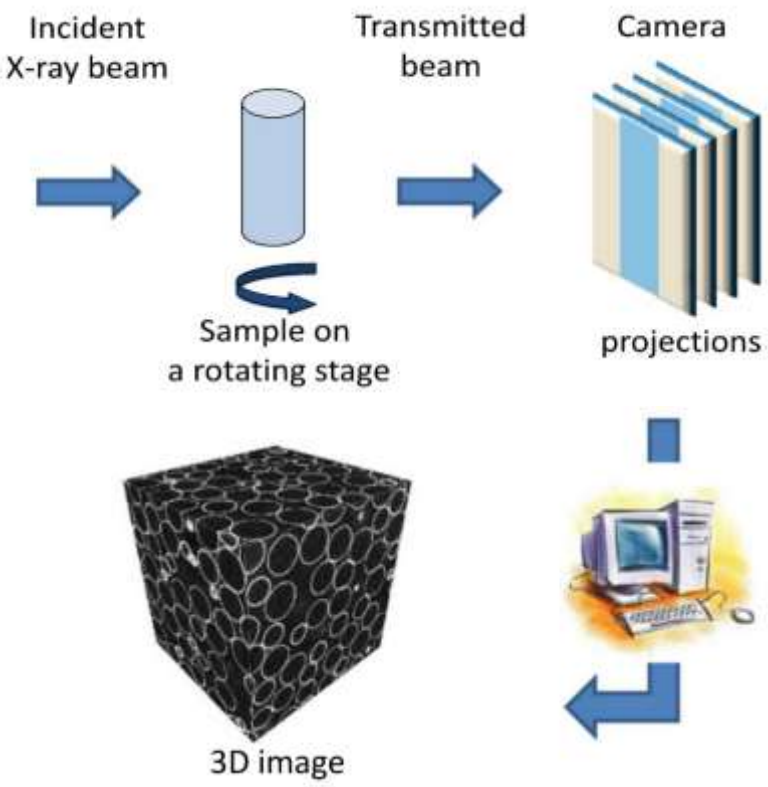

Figure III.2 Schematic of the X-ray microtomography system.

X-ray computed tomography (CT) has been extensively utilized for the three-dimensional modeling of foam structures. Several studies have employed X-ray CT to characterize and model various foam materials, including polymeric foams, closed-cell metallic foams, and expanded polystyrene (EPS) foams. The method is based on the characterization of foams with X-ray CT and the conversion of the data to finite element (FE) models [62, 63]. X-ray CT has been used to capture the macro-level detailing of foam structures [63, 67, 68], allowing for the generation of accurate three-dimensional foam models. These models have been employed to study deformation mechanisms, elastic-plastic behavior, and the mechanical properties of foam materials. X-ray CT has proven to be a valuable tool for the accurate characterization and modeling of foam structures, offering insights into their microstructure, thermal and mechanical properties, and deformation behavior [64].

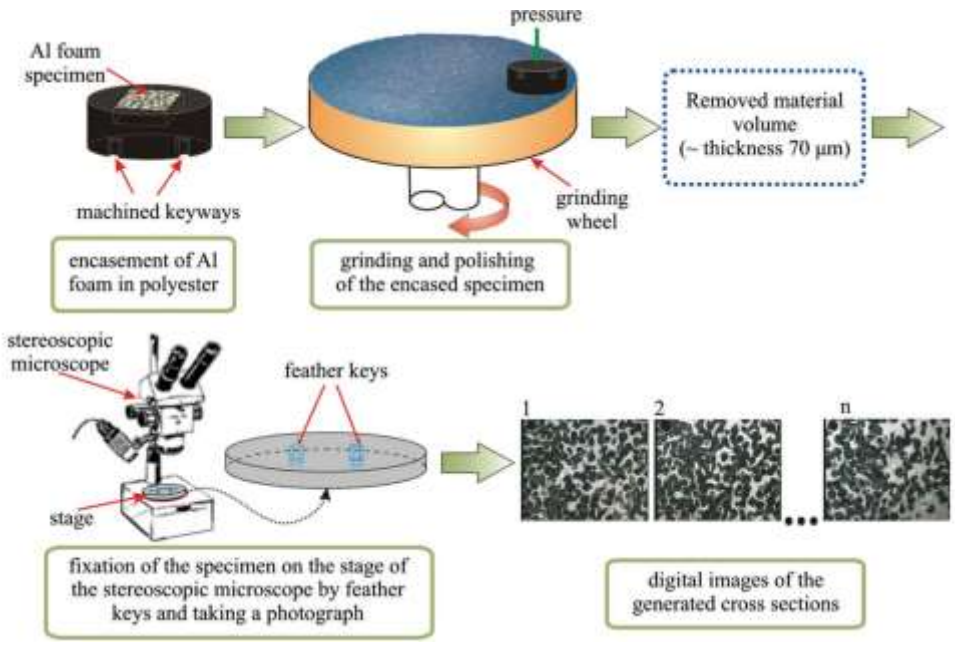

Figure III.3 Schematic representation of the procedure applied to obtain the digital images of the Al-foam sections.

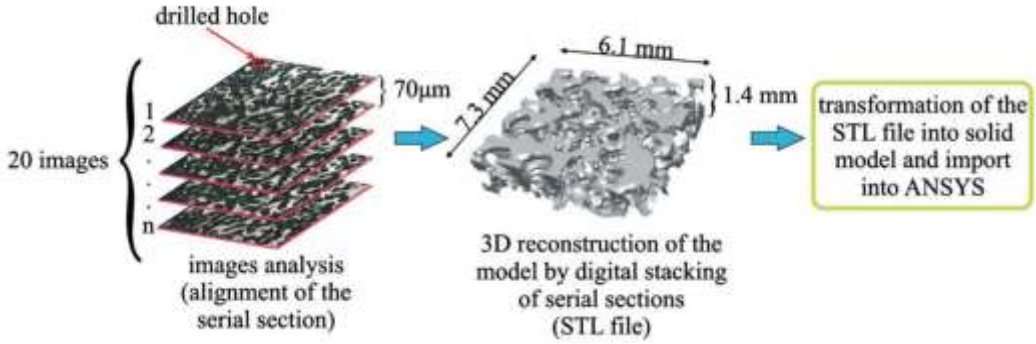

Figure III.4 Schematic diagram accounting for the image processing to obtain the 3D model of the Al-foam.

The limitations of using X-ray tomography to study foam structures include:

- Limited time resolution

The various processes observed in a foam take place on characteristic time scales, and until recently, tomography has been too slow to cope with the constant movement of expanding foams [69]. This can limit the ability to capture dynamic phenomena in real-time with high-time resolution.

- Limited sample size

The size of the sample that can be imaged using X-ray tomography is limited by the size of the X-ray beam and the detector [69]. This can limit the ability to study larger foam structures.

- Limited contrast

X-ray tomography relies on the contrast between different materials to produce images, and some foam structures may have limited contrast, making it difficult to distinguish between different features [66].

Despite these limitations, X-ray tomography remains a valuable tool for studying foam structures, providing high-resolution 2D and 3D images of their internal characteristics and dynamics.

X-ray tomography is a crucial tool in the field of material science for the detailed analysis and modeling of foam structures. Its ability to provide non-destructive, high-resolution insights into the internal structure of foams makes it invaluable for research, development, and quality control in various industrial applications

III.2.3. Voronoi method

The Voronoi method, widely used in material science and engineering, is a computer methodology utilized for modeling foam structures. It creates depictions of the foam's internal arrangement using the Voronoi tessellation concept. Presented below is a comprehensive explanation of the use of this strategy, along with recommendations for certain sorts of references that may provide more intricate and specific information.

Several studies used Voronoi tessellation to produce random models. This approach begins by creating 3d random seed points. Subsequently, a cell is created by defining the area that is nearer to its own seed point than to any other points [70]. The stochasticity of this arrangement is impacted by the seed locations. [71] introduced a 3D framework for OCF by using Laguerre-Voronoi tessellation. the study [72] conducted a validation of the LV tessellation modeling approach, which was previously published in the literature [71]. Additionally, they computed the permeability of OCF.

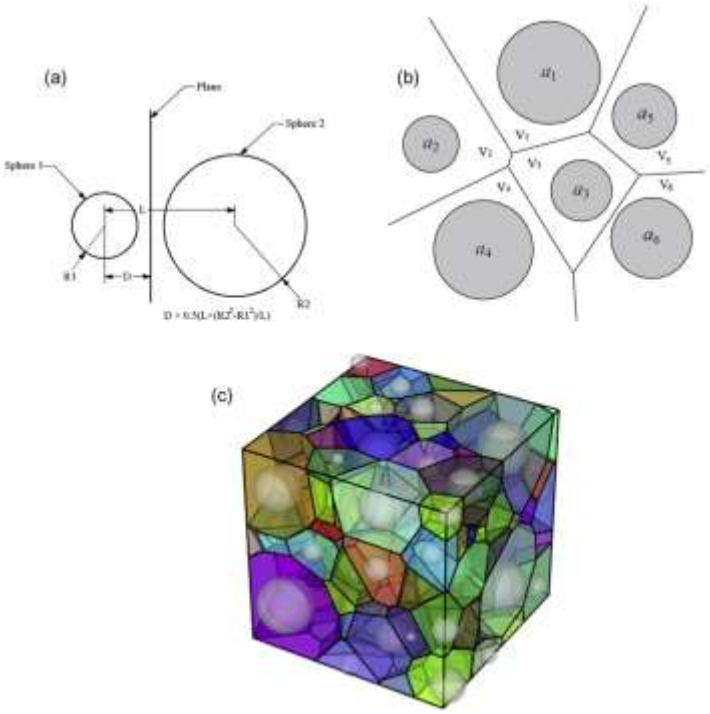

Figure III.5 a) Illustration of LV tessellation method, b) a 2D, c) a 3D Laguerre-Voronoi diagram.

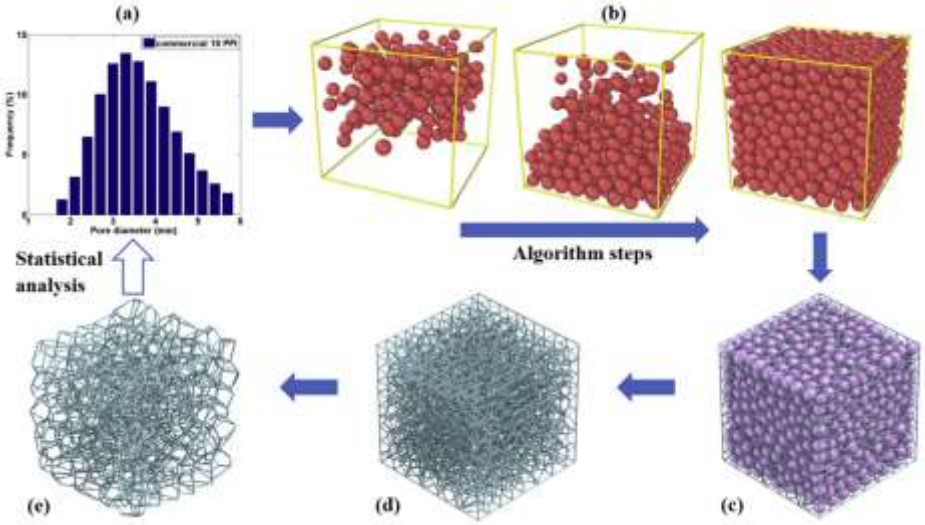

Figure III.6 Schematic illustration of the procedure for foam structure generation: (a) spheres of pre-selected volume distribution, (b) the algorithm of randomly packed spheres, (c) LV diagram based on randomly packed spheres, (d) LV-cells with cylindrical edges, and (e) foam structure with cylindrical struts.

Limitations of using Laguerre-Voronoi tessellations for modeling foam structures

- Computational Complexity

The use of Laguerre-Voronoi tessellations can be computationally expensive, requiring significant computational resources and time to generate accurate models [73].

- Limited Applicability

The Laguerre-Voronoi method may not be suitable for all types of foam structures, as it is primarily designed for modeling irregular and complex geometries [73].

- Modeling Errors

The accuracy of the Laguerre-Voronoi method depends on the quality of the input data and the assumptions made during the modeling process. Modeling errors can occur if the input data is incomplete or if the assumptions made during the modeling process do not reflect the real-world behavior of foam materials [73].

III.3. Proposed technique for design of stochastic open-cell foam structure

III.3.1. Design of stochastic OCF structure

The OCF structure exhibits a non-periodic and random architecture, as depicted in Figure III.7. This structure comprises cells that are randomly distributed and interconnected through pores. Each cell is formed by multiple struts attached to nodes [74]. However, many numerical studies represent the OCF structure by employing a simplified uniform three-dimensional (3D) finite element beam in their models. This simplification overlooks the variation in cross-section along the strut length and the mass concentration at the junctions, aspects that are present in real foam structures.

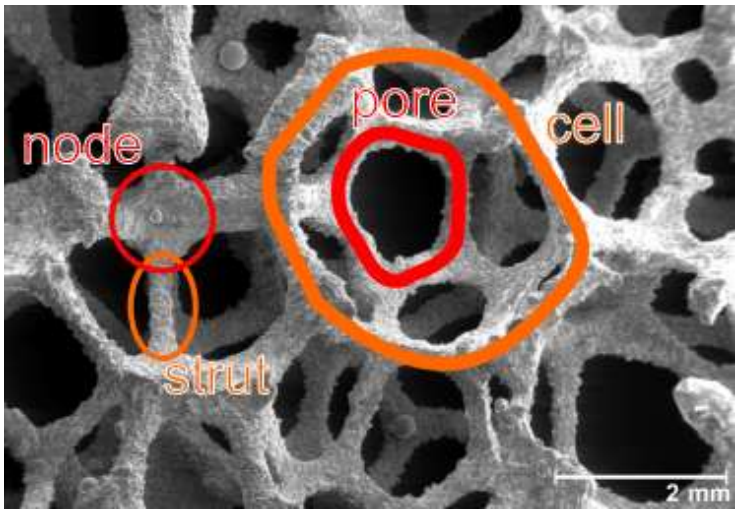

Figure III.7: Stochastic open-cell foam structure.

In this study, we employed the modelling approach introduced by Fantini [75, 76], which utilizes Voronoi diagrams to construct three-dimensional (3D) solid models of stochastic OCF, incorporating cross-section variations along the strut length.

The modelling process was executed using Rhinoceros3D 7 by Robert McNeel & Associates, supplemented with the Grasshopper graphical programming add-on for creating the intricate foam structures. The primary steps in this modeling process include:

- Generate a set of random points (Figure III.8(a)), some of which are considered as the number of seeds used to create a 3D Voronoi set of polyhedral cells (Figure III.8(b)) in the Rhinoceros3D software.
- Separate the generated polyhedral cells (Figure III.8(c)) by a scale factor to obtain voids (Figure III.8(d)) and a network of solid beams (Figure III.8(e)) in the structure.
- Smoothing and closing the 3D mesh model (Figure III.8(f)) using the Catmull-Clark algorithm [77], and the pufferfish plug-in provided by the Grasshopper.

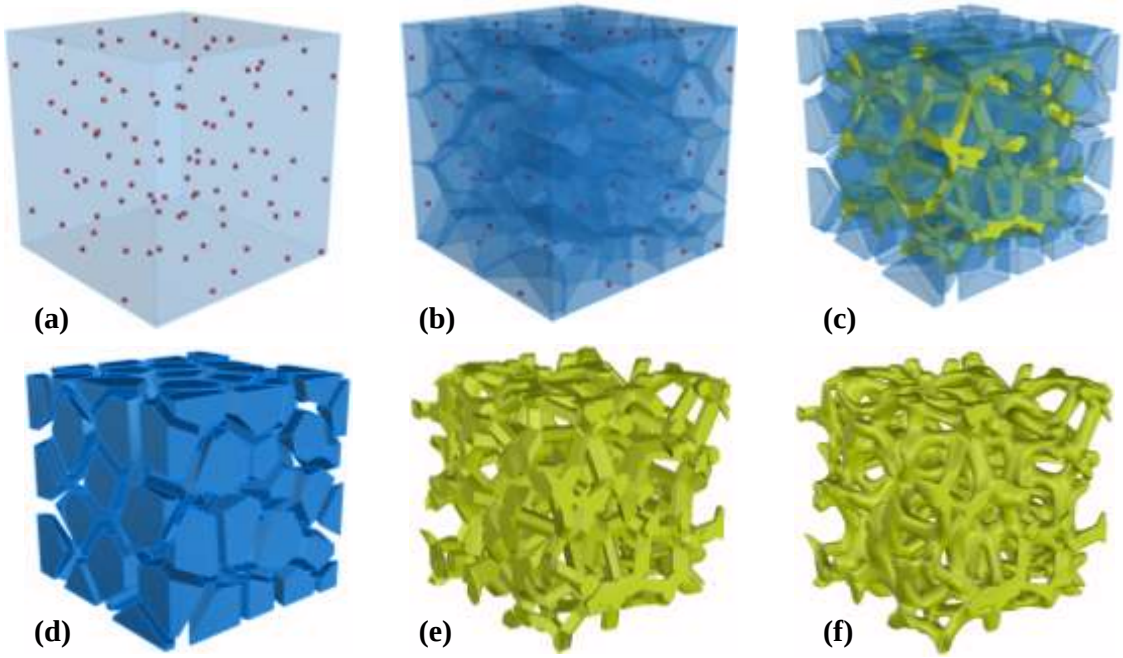

Figure III.8. Design steps of stochastic OCF based on Voronoi diagrams.

An example of a constructed geometric model of random open-cell foam with a circular cross-sectional shape of struts is presented in Figure III.9. Noting that relative density, pore number, and strut shapes in the generated model can be easily controlled.

The cross-section shape is obtained by changing the scaling ratio R for cells and faces in the algorithm defined as:

$$R = \frac{S_f}{S_v} \tag{III.1}$$

S_f is the polyhedrons faces scale factor;

S_v is the polyhedrons volume scale factor.

The cross-sectional shape can be approximately a circle or a triangle with smooth vertices and convex or concave edges.

In this thesis, to calculate easily the two input scale factors S_f and S_v for a given cross-sectional shape type and porosity P, analytical formulas summarizing the relationships between the three variables: scaling ratio, cross-sectional shape type, and porosity are proposed as:

- For circular shape

$$\begin{cases} R = 0.00139 * P + 0.760 \\ S_f = \frac{0.1*R}{(1-R)} \\ S_v = S_f + 0.1 \end{cases} \quad \text{(III.2)}$$

- For concave shape

$$\begin{cases} R = -0.00202 * P + 1.306 \\ S_f = \frac{0.1*R}{(R-1)} \\ S_v = S_f - 0.1 \end{cases} \quad \text{(III.3)}$$

- For convex shape

$$\begin{cases} R = 0.00434 * P + 0.151 \\ S_f = \frac{0.43*R}{(1-R)} \\ S_v = S_f + 0.43 \end{cases} \quad \text{(III.4)}$$

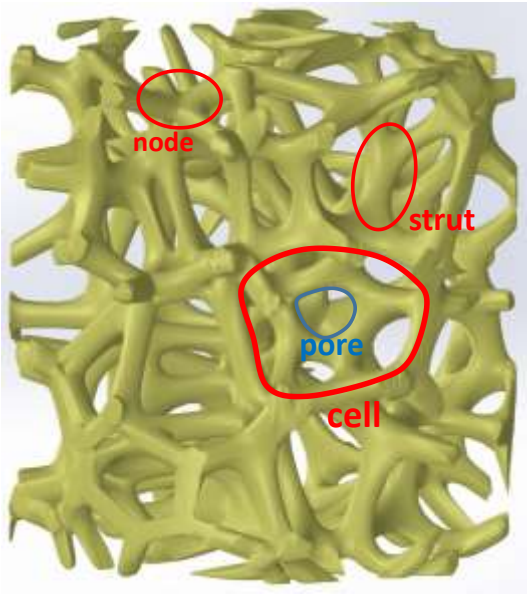

Figure III.9: Example of constructed geometric model of stochastic OCF.

The effectiveness of the generated geometries was verified by constructing 3D finite element models for two types of finite element modeling, namely shell and solid finite elements (see Appendix 1).

III.3.2. 3D printing of the developed models

A designed cylindrical 3D models with a diameter of 50 mm and a height of 50 mm, 100 pores, and three deferent relative densities ρ=0.213, ρ= 0.128, and ρ= 0.078 respectively (Figure III.10(a)) were printed as shown in (Figure III.10(b)) using Geeetech A10 3d printer. More details on the FDM technique used and the 3D printing of the developed models can be found in Appendix 2.

The basic mechanical properties of the PLA material and the printing parameters used in this study are listed in Table III.1.

Table III.1. 3D-printing parameters and mechanical properties of the PLA filament.

3D-printing parameters	
Layer Thickness (mm)	0.14
Infill density (%)	100
Print temperature (°C)	210
Build bed temperature (°C)	60
Print speed (mm/s)	40
Build bed adhesion	raft
Filament diameter (mm)	1.75
Mechanical properties	
Tensile modulus [MPa]	1451
Density (g/cm^3)	1.26
Ultimate tensile strength [MPa]	37
Yield strength [MPa]	27

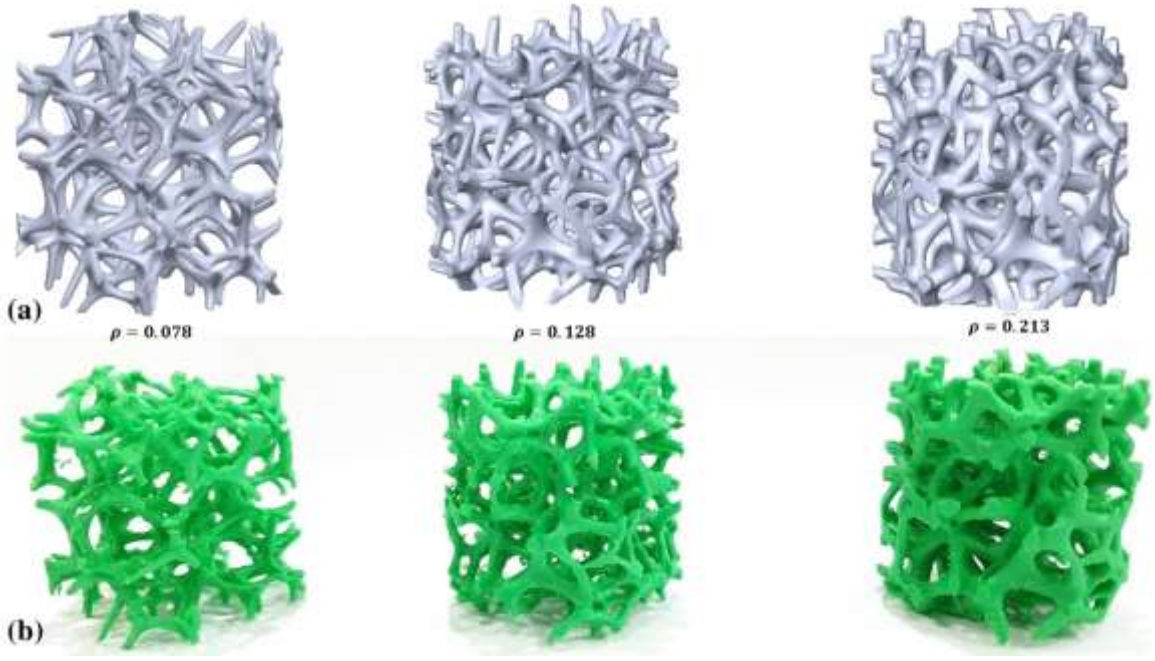

Figure III.10 Comparison between (a) Designed models and (b) 3D-printed models of random OCF structures with circular cross-section shape of struts.

The relative density of the fabricated sample is defined as the density ratio of the foam to the solid material, it has been calculated from Eq. (5):

$$\rho = \frac{\rho_{app}}{\rho_{PLA}} \tag{III.5}$$

ρ_{app} is the apparent density of the 3D-printed PLA sample, which is calculated by dividing the weight by the apparent volume.

ρ_{PLA} is the density of the rigid polymer ($\rho_{PLA} = 1.26\ g/cm^3$).

The relative density of the manufactured and designed samples is compared as shown in Figure III.11. It was found that there is a small deviation of the measured relative density of the fabricated PLA foams to the pre-set one, which may be explained by the partial loss of small parts during printing [78].

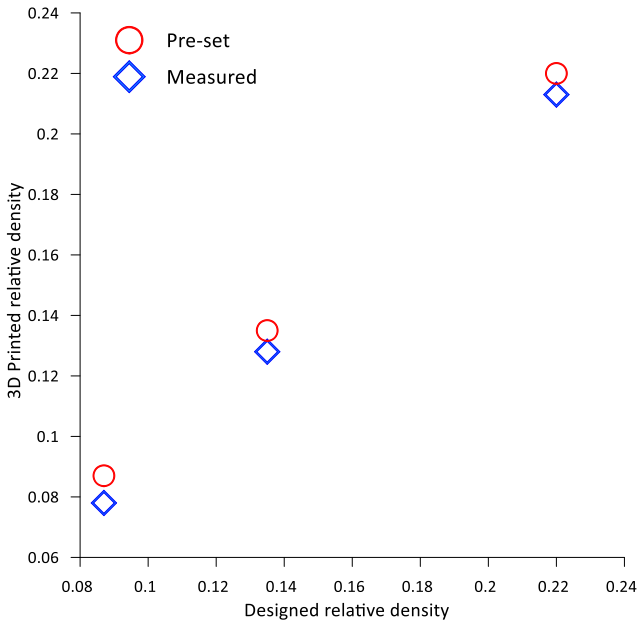

Figure III.11 Comparison of measured relative density between designed and 3D-printed models of random OCF.

III.4. Conclusion

In this chapter, we have explored the diverse spot of methodologies used in the generation and modeling of OCF structures, each offering unique insights and capabilities.

From the intricate details captured through phase-field modeling, which excels in handling the complexities of foam microstructures, to the high-resolution internal imaging provided by X-ray tomography, these methods have significantly advanced our understanding and capabilities in material science.

The Voronoi method, with its mathematical elegance, offers a different yet effective approach to simulating the irregular and stochastic nature of foam geometries. It highlights the importance of computational geometry in material modeling, presenting a balance between geometric accuracy and computational efficiency.

The 3D morphology of the 3-D printed PLA stochastic OCF proposed in this work is constructed using the Voronoi technique. The main contributions of the proposed technique are:

- Offering suitable numerical models for Additive Manufacturing (AM) technology.
- The output can be defined in various formats, e.g. Parasolid, Iges, Step, Sat and Stl files,.
- The 3D model can be scaled to nano, micro, meso, and macro levels without any structural defects.

Based on the proposed numerical models in this study, plenty of experimental works on OCF can be reduced for engineering applications.

CHAPTER IV

3D-PRINTED OPEN-CELL FOAMS UNDER COMPRESSION TEST

IV.1. Introduction

This chapter delves into the influence of microstructural properties on the mechanical behavior of open-cell foams, extending the discussions from previous chapters. It focuses on the applicability of the proposed approach of foam generation using the Voronoi technique, coupled with additive manufacturing (3D printing).

This innovative method allows for a detailed investigation into how foam mechanics are affected by morphological parameters using the Polylactic Acid (PLA) material.

A significant challenge in this area of research lies in the detailed experimental analysis of each morphological feature. Traditional methods and models often fail to capture the complex geometries and intricate details of real-life OCF, especially in medium-density variants. These conventional approaches, such as shell formulations or computed tomography, are limited in scope and often come with high computational costs and complexity. They tend to focus on smaller-scale structures or offer only partial analysis of foam behavior, particularly in terms of compression strains and densification processes.

In contrast, this work introduces a detailed 3D solid model that accurately represents the complex geometries of real open-cell foams. By leveraging the unique Voronoi-based technique for foam generation, we have succeeded in creating models with varied relative densities where we could control most of the morphological parameters in open-cell foam.

This experimental approach enables a comprehensive evaluation of the effects of various morphological parameters, such as cell size, randomness in cell distribution, strut shape and length, pore number, and relative density, on the mechanical properties of OCF fabricated through advanced 3D printing techniques.

IV.2. Quasi-static compression experiment

The specimens underwent quasi-static compression testing using the WDW-100S universal testing equipment. The tests were performed under displacement control, maintaining a constant speed of 10 mm/min [79, 80], following the guidelines outlined in the ISO 13314-11 standard [30].

Cylindrical specimens with a diameter and height of 50 mm each were utilized and compressed along the longitudinal axis using layer deposition orientation until the desired deformation was attained.

Drawing upon previous research on foams [82-84], the compressive behavior is typically evaluated based on three key parameters: collapse stress σ_c, plateau stress σ_{pl}, and densification strain ε_d. Our focus is on assessing the densification strain and plateau stress of random open-cell PLA foams under quasi-static compression. This will be achieved using the energy absorption efficiency method [84-89], as follows:

$$\eta(\varepsilon_a) = \frac{\int_0^{\varepsilon_a} \sigma(\varepsilon) d\varepsilon}{\sigma_a}, \qquad 0 \leq \varepsilon_a \leq 1 \tag{IV.1}$$

Where σ_a and ε_a are the stress and corresponding strain, respectively.
The densification strain ε_d denotes when the energy absorption efficiency η has reached the maximum as:

$$\left.\frac{d\eta(\varepsilon_a)}{d\varepsilon}\right|_{\varepsilon_a=\varepsilon_d} = 0, \qquad 0 \leq \varepsilon_d \leq 1 \tag{IV.2}$$

The plateau stress σ_{pl} is derived as follows:

$$\sigma_{pl} = \frac{\int_0^{\varepsilon_d} \sigma(\varepsilon) d\varepsilon}{\varepsilon_d} \tag{IV.3}$$

IV.3. Results and discussion

IV.3.1. Effect of relative density

Figure IV.1 displays the stress-strain curves and deformation process of the 3D printed PLA foam under the quasi-static compression test for the three distinct relative densities, ρ=0.213, ρ=0.128, and ρ= 0.078. There is a strong correlation between the quasi-static stress-strain curves and the relative density. Like metallic foam (see, for example, [90]), each curve displays three distinct stages: a linear elasticity stage, a lengthy plastic plateau, and a rapid compression stage.

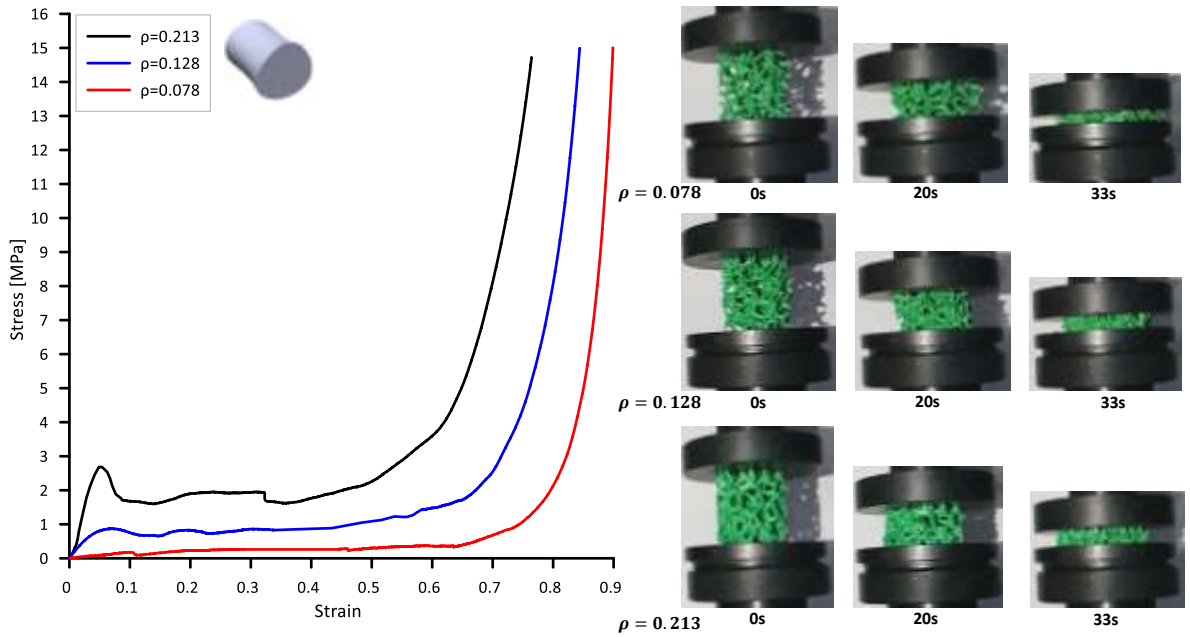

Figure IV.1 Stress-strain curves and deformation process under quasi-static compression test of 3D printed open-cell foams for three different relative densities.

Figure IV.2 shows the corresponding energy absorption efficiency against strain curves. The experimental findings shown that energy absorption efficiency decreases when strain exceeds densification strain and rises with compressive strain up to a maximum value.

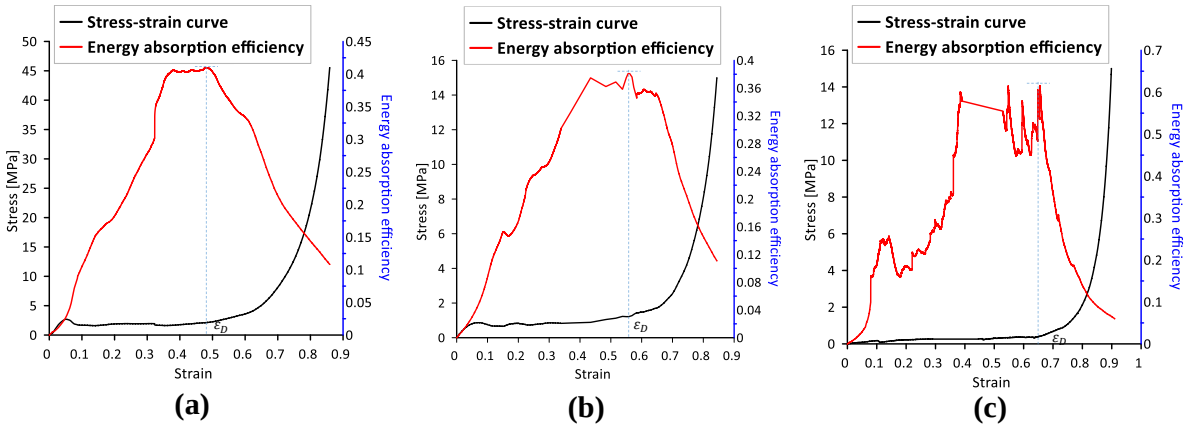

Figure IV.2 Stress-strain and energy absorption efficiency–strain curves of 3D printed open-cell foams for different relative densities: (a) ρ=0.213, (b) ρ= 0.128, and (c) ρ= 0.078.

Table IV.1 lists the primary computed mechanical parameters of the foams under investigation.

Table IV.1: Quasi-static compressive properties of 3D printed open-cell PLA foam specimens for three different relative densities.

Relative density (%)	Collapse stress (MPa)	Plateau stress (MPa)	Densification strain (%)
0.213	2.71	1.81	0.47
0.128	0.87	0.74	0.56
0.078	0.18	0.19	0.64

IV.3.2. Effect of cell number

By comparing two 3D-printed specimens with 100 and 200 pores, respectively, under quasi-static compression, the impact of cell number on the compressive behavior of the specified models is examined at a constant relative density. Figure IV.3 displays the 200-pore specimens that were created and 3D printed for the three distinct relative densities (ρ=0.213, ρ=0.128, and ρ= 0.078).

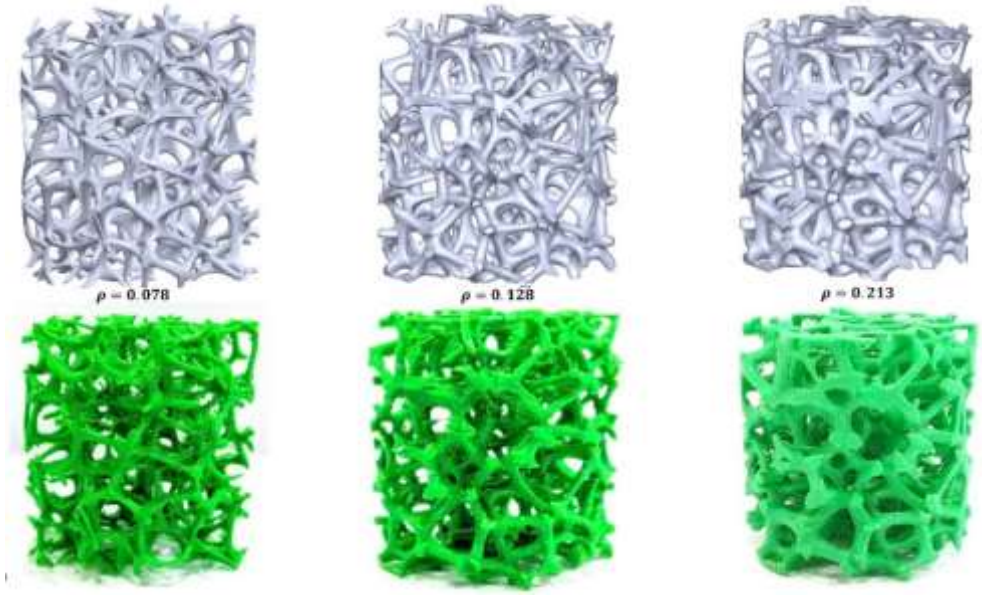

Figure IV.3 Comparison between (a) Designed models and (b) 3D-printed models of OCF structures with 200 pores for three different relative densities.

Figure IV.4 displays the stress-strain curves and the deformation process; Figure IV.5 compares the related energy absorption efficiency vs strain curves.

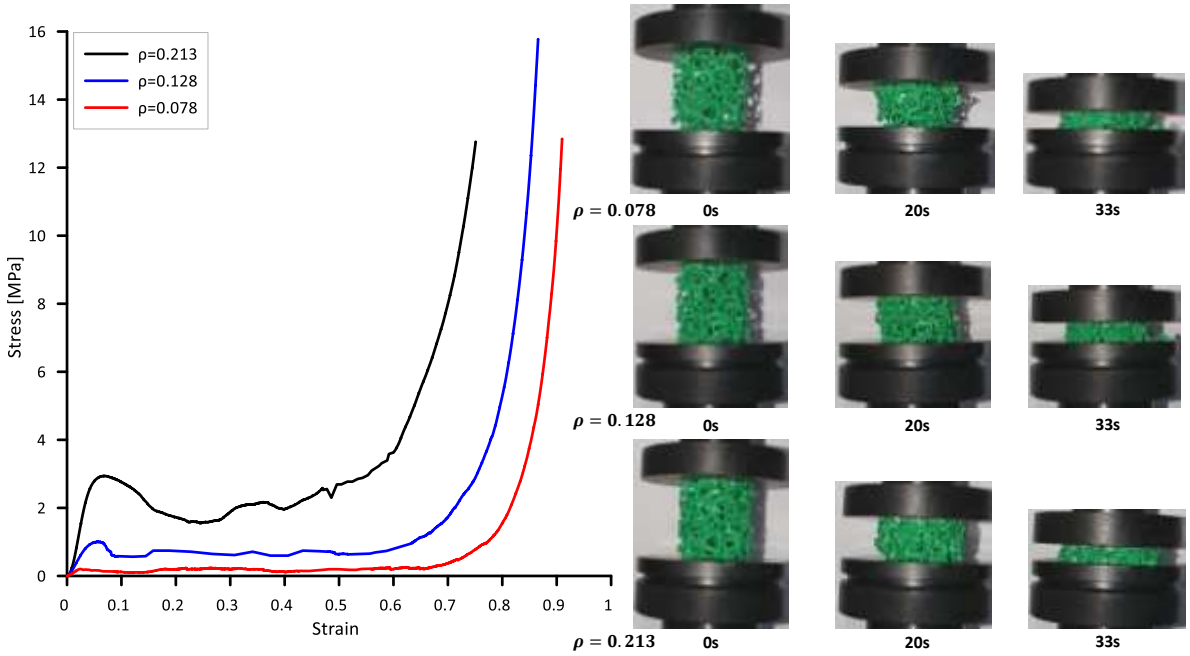

Figure IV.4: Quasi-static compressive stress-strain curves and deformation process of 3D printed OCF with 200 pores for three different relative densities.

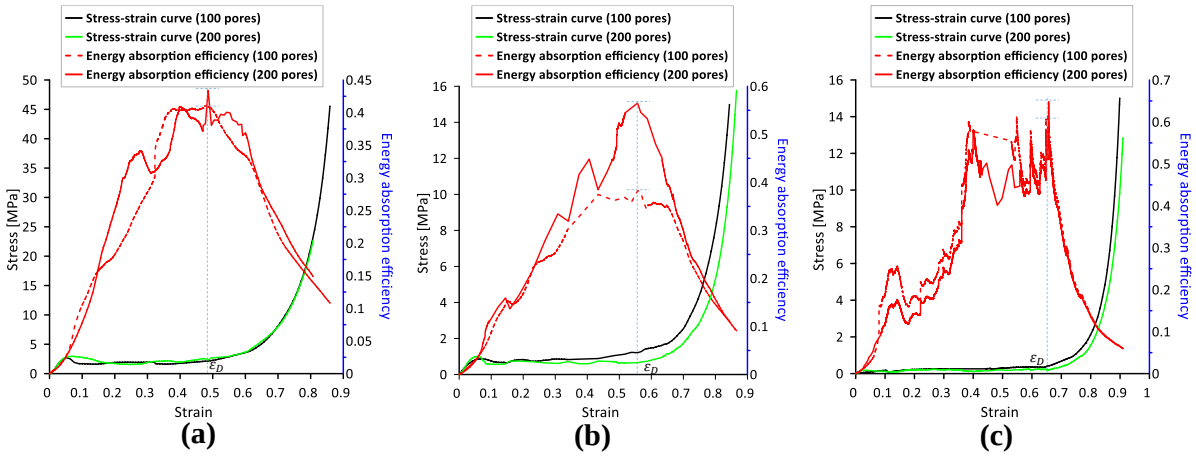

Figure IV.5: Comparison of Stress–strain and energy absorption efficiency–strain curves of 3D printed OCF for different pores number and relative densities: (a) ρ=0.213, (b) ρ= 0.128, and (c) ρ= 0.078.

The results of collapse stress, plateau stress, and densification strain are compared in Table IV.2.

Table IV.2: Quasi-static compressive property of 3D printed open-cell foams for different pores number and relative densities.

Relative Density (%)	Collapse stress (MPa)		Plateau stress (MPa)		Densification strain (%)	
	100 pores	200 Pores	100 pores	200 pores	100 pores	200 pores
0.213	2.71	2.93	1.81	1.82	0.47	0.48
0.128	0.87	1.00	0.74	0.68	0.56	0.56
0.078	0.18	0.21	0.19	0.17	0.64	0.65

The stress-strain profiles of the samples under comparison, characterized by three distinct relative densities, exhibit a notable degree of superposition across the three discernible stages—namely, the linear elastic phase, prolonged plastic plateau, and the subsequent densification stage. The investigation reveals a marginal variance in the tested pore numbers between the samples.

IV.3.3. Effect of random realization

In order to verify the accuracy of the acquired results, three separate instances of disordered pore distributions are created (Figure IV.6 (a)) and reproduced (Figure IV.6 (b)), all with an identical relative density of ρ=0.128.

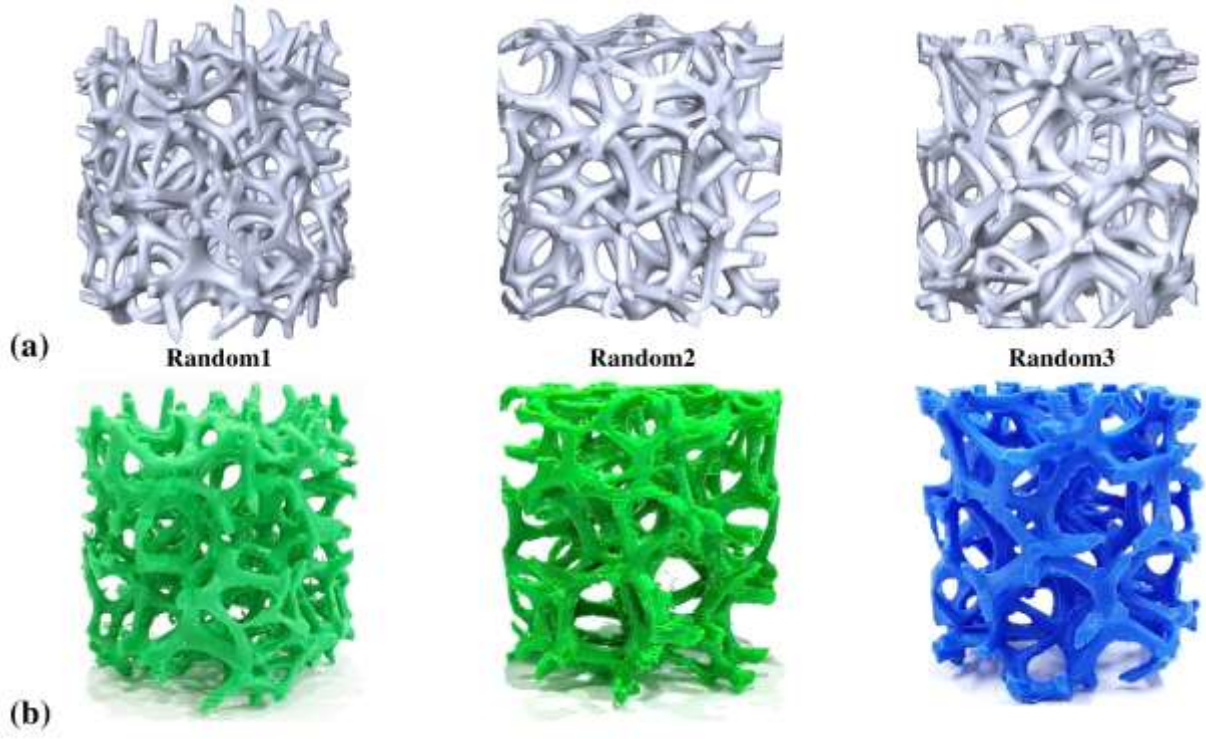

Figure IV.6: Comparison between (a) Designed models and (b) 3D-printed models of open-cell foam structures with three different configurations, and a similar relative density ρ=0.128.

The stress-strain, energy absorption efficiency curves, and deformation process of the three tested designs under quasi-static compression are illustrated in Figure IV.7. The curves exhibit overlap throughout all three stages of deformation.

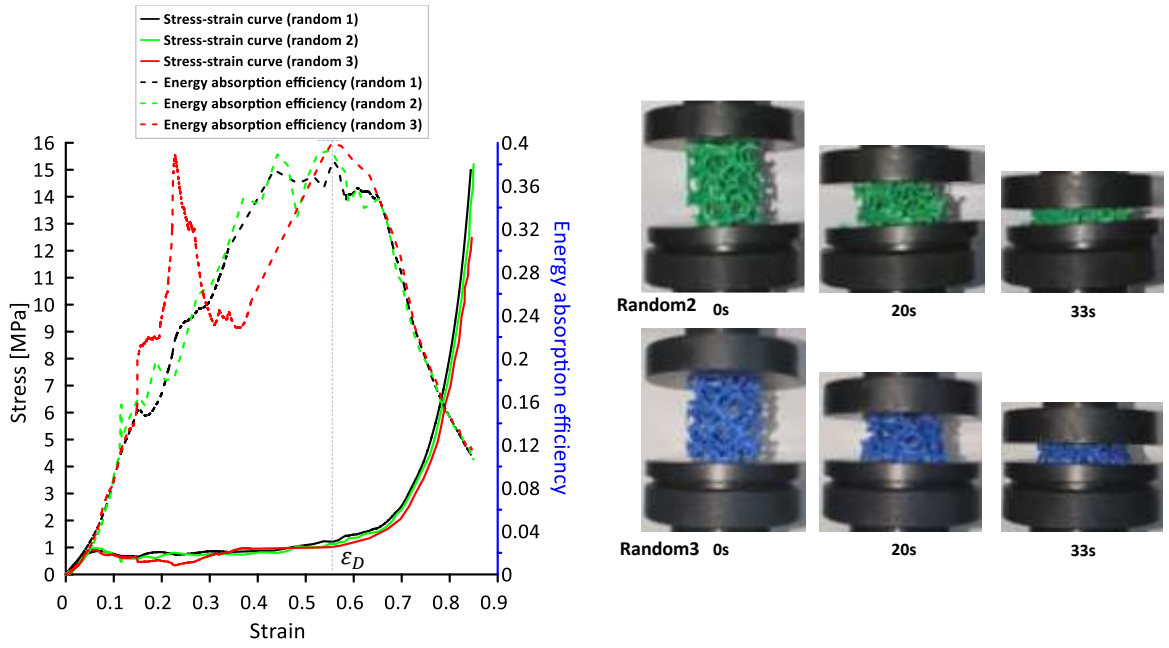

Figure IV.7: Comparison of stress-strain, energy absorption efficiency–strain curves, and deformation process of 3D printed OCF with three different configurations.

The mechanical properties acquired are presented in Table IV.3. The results exhibit comparable characteristics for the three configurations that were evaluated, with a little discrepancy noted in the third configuration as a result of the variations observed in its stress-strain response.

Table IV.3 Obtained collapse stress, plateau stress, and densification strain of foam specimens with three different configurations.

Sample	Collapse stress (MPa)	Plateau stress (MPa)	Densification strain (%)
Random1	0.87	0.74	0.56
Random2	0.91	0.74	0.55
Random3	0.9	0.75	0.56

This observation suggests that a Representative Volume Element (RVE) can be effectively represented with a modest count of 100 pores, implying that such a configuration adequately captures the macroscopic mechanical behavior of the material under consideration.

IV.3.4. Effect of cross-sectional shape

An investigation is conducted to examine the impact of cross-sectional form on the overall behavior of random PLA foams. This is achieved by comparing three distinct cross-section shapes. The average diameter of cell struts for the three different cross-section geometries, each with varying relative densities, is recorded in Table IV.4.

Table IV.4: Measured average diameter.

Relative density (%)	**Measured average diameter (mm)**		
	Convex	Circle	Concave
0.213	2.08	2.45	2.0495
0.128	1.68	1.92	1.525
0.078	1.33	1.5	1.19

Figure IV.8 depicts many open-cell foam structures that have been created, each exhibiting distinct cross-sectional forms of struts.

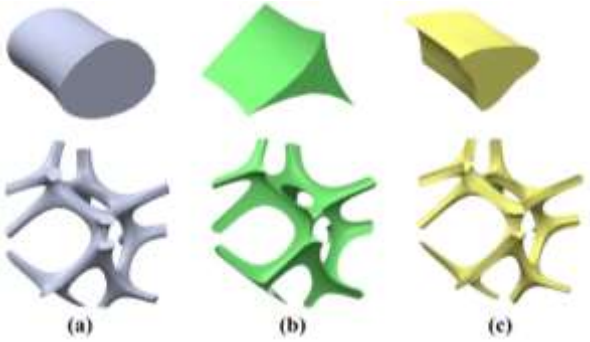

Figure IV.8 Example of generated OCF structures with different cross- sectional shapes of strut (a) circlelike, (b) triangular one with convex edges, and (c) triangular one with concave edges.

The PLA foam structures with concave and convex cross-section shapes are depicted in Figure IV.9 and Figure IV.10, respectively.

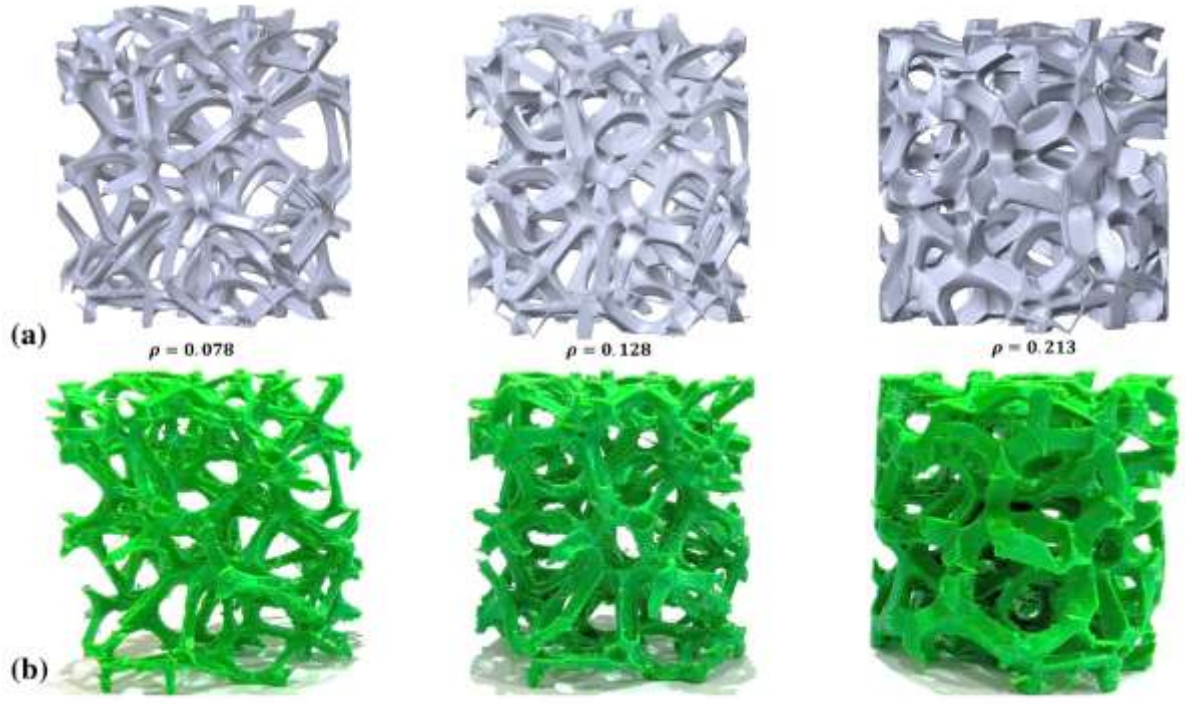

Figure IV.9 Designed and 3D-Printed open foam structures with a triangular cross-sectional shape with concave edge for three different relative densities.

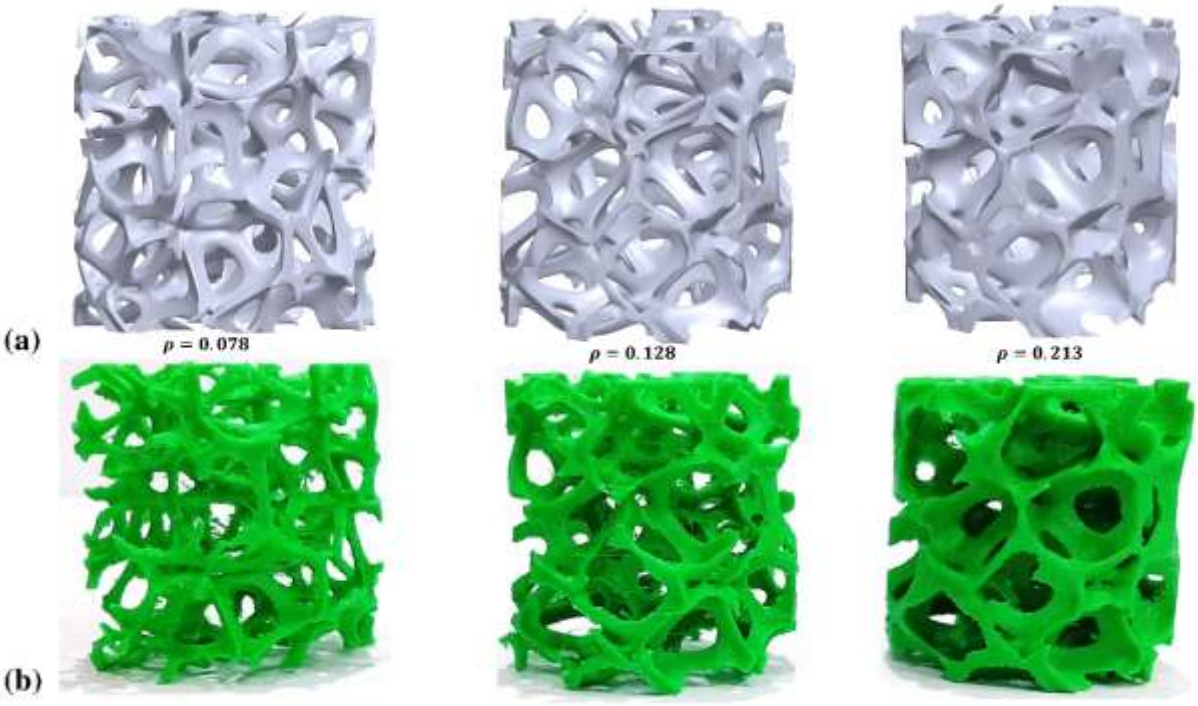

Figure IV.10 Designed and 3D-Printed open foam structures with a triangular cross-sectional shape with convex edge.

Figure IV.11 displays the stress-strain curves of 3D printed PLA foams with concave strut shapes, while Figure IV.12 shows the deformation process of foams with convex strut shapes.

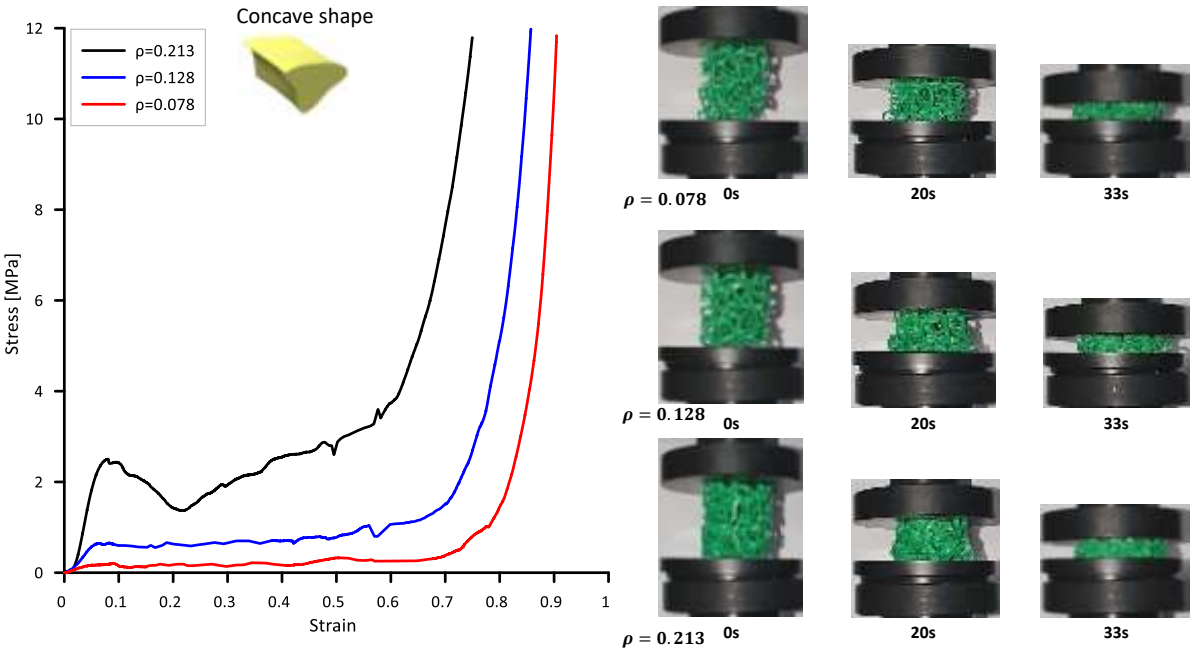

Figure IV.11 Stress-strain curves and deformation process under quasi-static compression test of the 3D printed PLA foam with concave strut shape for three different relative densities.

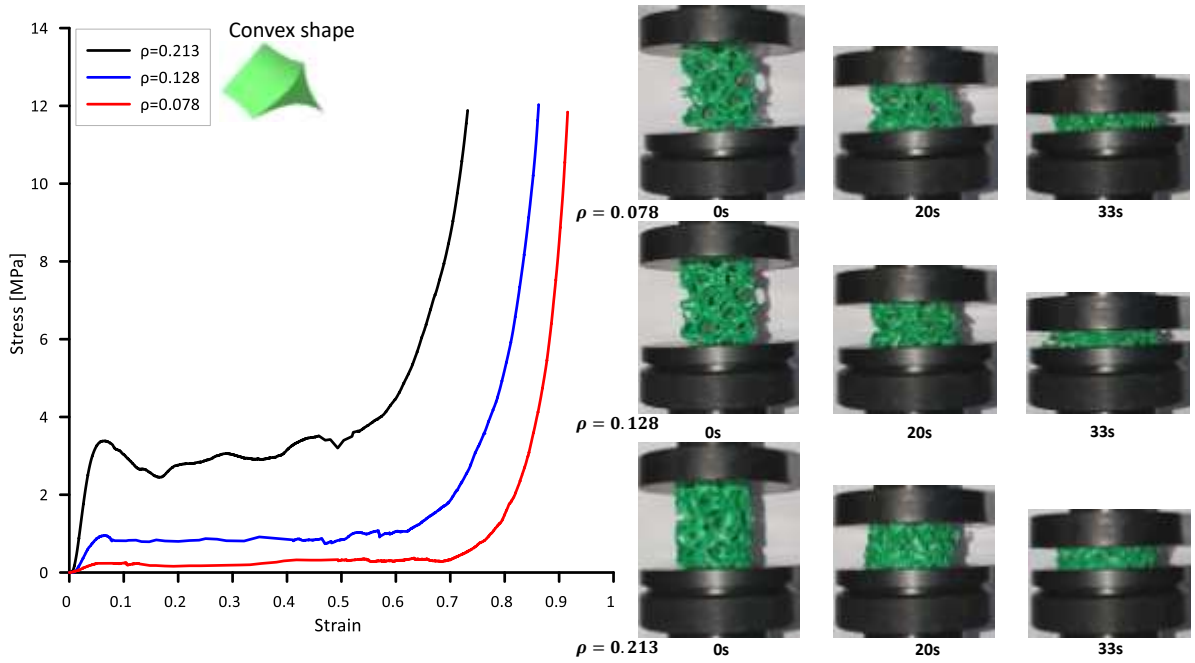

Figure IV.12 Stress-strain curves and deformation process under quasi-static compression test of the 3D printed PLA foams with convex strut shape.

Figure IV.13 displays the mechanical response, whereas Figure IV.14 shows the matching energy absorption efficiency–strain curves.

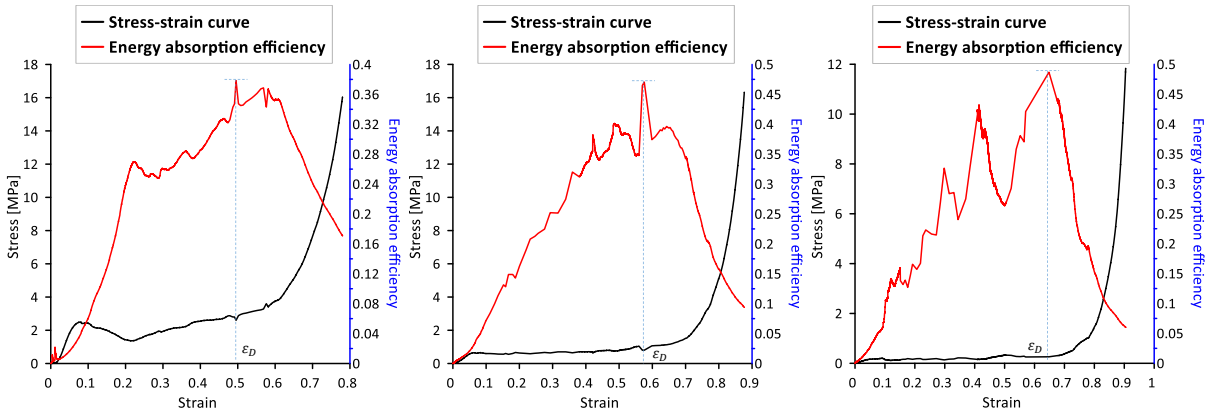

Figure IV.13: Stress–strain and energy absorption efficiency–strain curves of 3D printed OCF with triangle concave edges strut shape for different relative density: (a) ρ=0.213, (b) ρ= 0.128, and (c) ρ= 0.078.

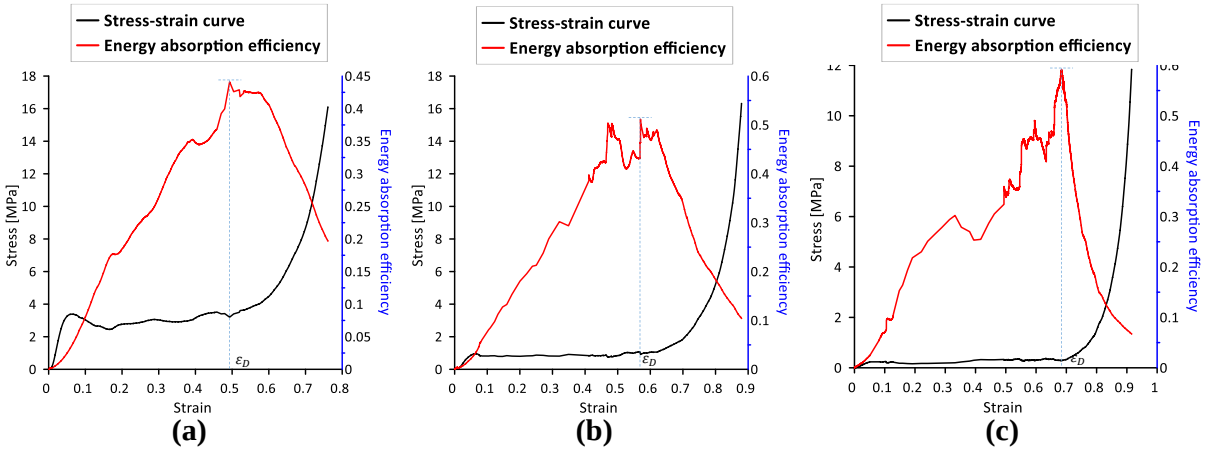

Figure IV.14: Stress–strain and energy absorption efficiency–strain curves of 3D printed MF with triangle convex edges strut shape for different relative density: (a) ρ=0.213, (b) ρ= 0.128, and (c) ρ= 0.078.

Figure IV.15 compares the mechanical reactions of OCF with three distinct cross-section forms that have been manufactured. There is a significant disparity in the curves of the three cross-section shapes, particularly during the elastic and plateau phases of deformation. This example demonstrates that the random structure of PLA foam can be considerably influenced by the sort of cross-section shape.

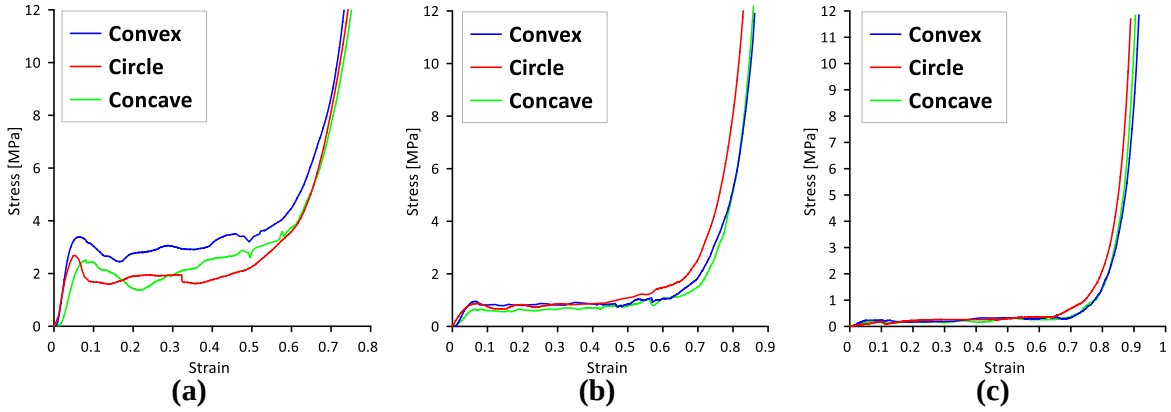

Figure IV.1: Comparison of mechanical responses of fabricated open-cell foams with three different cross-section shapes under quasi-static compression for different relative density: (a) ρ=0.213, (b) ρ= 0.128, and (c) ρ= 0.078.

The mechanical properties of the OCF, which were manufactured with three distinct cross-section shapes, are presented in Table IV.5.

Table IV.5: Obtained mechanical properties of PLA OCF with three different cross-section shapes.

Relative density (%)	Collapse stress (MPa)			Plateau stress (MPa)			Densification strain (%)		
	Convex	Circle	Concave	Convex	Circle	Concave	Convex	Circle	Concave
0.213	3.38	2.71	2.48	2.5	1.81	1.69	0.48	0.47	0.49
0.128	0.95	0.87	0.65	0.75	0.74	0.6	0.58	0.56	0.57
0.078	0.23	0.18	0.20	0.21	0.19	0.16	0.66	0.64	0.64

The sensitivity of collapse stress and plateau stress to the strut section shape is higher compared to the densification strain. The convex cross-section shape has superior mechanical performance compared to both round and concave shapes. The impact of strut shape on the mechanical characteristics of the examined foam was significant, particularly at high relative density values. The magnitude of this phenomenon diminishes as one moves towards lower relative density, resulting in a correlation between the mechanical response values. The potential cause could be attributed to the diminutive size of the strut diameter, which undergoes deformation at low density (see to [40] for further details). Figure IV.16 illustrates a comparison of cross-section shapes for low and high relative densities. The Figure clearly demonstrates that the disparity in cross-section shapes is more pronounced in the case of high relative density compared to low relative density.

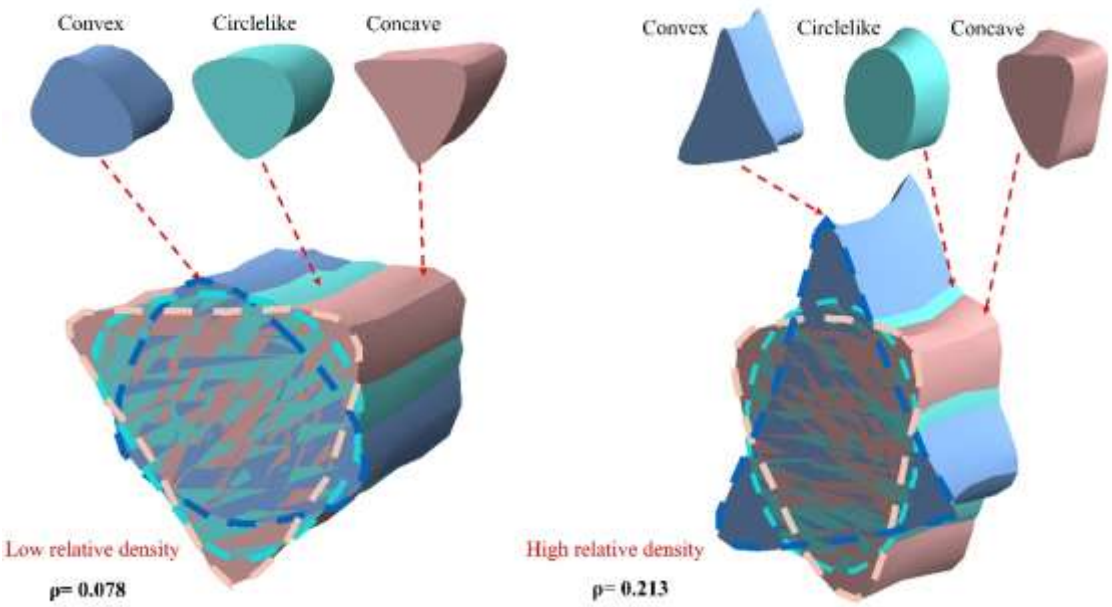

Figure IV.16 Comparison of cross-sectional shapes in the case of low relative density and high relative density.

IV.3.5. Quasi-static compressive properties estimation

In order to provide a precise numerical representation of the changes in collapse stress, plateau stress, and densification strain across various sectional forms under study, the correlation between these attributes and relative density can be represented as follows:

- Power law function to calculate the collapse stress and plateau stress:

$$Y = A\sigma_y(\rho)^B \quad \text{(IV.4)}$$

Where $\sigma_y = 27$ MPa is the yield strength determined from the tensile test.

- A simple first-degree polynomial equation to calculate the densification strain:

$$\varepsilon_D = \alpha + \beta(\rho) \quad \text{(IV.5)}$$

The proposed functions (Eq. (IV.4) and Eq. (IV.5)) are used to fit the experimental data. The values of the fitting parameters A, B, α, and β can be found in Table IV.6.

Table IV.6 Values of fitted parameters A, B, α, and β for different cross-sectional shapes.

Cross-Sectional shape	Collapse stress (MPa)		Plateau stress (MPa)		Densification strain (%)	
	A	B	A	B	α	β
Convex	6.314	2.534	3.740	2.391	0.757	-1.316
Circle	3.792	2.346	1.342	1.93	0.729	-1.237
Concave	5.110	2.599	1.690	2.129	0.719	-1.093

The computed values obtained from equations (IV.4) and (IV.5) were graphed alongside the empirical data in Figure IV.17. The fitted parameter 'B' exhibits values within the range of 1 to 4, which align well with the values reported for foams during compression testing [16].

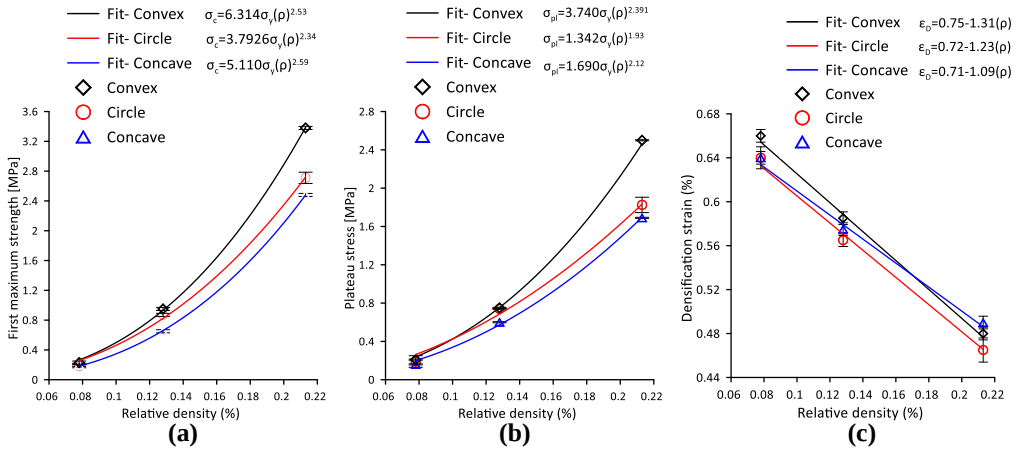

Figure IV.17 Comparison between fitted and experimental results of mechanical properties for different cross-sectional shapes: (a) Collapse stress, (b) Plateau stress, and (c) Densification strain.

IV.4. Conclusion

In this study, we systematically explore the quasi-static compression experiments of the fabricated OCF samples. Our approach involves the experimental investigation of various parameters.

The experimental setup involves quasi-static compression tests conducted using a universal testing machine system. The obtained results provide valuable insights into the compressive mechanical behavior of the fabricated PLA foam. Through a meticulous analysis of the experimental data, the following conclusions can be drawn:

- The compressive mechanical responses of the fabricated PLA foam were notably influenced by relative density, showcasing a strong dependence on this parameter.
- Increasing the pore number did not significantly impact the compressive properties of the PLA specimens. Remarkably, the study suggests that a representation with as few as 100 pores is sufficient to capture the essential characteristics of the foam microstructure.
- The strut geometry effect on the mechanical properties of the fabricated foam was particularly pronounced at large relative density values. The analysis revealed that stress properties exhibited higher sensitivity to the strut section shape compared to densification strain.
- The mechanical characteristics of the 3D-printed foams are quantified using two widely recognized formulas present in the literature. Specifically, a power law function is employed for stress properties, while a first-order polynomial equation is utilized for densification strain.
- The application of these formulas allows for the effective expression of the foam's compressive properties across diverse cross-sectional shapes.

GENERAL CONCLUSION

Conventional processes can be employed to create foams. Although these technologies allow for the alteration of particular characteristics, the complex and costly nature of production methods and experimental tests provide challenges in isolating and analyzing the effects of specific morphological aspects. As a result, these strategies have limited applicability.

Rapid prototyping, often known as 3D printing, has emerged as a viable alternative to traditional manufacturing methods for creating various structures based on three-dimensional model data. This technology offers greater flexibility compared to conventional manufacturing procedures.

The mechanical response of metal foams is crucial for their effective incorporation into many engineering applications. A comprehensive of the mechanical behavior of metal foams under different mechanical tests is crucial in several fields such as crashworthiness for automobiles, load-bearing structures in construction, and biomedical implants.

In this work, the mechanical behavior of 3D-printed stochastic open-cell foam was experimentally studied under a quasi-static compression test. PLA foam specimens with irregular cell geometry and variable strut sections are constructed numerically using the Voronoi diagrams and prepared with fused deposition modeling.

The effect of morphological characteristics on the mechanical performance of open-cell foam material was examined in detail. Compression experiments prove that the mechanical properties of fabricated PLA foams are significantly dependent on the relative density and strut section shape.

An extensive analysis of quasi-static compression tests is conducted to demonstrate the impact of many factors, including design parameters and pore morphology, on the compressive mechanical properties of the formed foam. The results of the experiment allow us to draw the following conclusions:

- The manufactured PLA foam displayed a significant correlation between its mechanical responses and relative density.
- The obtained compressive properties remain unaffected by an increase in the number of pores. It has been shown that a total of 100 pores are sufficient to accurately mimic the foam microstructure.
- The impact of strut shape on the foam's mechanical properties was significant, especially when the relative density is large.

- Results have revealed that the properties at the first and second stages of the stress-strain curve are more responsive to changes compared to the final stage property.
- The foam's mechanical characteristics are quantified for various cross-sectional geometries using the two prevailing equations found in the literature. The power law function is used to describe the relationship between collapse stress and plateau stress, whereas a simple first-degree polynomial equation is used to represent the densification strain.

In perspective, many 3D models of stochastic foams can be inspired by nature and analyzed using the additive manufacturing technique for enhancing mechanical performances, examining more relevant geometrical features.

Bibliography

[1] Duarte, I., et al., Special issue on cellular materials. Science and Technology of Materials, 2018. 30(1): p. 1-3.

[2] Schaedler, T.A. and Carter, W.B., Architected cellular materials. Annual Review of Materials Research, 2016. 46: p. 187-210.

[3] Zhang, F. and Schechter, D.S., Gas and foam injection with CO2 and enriched NGL's for enhanced oil recovery in unconventional liquid reservoirs. Journal of Petroleum Science and Engineering, 2021. 202: p. 108472.

[4] Banhart, J., Manufacture, characterisation and application of cellular metals and metal foams. Progress in materials science, 2001. 46(6): p. 559-632.

[5] Ashby, M. F., Anthony, G. Evans., Norman A. Fleck, Lorna J. Gibson, John W. Hutchinson, H. N. G. Wadley and Feridun Delale. Metal Foams: A Design Guide. (2000).

[6] Bisht, A., Gangil, B. and Patel, V.K., Selection of blowing agent for metal foam production: A review. Journal of Metals, Materials and Minerals, 2020. 30(1).

[7] Sharma, S. and Rajpoot, Y., Development of aluminum metal foam using blowing agent. in IOP Conference Series: Materials Science and Engineering. 2018. IOP Publishing.

[8] Kulshreshtha, A. and Dhakad, S., Preparation of metal foam by different methods: A review. Materials Today: Proceedings, 2020. 26: p. 1784-1790.

[9] Behymer, N. and Morsi, K., Closed-Cell Metallic Foams Produced via Powder Metallurgy. Metals, 2023. 13(5): p. 959.

[10] Tan, Koon Tatt. “Review on Manufacturing of Metal Foams.” *ASM Science Journal*, vol. 16, Academy of Sciences Malaysia, July 2021, pp. 1–8.

[11] Wu, Z., et al., Study of powder gas entrapment and its effects on porosity in 17-4 PH stainless steel parts fabricated in laser powder bed fusion. JOM, 2021. 73: p. 177-188.

[12] Changdar, A. and Chakraborty, S.S., Laser processing of metal foam-A review. Journal of Manufacturing Processes, 2021. 61: p. 208-225.

[13] dubinin, o., bondareva, kuzminova, N., V, j., O, y., et al. A promising approach to 3d printing of metal foam with defined porosity. Journal of porous materials, 2023, p. 1-9.

[14] Rajak, D.K. and Gupta, M., An Insight Into Metal Based Foams. Singapore, Springer, DOI, 2020. 10: p. 978-981.

[15] Lefebvre, L.P., Banhart, J. and Dunand, D.C., Porous metals and metallic foams: current status and recent developments. Advanced engineering materials, 2008. 10(9): p. 775-787.

[16] Dukhan, N., Metal foams: fundamentals and applications. 2013: DEStech Publications, Inc.

[17] Banhart, J., Light-metal foams—history of innovation and technological challenges. Advanced Engineering Materials, 2013. 15(3): p. 82-111.

[18] Sharma, S.S., et al., Application of metallic foam in vehicle structure: A review. Materials Today: Proceedings, 2022. 63: p. 347-353.

[19] Degischer, H.-P. and Kriszt, B., Handbook of cellular metals. Vol. 71. 2002: Wiley-VCH, Weinheim.

[20] Banhart, J. and Weaire, D., On the road again: metal foams find favor. Physics Today, 2002. 55(7): p. 37-42.

[21] Liu, H., Wei, J. and Qu, Z., Prediction of aerodynamic noise reduction by using open-cell metal foam. Journal of Sound and Vibration, 2012. 331(7): p. 1483-1497.

[22] ensarioglu, Cihat., bakirci, Altug., koluk, Huseyin. et al., Metal foams and their applications in aerospace components. In: Materials, Structures and Manufacturing for Aircraft. Cham: Springer International Publishing, 2022. p. 27-63.

[23] Ullen, N.B., Karabulut, G., The place of metal foams in biomaterial applications, in: 2nd International Eurasian Conference on Science, Engineering and Technology (EurasianSciEnTech 2020), 2020, pp. 473–479.

[24] han, Xiao-Hong., wang, Qin., park, Young-Gil. et al. A review of metal foam and metal matrix composites for heat exchangers and heat sinks. Heat Transfer Engineering, 2012, vol. 33, no 12, p. 991-1009.

[25] Hafeez, P., Heat transfer in metal foam heat exchangers at high temperature. 2016: University of Toronto (Canada).

[26] Gibson, Lorna J., and Ashby Michael F., Cellular Solids. Cambridge University Press, 1997.

[27] Ashby, M.F., et al., Metal foams: a design guide. 2000: Elsevier.

[28] Gibson, L.J., et al., The mechanics of two-dimensional cellular materials. Proceedings of the Royal Society of London. A. Mathematical and Physical Sciences, 1982. 382(1782): p. 25-42.

[29] Vogel, J., et al., Characterisation of strength behaviour of aluminium foam sandwiches under static load. Strain, 2011. 47: p. e234-e242.

[30] DIN 53 291 (1982) Testing of Sandwiches; Flatwise Compression Test. Beuth Verlag GmbH, Berlin, p. 4 (in Germany)

[31] Mysarh, A. and Abdelshafy, M., Quasi static compressive behavior of aluminum foam. in Journal of Physics: Conference Series. 2022. IOP Publishing.

[32] Wang, E., et al., On multiaxial failure behavior of closed-cell aluminum foams under medium strain rates. Thin-Walled Structures, 2021. 160: p. 107278.

[33] Bensalem, I., & Benhizia, A, Novel design of irregular closed-cell foams structures based on spherical particle inflation and evaluation of its compressive performance. Thin-Walled Structures, 2022.

[34] Luo, G., Xue, P. and Li, Y., Experimental investigation on the yield behavior of metal foam under shear-compression combined loading. Science China Technological Sciences, 2021. 64(7): p. 1412-1422.

[35] Tan, P., Reid, S. and Harrigan, J., On the dynamic mechanical properties of open-cell metal foams–A re-assessment of the 'simple-shock theory'. International Journal of Solids and Structures, 2012. 49(19-20): p. 2744-2753.

[36] Soni, B. and Biswas, S., Mechanical Behaviour under Quasi-Static Loading of Open-Cell Foams of 6061-T6 Al Alloys Processed by Pressurized Salt Infiltration Technique. Key Engineering Materials, 2016. 706: p. 23-28.

[37] Khezrzadeh, O., et al., Anisotropic compressive behavior of metallic foams under extreme temperature conditions. Materials, 2020. 13(10): p. 2329.

[38] Wang, N., et al., Compressive performance and deformation mechanism of the dynamic gas injection aluminum foams. Materials Characterization, 2019. 147: p. 11-20.

[39] Guo, Q., et al., Mechanical Properties and Constitutive Model Applied to the High-Speed Impact of Aluminum Foam That Considers Its Meso-Structural Parameters. Materials, 2021. 14(20): p. 6206.

[40] Hajizadeh, M., et al., An experimental investigation into the quasi-static compression behavior of open-cell aluminum foams focusing on controlling the space holder particle size. Journal of Manufacturing Processes, 2021. 70: p. 193-204.

[41] Członka, S., et al., Composites of rigid polyurethane foams reinforced with POSS. Polymers, 2019. 11(2): p. 336.

[42] linul, Emanoil., marsavina, Liviu., kovacik, Jaroslav. et al. Dynamic and quasi-static compression tests of closed-cell aluminium alloy foams. In: Proc. Rom. Acad. Ser. A. 2017. p. 361-369.

[43] kanetake, N., hipke, T., miyoshi, T., nakajima, H., ono, F., krupp, U., International Standard for Compression Test of Porous and Cellular Metals, Proc. of the 6th Int. Conf. on Porous Metals and Metallic Foams, Bratislava, 1–4 Sept 2009.

[44] Rajak, D.K., and Linul, E., Crushing response of Composite Metallic Foams: Density and High Strain Rate effects. Journal of Alloys and Compounds, 2021. 871: p. 159614.

[45] Jung, A., Lach, E., and Diebels, S., New hybrid foam materials for impact protection. International Journal of Impact Engineering, 2014. 64: p. 30-38.

[46] Fíla, T., et al., Impact testing of polymer-filled auxetics using split Hopkinson pressure bar. Advanced Engineering Materials, 2017. 19(10): p. 1700076.

[47] Bertholf, L. and Karnes, C., Two-dimensional analysis of the split Hopkinson pressure bar system. Journal of the Mechanics and Physics of Solids, 1975. 23(1): p. 1-19.

[48] Kaczyński, P., Ptak, M., and Gawdzińska, K., Energy absorption of cast metal and composite foams tested in extremely low and high-temperatures. Materials & Design, 2020. 196: p. 109114.

[49] Guo-yin, zu., Ri-huan, lu., Xiao-bing, li., et al. Three-point bending behavior of aluminum foam sandwich with steel panel. Transactions of Nonferrous Metals Society of China, 2013, vol. 23, no 9, p. 2491-2495.

[50] Wang, X., Cao, Z., and Fu, G., Quasi-Static Three-Point Bending Behavior of Aluminum Foam Sandwich with CFRP Face-Sheets. Metals, 2022. 12(8): p. 1393.

[51] Kalpakoglou, T., and Yiatros, S., Metal foams: A review for mechanical properties under tensile and shear stress. Frontiers in Materials, 2022. 9: p. 998673.

[52] Deshpande, V.S. and Fleck, N.A., Isotropic constitutive models for metallic foams. Journal of the Mechanics and Physics of Solids, 2000. 48(6-7): p. 1253-1283.

[53] Mei, Y., et al., Tensile Behavior and Performance of Syntactic Steel Foams Prepared by Infiltration Casting. Metals, 2022. 12(4): p. 668.

[54] Yang, Q., et al., Innovative compound casting technology and mechanical properties of steel matrix syntactic foams. Journal of Alloys and Compounds, 2021. 853: p. 156572.

[55] Vengatachalam, B., et al., Initial yield behaviour of closed-cell aluminium foams in biaxial loading. International Journal of Mechanical Sciences, 2021. 191: p. 106063.

[56] Uehara, T., Phase-Field Modeling for the Three-Dimensional Space-Filling Structure of Metal Foam Materials. Open Journal of Modelling and Simulation, 2015. 3(03): p. 120.

[57] Maruyama, B., et al., A new technique for obtaining three-dimensional structures in pitch-based carbon foams. Scripta materialia, 2006. 54(9): p. 1709-1713.

[58] Gan, Y., Chen, C., and Shen, Y., Three-dimensional modeling of the mechanical property of linearly elastic open cell foams. International Journal of Solids and Structures, 2005. 42(26): p. 6628-6642.

[59] Sahu, S., et al., Three dimensional modelling of aluminum foam through computed tomography scan technique. World Journal of Engineering, 2022. 19(3): p. 340-345.

[60] Mancini, E., et al., Mechanical Testing of Metallic Foams for 3d Model and Simulation of Cell Distribution Effects. Procedia Manufacturing, 2020. 47: p. 1490-1495.

[61] Vakili, S., Steinbach, I., and Varnik, F., Multi-phase-field simulation of microstructure evolution in metallic foams. Scientific reports, 2020. 10(1): p. 19987.

[62] Osipov, S., et al., Algorithms for modeling the formation and processing of information in X-ray tomography of foam materials. Russian Journal of Nondestructive Testing, 2021. 57(3): p. 238-250.

[63] Wismans, J., et al. X-ray computed tomography based modelling of polymeric foams. in Materials Science Forum. 2010. Trans Tech Publ.

[64] Ghazi, A., et al., Computed tomography based modelling of the behaviour of closed cell metallic foams using a shell approximation. Materials & Design, 2020. 194: p. 108866.

[65] Carmignato, S., Dewulf, W., and Leach, R., Industrial X-ray computed tomography. Vol. 10. 2018: Springer.

[66] Salvo, L., et al., 3D imaging in material science: Application of X-ray tomography. Comptes Rendus Physique, 2010. 11(9-10): p. 641-649.

[67] Vabre, A., et al., Metallic foams characterization with X-ray microtomography using Medipix2 detector. Nuclear Instruments and Methods in Physics Research Section A: Accelerators, Spectrometers, Detectors and Associated Equipment, 2007. 576(1): p. 169-172.

[68] Bock, J. and Jacobi, A.M., Geometric classification of open-cell metal foams using X-ray micro-computed tomography. Materials Characterization, 2013. 75: p. 35-43.

[69] García-Moreno, F., et al., Using X-ray tomoscopy to explore the dynamics of foaming metal. Nature communications, 2019. 10(1): p. 3762.

[70] Elkhoury, J.E., Shankar, R., and Ramakrishnan, T., Resolution and limitations of X-ray micro-CT with applications to sandstones and limestones. Transport in Porous Media, 2019. 129(1): p. 413-425.

[71] Nie, Z., Lin, Y., and Tong, Q., Modeling structures of open cell foams. Computational Materials Science, 2017. 131: p. 160-169.

[72] Wejrzanowski, T., et al., Structure of foams modeled by Laguerre–Voronoi tessellations. Computational Materials Science, 2013. 67: p. 216-221.

[73] Lautensack, C., Fitting three-dimensional Laguerre tessellations to foam structures. Journal of Applied Statistics, 2008. 35(9): p. 985-995.

[74] Billiet, M., et al., Influence of orientation and radiative heat transfer on aluminum foams in buoyancy-induced convection. Materials, 2015. 8(10): p. 6792-6805.

[75] Fantini, M., Curto, M., and De Crescenzio, F., A method to design biomimetic scaffolds for bone tissue engineering based on Voronoi lattices. Virtual and Physical Prototyping, 2016. 11(2): p. 77-90.

[76] Fantini, M. and Curto, M., Interactive design and manufacturing of a Voronoi-based biomimetic bone scaffold for morphological characterization. International Journal on Interactive Design and Manufacturing (IJIDeM), 2018. 12: p. 585-596.

[77] Catmull E, Clark J. Recursively generated B-spline surfaces on arbitrary topological meshes. Comput-Aided Des. 1978; 10(6): 350–355.

[78] Wang, S., et al., Crushing and densification of rapid prototyping polylactide foam: Meso-structural effect and a statistical constitutive model. Mechanics of Materials, 2018. 127: p. 65-76.

[79] Movahedi, N. and Linul, E., Quasi-static compressive behavior of the ex-situ aluminum-alloy foam-filled tubes under elevated temperature conditions. Materials Letters, 2017. 206: p. 182-184.

[80] Movahedi, N. and Linul, E., Radial crushing response of ex-situ foam-filled tubes at elevated temperatures. Composite Structures, 2021. 277: p. 114634.

[81] ISO13314. Mechanical testing of metals – ductility testing –compression test for porous and cellular metals. 2011.

[82] Soni, B., and Biswas, S., Evaluation of mechanical properties under quasi-static compression of open-cell foams of 6061-T6 Al alloy fabricated by pressurized salt infiltration casting method. Materials Characterization, 2017. 130: p. 198-203.

[83] Jing, L., et al., Compressive strain rate dependence and constitutive modeling of closed-cell aluminum foams with various relative densities. Journal of Materials Science, 2018. 53: p. 14739-14757.

[84] Zhao, Y., et al., Dynamic mechanical properties of closed-cell aluminum foams with uniform and graded densities. Journal of Materials Research, 2020. 35(19): p. 2575-2586.

[85] Li, Q., Magkiriadis, I., and Harrigan, J.J., Compressive strain at the onset of densification of cellular solids. Journal of cellular plastics, 2006. 42(5): p. 371-392.

[86] Li, L., et al., Insight into cell size effects on quasi-static and dynamic compressive properties of 3D foams. Materials Science and Engineering: A, 2015. 636: p. 60-69.

[87] Habib, F., et al., Fabrication of polymeric lattice structures for optimum energy absorption using Multi Jet Fusion technology. Materials & Design, 2018. 155: p. 86-98.

[88] Duan, Y., et al., Quasi-static and dynamic compressive properties and deformation mechanisms of 3D printed polymeric cellular structures with Kelvin cells. International Journal of Impact Engineering, 2019. 132: p. 103303.

[89] Wang, N., et al., Compressive performance and deformation mechanism of the dynamic gas injection aluminum foams. Materials Characterization, 2019. 147: p. 11-20.

[90] Lu, Z.-x., Huang, J.-x., and Yuan, Z.-s., Effects of microstructure on uniaxial strength asymmetry of open-cell foams. Applied Mathematics and Mechanics, 2015. 36(1): p. 37-46.

Appendix 1

3D Finite Element Model

The generated geometric model of random open-cell foam using the proposed technique can be included in two kinds of modeling i.e. Shell and Solid finite elements.

Examples of 3D finite element models are constructed and shown in Figure 1 and Figure 2.

For Shell modeling

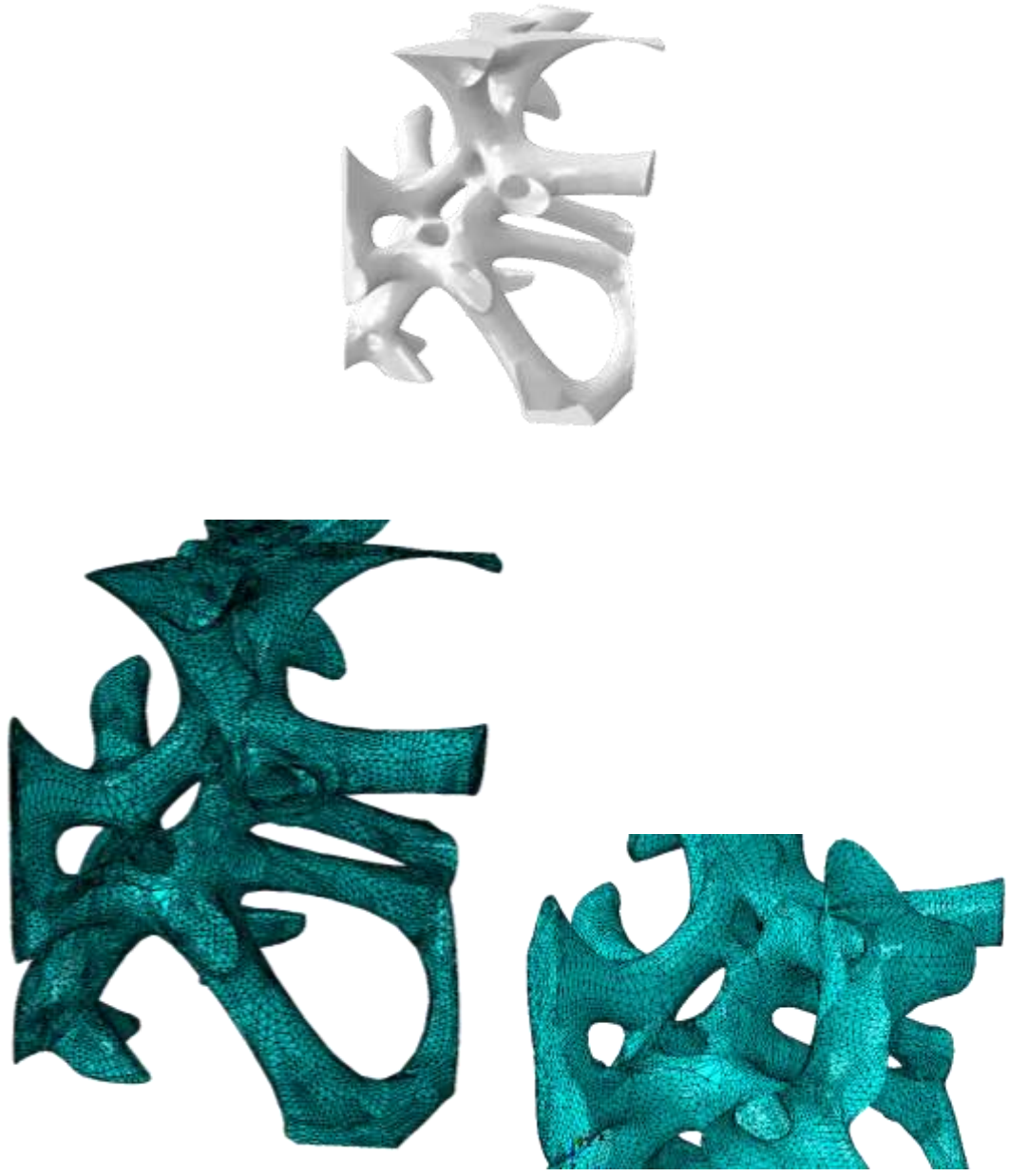

Figure 2: 3D finite element model based on shell geometry.

For Solid modeling

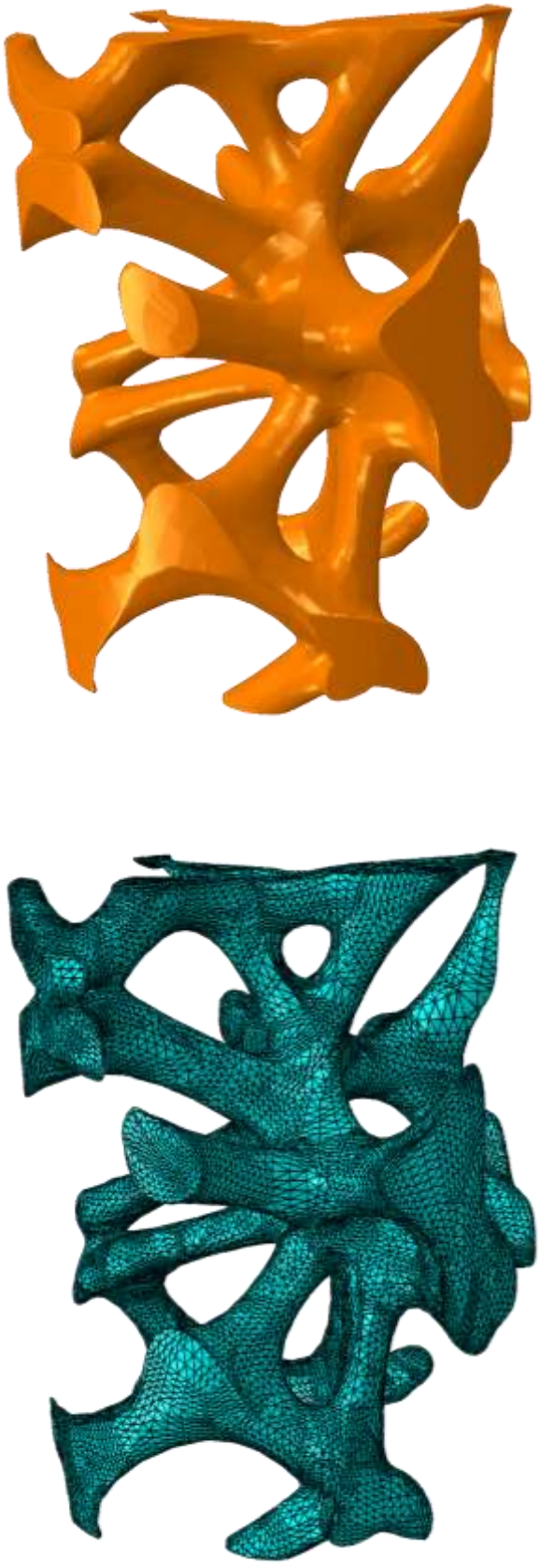

Figure 2: 3D finite element model based on solid geometry.

Appendix 2

Fused deposition modeling

1. Principle

Fused Deposition Modeling (FDM) is a 3D printing technology that involves building objects by depositing successive layers of material with an extruded thermoplastic filament. This process is known for its precision, reliability, and repeatability, and it offers valuable efficiencies over conventional manufacturing methods, allowing for the production of a wide range of applications, from functional prototyping to end-use parts. FDM 3D printers work by depositing melted filament material over a build platform layer by layer until a completed part is obtained. The technology uses thermoplastic filaments, which are melted and extruded onto a build platform, and it is widely used due to its high accuracy, low cost, and large material selection. FDM is recognized for its simplicity of use and is commonly used for form/fit testing, functional testing, rapid tooling patterns, small detailed parts, and presentation models. Figure 1 shows the schematic illustration of the FDM process.

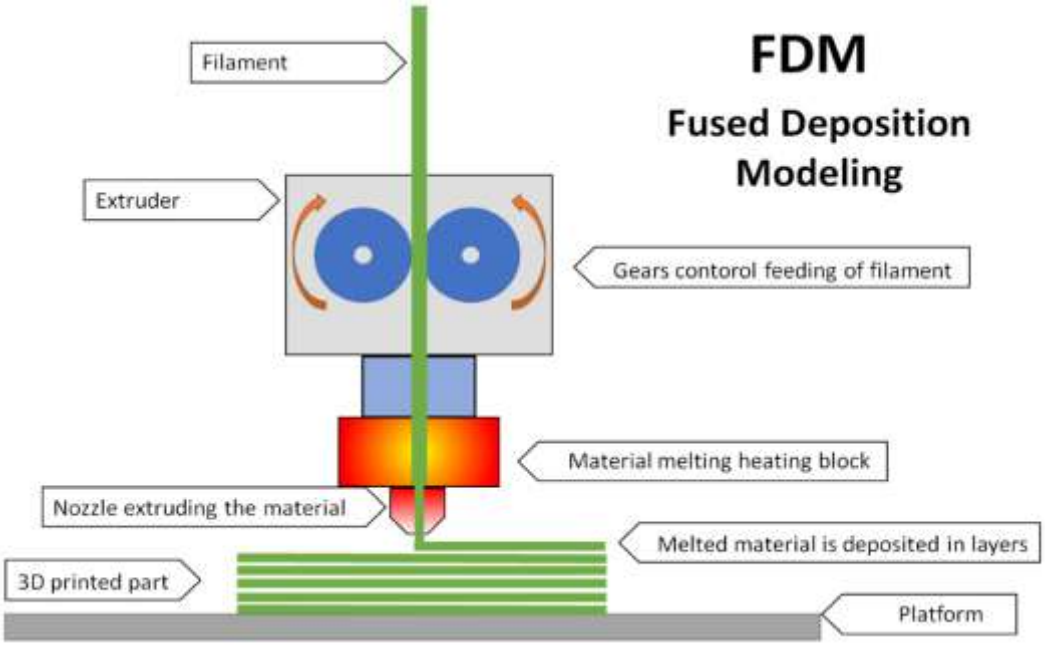

Figure 1: Schematic illustration of the FDM process.

2. 3D Printer description

The 3D printing of the designed Samples in chapter three was done by the **Geeetech A10** 3D printer. It is a noteworthy example, distinguished by its utilization of an open-source GT2560 control board. This board's open-source nature encourages customization and experimentation, fostering the printer's capability to produce objects with mixed colors, thus contributing to a more diversified and engaging 3D printing experience.

Figure 2: Geeetech A10M FDM printer.

- *Material Filament*: FDM printers use a thermoplastic filament, typically made of materials like ABS (Acrylonitrile Butadiene Styrene), PLA (Polylactic Acid), PETG, or others. The filament is fed into the 3D printer through a heated nozzle.

Figure 3: PLA Filament with different colors.

- ***Heating and Extrusion***: Inside the printer, the filament is heated to its melting point within the nozzle. Once it's in a molten state, the nozzle moves along a predefined path (based on the 3D model) and extrudes the material layer by layer onto a build platform.

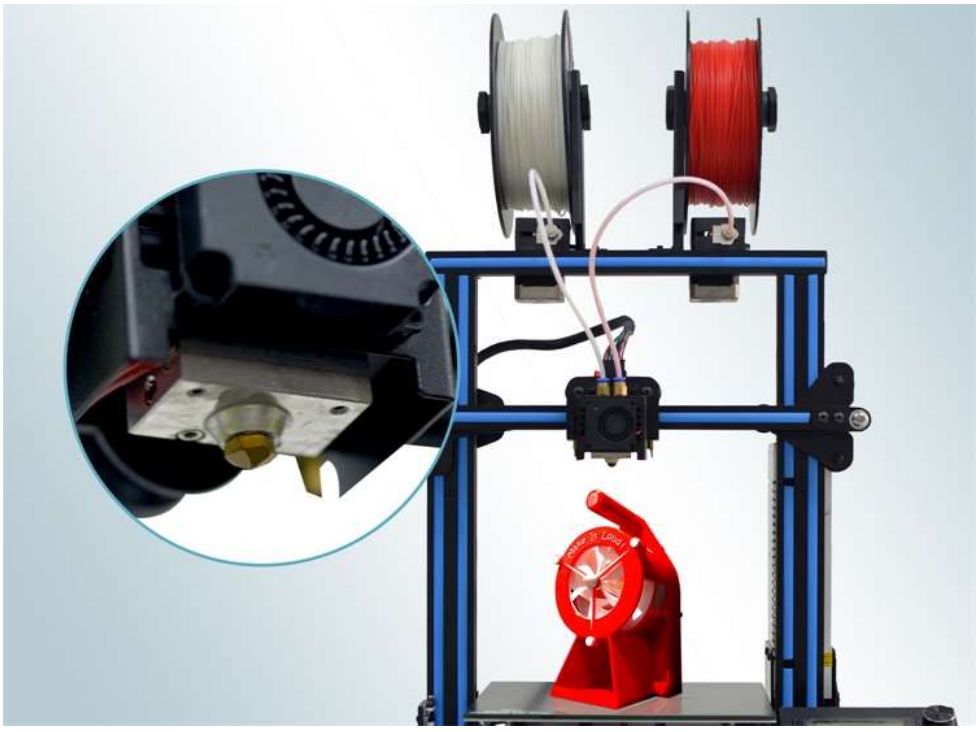

Figure 4: Hotend and nozzle of geeetech a 10.

- ***Layer-by-Layer Build***: As each layer of material is extruded, it quickly cools down and solidifies, bonding with the previously deposited layers. This process is repeated, layer by layer, until the entire 3D object is created.

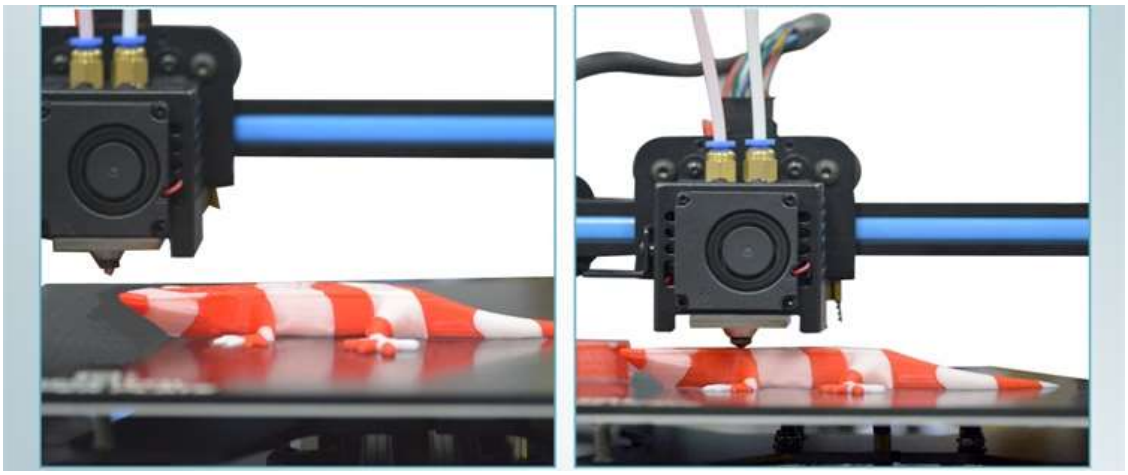

Figure 5: The geeetech A10 printer in the printing process (layer by layer).

- ***Cooling and Solidification:*** As mentioned earlier, the material cools and solidifies quickly after being deposited, ensuring that the layers adhere to each other and form a solid object.

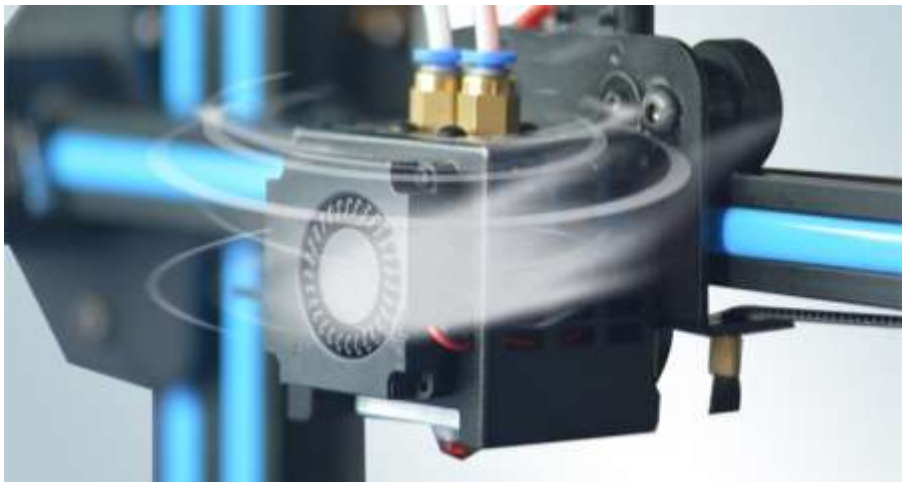

Figure 6: A10 extruder 360° ventilation design.

3. 3D printing process of developed open-cell foam structures

Open cell foam specimens, each with dimensions of 50 mm × 50 mm × 50 mm, were systematically produced using a Geeetech A10 3D printer, employing PLA as the filament material. The optimization of printing parameters was conducted through an iterative process, utilizing the Ultimaker_Cura-4.12.1 slicing software. This methodology aimed to refine the outcomes, achieving the optimal print quality as demonstrated in Figure 7.

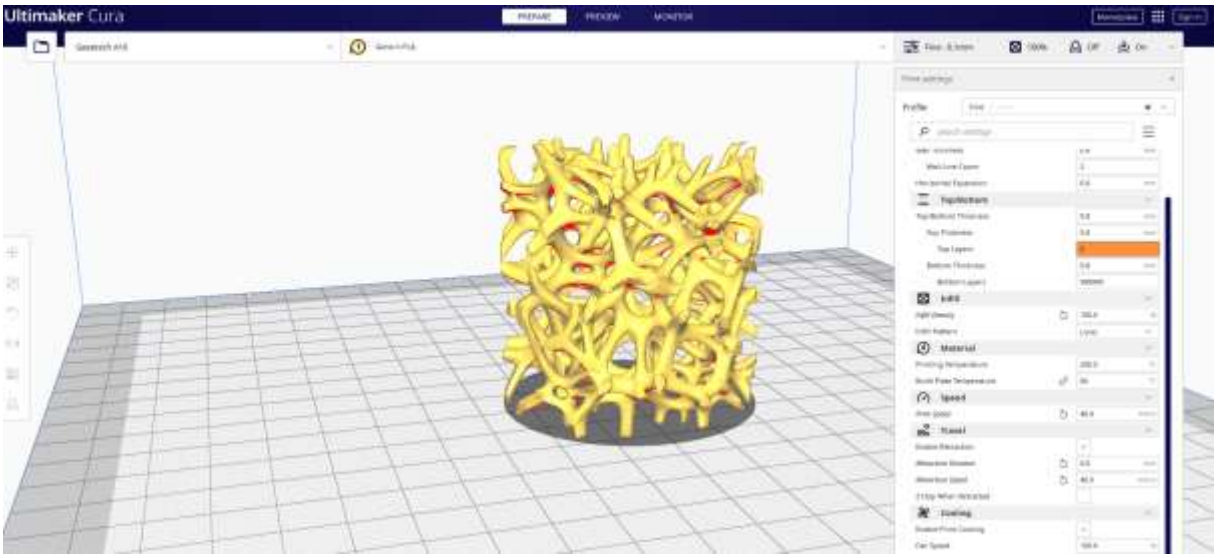

Figure 7: the basics print setting used for open cell foam manufacturing.

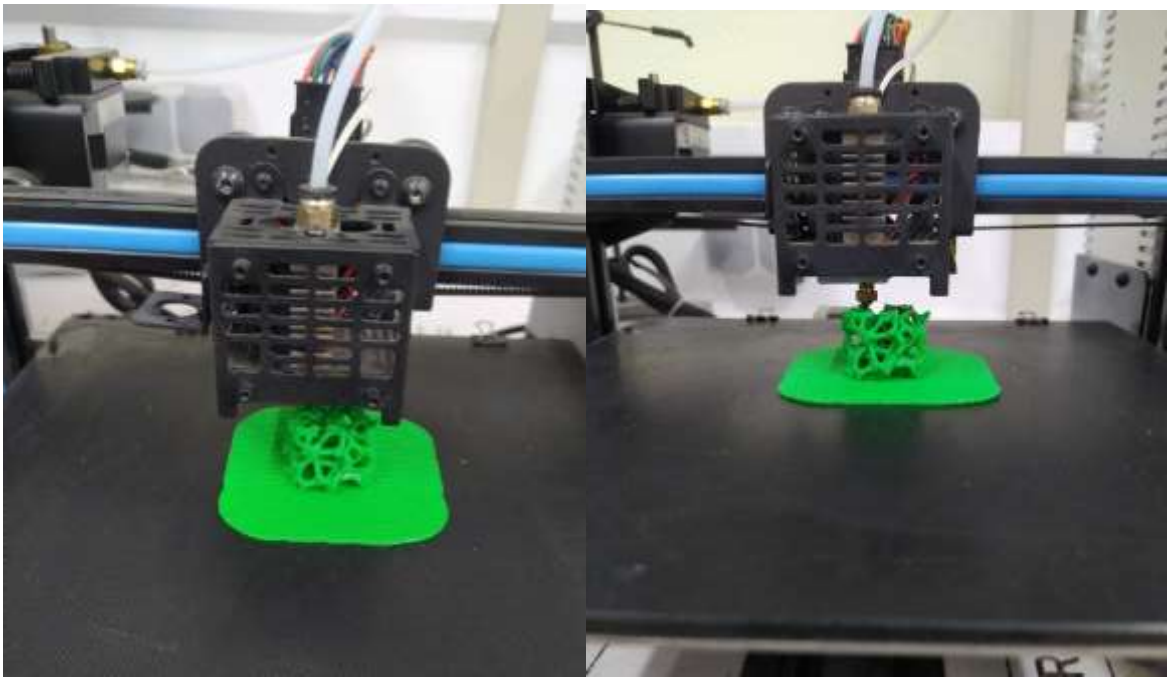

Figure 8: The 3d printing process of open cell foam.

- Example of 3D printed simples

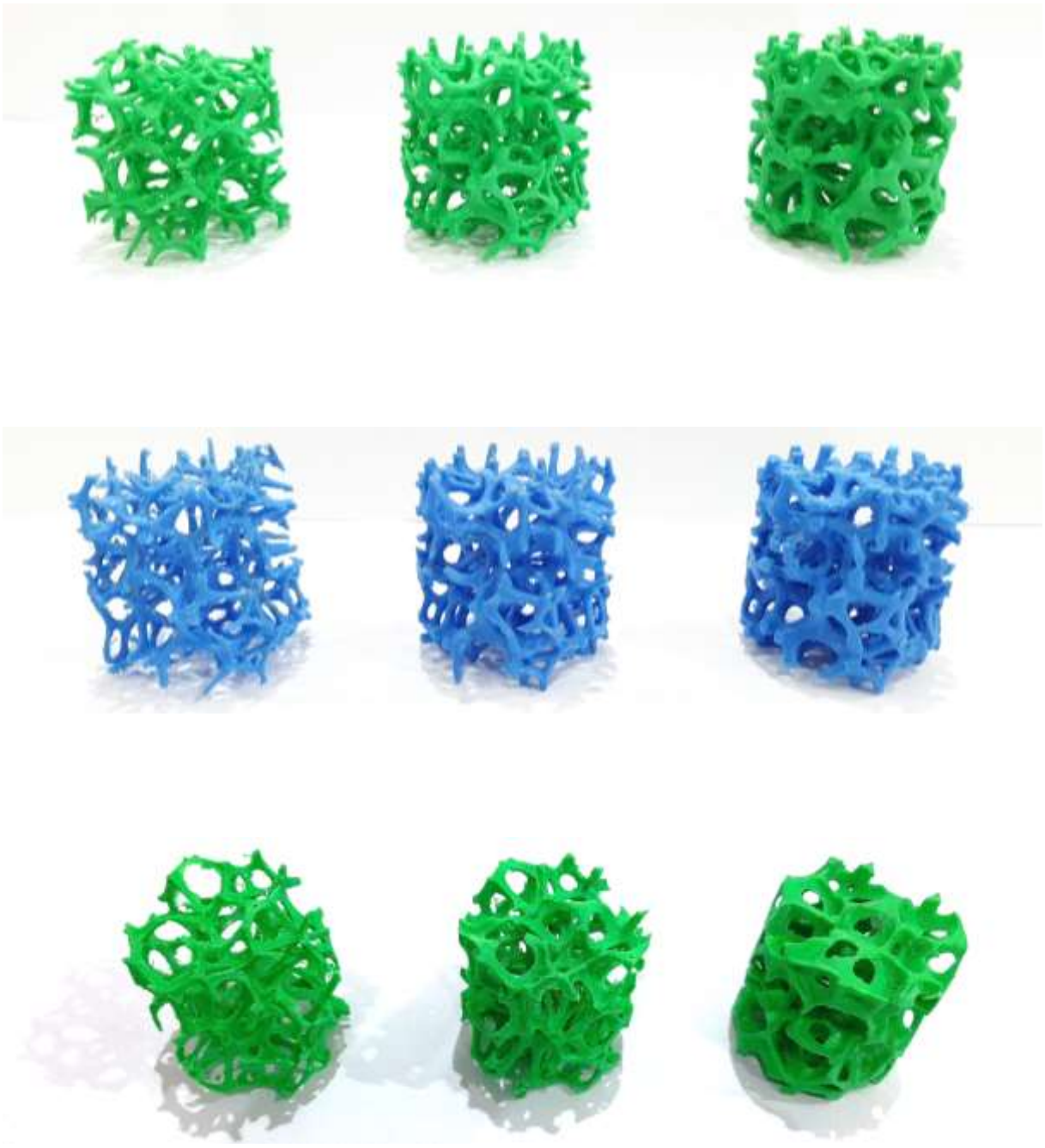

Figure 9: Example of 3D printed simples using geeetech A10 3D-printer

ملخص

تمت دراسة خصائص التشوه والسلوك الميكانيكي لهياكل الرغوة ذات الخلايا المفتوحة العشوائية المطبوعة ثلاثية الأبعاد بشكل تجريبي تحت اختبار الضغط شبه الثابت. يتم إنشاء عينات رغوة PLA ذات هندسة الخلايا غير المنتظمة وأقسام الدعامات المتغيرة والكثافة النسبية الموصوفة رقميًا باستخدام مخططات فورونوي وإعدادها باستخدام نمذجة الترسيب المنصهر. يتيح إجراء التصميم التحكم في طوبولوجيا الدعامة بسهولة، مما يجعل النموذج الهندسي مناسبًا لدراسة تأثير الخصائص المورفولوجية المحلية على الأداء الميكانيكي لمادة الرغوة ذات الخلية المفتوحة. تم فحص تأثير الخصائص المورفولوجية المختلفة على السلوك الميكانيكي المضغوط لرغوة PLA المصنعة بالتفصيل. أثبتت تجارب الضغط أن الخواص الميكانيكية تعتمد بشكل كبير على الكثافة النسبية وشكل قسم الدعامة. تم الحصول على الخواص الميكانيكية الرئيسية لرغاوي PLA المطبوعة ثلاثية الأبعاد لأشكال مقطعية مختلفة من الدعامات عبر الطريقة الموفرة للطاقة وتم التعبير عنها بالصيغتين الشائعتين الموجودتين في الأدبيات.

Abstract

The deformation characteristics and mechanical behaviour of 3D-printed stochastic open-cell foam structures were experimentally studied under a quasi-static compression test. PLA foam specimens with irregular cell geometry, variable strut sections and prescribed relative density are constructed numerically using the Voronoi diagrams and prepared with fused deposition modelling. The design procedure allows controlling the strut topology easily, which makes the geometrical model suitable for studying the effect of local morphological characteristics on the mechanical performance of open-cell foam material. The effect of different morphological characteristics on the compressive mechanical behaviour of the fabricated PLA foam was examined in detail. Compression experiments prove that the mechanical properties significantly dependent on the relative density and strut section shape. The main mechanical properties of the 3D-printed PLA foams for different cross-sectional shapes of struts were obtained via the energy-efficient method and expressed with the two common formulas existing in the literature.

Résumé

Les caractéristiques de déformation et le comportement mécanique de structures de mousse stochastique à cellules ouvertes imprimées en 3D ont été étudiées expérimentalement dans le cadre d'un test de compression quasi-statique. Des échantillons de mousse PLA avec une géométrie cellulaire irrégulière, des sections de support variables et une densité relative prescrite sont construits numériquement à l'aide des diagrammes de Voronoï et préparés avec une modélisation de dépôt fondu. La procédure de conception permet de contrôler facilement la topologie des entretoises, ce qui rend le modèle géométrique adapté à l'étude de l'effet des caractéristiques morphologiques locales sur les performances mécaniques du matériau en mousse à cellules ouvertes. L'effet de différentes caractéristiques morphologiques sur le comportement mécanique en compression de la mousse PLA fabriquée a été examiné en détail. Les expériences de compression prouvent que les propriétés mécaniques dépendent de manière significative de la densité relative et de la forme de la section de support. Les principales propriétés mécaniques des mousses PLA imprimées en 3D pour différentes formes de section transversale d'entretoises ont été obtenues via la méthode économe en énergie et exprimées avec les deux formules courantes existant dans la littérature.